WRF Rainfall Parameterisation and Verification

Report to the
WATER RESEARCH COMMISSION

by

Michael Weston & Paulo Kagoda
EScience Associates (PTY) LTD.

WRC Report No. 2162/1/14
ISBN 978-1-4312-0598-1

November 2014

Obtainable from
Water Research Commission
Private Bag X03
Gezina, 0031

email: orders@wrc.org.za or download from www.wrc.org.za

EXECUTIVE SUMMARY

BACKGROUND

Numerical weather prediction models (NWPs) are tools used to forecast rainfall based on current meteorological conditions and how they are expected to develop. Some challenges when modelling are: it is impossible to solve all atmospheric processes explicitly as they are too numerous and often involve more unknown variables than those known, and a single process may be driven by multiple forces, which are represented to a greater or lesser extent in the model. The aim of this work is to simulate rainfall using a NWP, and determine which parameterisation schemes within the model produce the best results.

RATIONALE

The Weather Research and Forecast (WRF) model is a numerical weather prediction model that simulates grid scale saturation and convective rainfall, which is a sub grid scale process. Several parameterisation schemes are available for each of these processes, which perform with varying degrees of success. Thus, when running a forecast which may cover a large area like the whole of South Africa that experiences both rainfall types, only a single combination of schemes is applied. This may then favour one rainfall type, like convective rainfall, to the detriment of non-convective rainfall forecasts.

OBJECTIVES AND AIMS

The aim of this research is to determine the most suitable parameterisation of WRF to represent observed rainfall events in both convective and non-convective rainfall areas in South Africa and to create institutional and professional capacity in:

- Numerical weather prediction models in simulating and verifying rainfall using the WRF model (v3.4.1)
- Hydrological modelling using the PyTopkapi model
- WRFChem modelling and its effects on rainfall

These aims were achieved through simulation of rainfall over two catchments in South Africa: the Berg River catchment in the Western Cape Province and the Liebenbergsvlei catchment in the Free State Province. Verification of rainfall was achieved through 1) WRF to rain gauge comparison, and 2) WRF rainfall entered into a hydrological model, PyTopkapi and compared to stream flow data.

The final objective was achieved through running WRFChem over the industrialised Highveld of South Africa, where emissions are expected to change the concentration of cloud condensation nuclei and therefore cloud droplet physics and rainfall patterns.

METHODOLOGY

WRF Rainfall

Results are presented for 3 month periods, covering the winter rainfall period for the Berg River catchment (May to July 2000) and summer months for the Liebenbergsvlei catchment (October to December 2000). Nested domains were used in WRF covering resolutions of 36-12-4 km, with the parent domain covering Africa South of the equator to 40 degrees south. The 12 km domain covers South Africa. The 4 km domains covered the catchment of interest.

Combinations of parameterisation schemes of grid scale saturation were implemented in the model. Further tests were run to increase frequency of forcing lateral boundary condition, radiation physics solvers (radt) and cumulus physics solvers (cudt).

PyTOPKAPI

TOPKAPI is an acronym which stands for **TO**Pographic **K**inematic **AP**proximation and **I**ntegration, and is a physically-based distributed rainfall-runoff model, originally proposed by Liu and Todini (2002). In this study, PyTOPKAPI (Vischel et al., 2007), a BSD licensed Python library version of Topkapi was used. The PyTopkapi model was calibrated using observed rainfall as input and verified against observed stream flow. Once calibrated, WRF rainfall was used as input and then verified against stream flow gauge data.

WRFChem

WRFChem simulations were initiated for rainfall case studies of a few days from 1-5 October 2000 where observed rainfall was recorded on each day. Emissions of anthropogenic sulphur dioxide (SO_2) and particulate matter (PM) were obtained from a global emissions inventory (EDGAR). Emissions were entered into the 36 km domain where dynamic interactions with cloud droplets were modelled.

RESULTS AND DISCUSSION

WRF Rainfall

We found that WRF had a positive daily bias for the Liebenbergsvlei catchment, ranging from < 1 mm to > 4 mm for 12 km resolution domains. The Berg River catchment produced positive bias results of < 2 mm for the same domain. Three factors that cause the positive bias over Liebenbergsvlei were identified. These were;

1) Surplus rain days in the model (Figure 1)
2) Early triggering and formation of convective rainfall and
3) Excessive grid scale saturation and rainfall at night.

The most defensible scenarios, in terms of physics and frequency of calls to the solvers, were WSM3-Tiedtke-cudt0 and Lin-Tiedtke-cudt0 (radt=12 for both scenarios) and produced daily bias of less than 2 mm. Both schemes struck a balance between achieving hits, while minimising false alarms. Thus, considering all metrics presented, these two scenarios performed most favourably across the board. It is shown that for these schemes, false alarm events are not as high (in terms of mm rainfall) as other schemes, and that over predictions are not as high (< 5 mm). In terms of total rainfall in the catchment over a 3 month period, the WSM3-Tiedtke combination of schemes produced the most realistic results. Observed rainfall shows a diurnal cycle where most rainfall occurs after midday. The WRF model shows that convective rainfall triggers too early for all scenarios.

Non-convective rainfall is the dominant observed rainfall for this catchment, and as such, the Betts-Miller-Janjic convective scheme, with either the WSM3 or Lin microphysics was suitable for the Berg River.

The 4 km domains produced lower positive bias over Liebenbergsvlei. Three scenarios were run; Thompson microphysics, WSM3-BMJ and WSM3-Grell-3D. The daily bias was 1.31 mm, 1.06 mm and 1.84 mm respectively.

PyTOPKAPI

Rainfall from WRF over the Berg domain performed surprisingly well, achieving a Nash-Sutcliffe Efficiency of 0.479 (Figure 2). For Liebenbergsvlei further improvements to WRF rainfall simulations are required before further use of WRF rainfall in PyTopkapi. It was decided, based on results, to cease any further hydrological modelling as it would not yield meaningful results.

WRFChem

WRFChem results showed an overall increase in rainfall over the region when emissions from the global emissions inventory was switched on. This increase was attained through an increase in non-convective rainfall. The increase in non-convective rainfall was achieved during low rainfall events when emissions of SO_2 and particulate matter and associated feedback mechanisms were implemented.

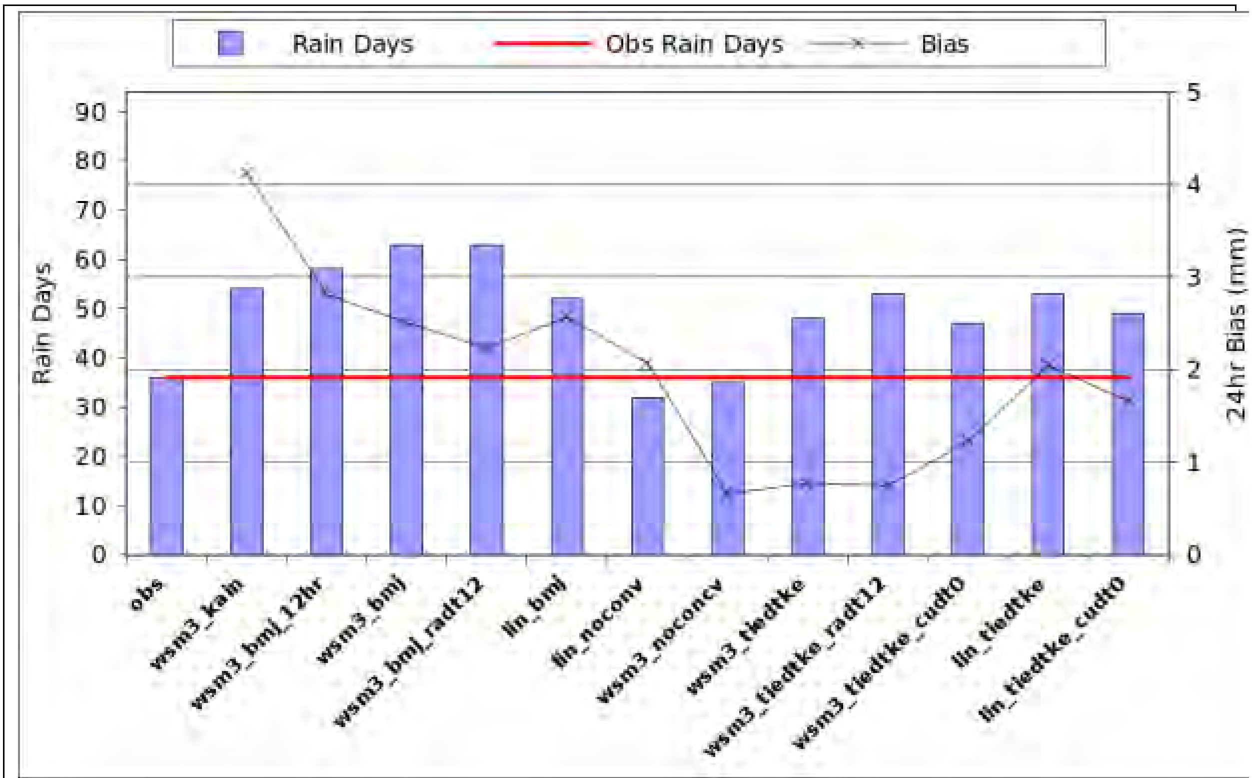

Figure 1: Rain days (>1 mm/d threshold) and 24hr bias for Liebenbergsvlei 12 km WRF domain.

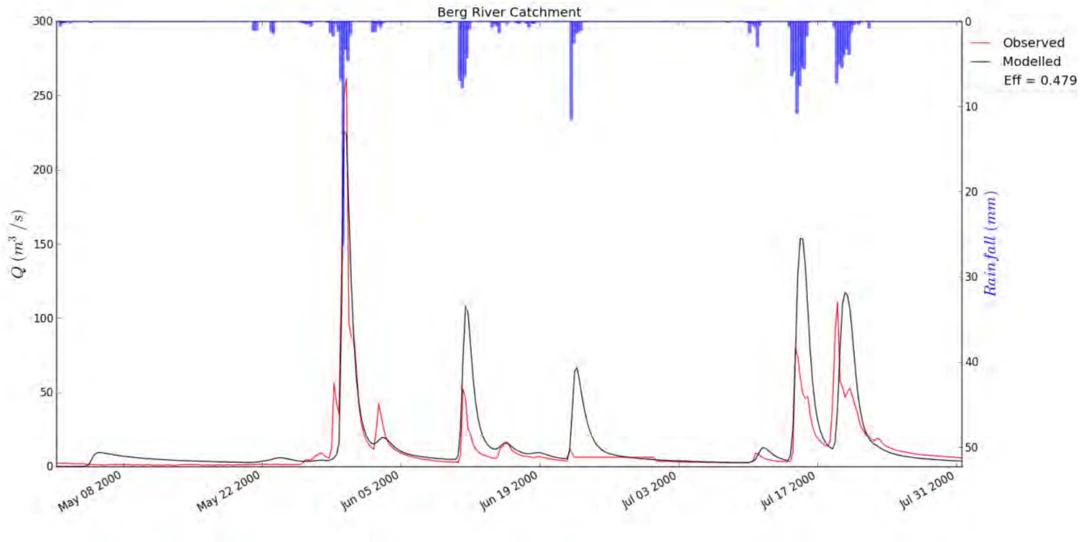

Figure 2: Berg River – WRF (scenario Lin/BMJ 12 km) vs. calibrated stream flow from May-Jul 2000.

CONCLUSIONS

Each catchment required different schemes to suitably model daily rainfall when running 12 km model domains. The best performing schemes for modelling rainfall over Liebenbergsvlei were the WSM3-Tiedtke-cudt0 and Lin-Tiedtke-cudt0. These schemes were implemented at a 12 km resolution, but both schemes trigger too early in the day and cause excessive rain days. Subsequently WRF is currently over-active at modelling convective rainfall over the eastern part of South Africa at this resolution and improvements to the model are required when modelling at this resolution.

The Liebenbergsvlei 4 km results did not show a significant improvement, but may indicate why the model is over predicting rainfall. These results suggests that there is either too much moisture in the model, which condenses and rains, or that the temperature profile is not correct causing too much cooling, or it is a combination of both.

The Betts-Miller-Janjic convective scheme, with either the WSM3 or Lin microphysics was suitable for the Berg River 12 km domain. However, these schemes did not perform well for Liebenbergsvlei.

Arguably, the 4 km domain results did not outperform the 12 km results presented in section 8.6, as the hit rates, hit ratios and daily bias results were less favourable compared to the WSM3-BMJ and Lin-BMJ scenarios.

RECOMMENDATIONS FOR FUTURE RESEARCH

Two possibilities exist for future research. The first is to include a larger sample size for comparing the mode to observed data. This would require modelling 6 months, instead of 3, over five seasons. This may be long enough to negate any bias in choosing a single observed rainfall season, which may be the anomaly in a 5 or 10 year period. The second option is to investigate the model code and determine why rainfall is triggered early. If identified, this can then be adjusted so that the early trigger is delayed. However, this requires much testing as it may create errors elsewhere in the model.

Two recommendations are made. The first is to model at 4 km resolution whenever possible using the correct microphysics scheme for the study area. However, this is not always feasible in which case the following suggestion is made for modelling rainfall at 12 km resolution: choose the correct schemes for your area of interest. If your domain contains both areas, e.g. Western Cape and Eastern Escarpment, and you are running a forecast, run two instances of the model, one with each set up.

CAPACITY BUILDING

Students

Two students were involved in this project and were involved in the hydrological modelling.

Paulo Kagoda is completing is PhD at the University of the Witwatersrand and was instrumental in calibrating the PyTopkapi model for the catchment areas. Once calibrated, Sintu Mhlonyane installed PyTopkapi and ran several simulations using WRF rainfall as input. Both students were present at meetings with the reference group.

Institutional

This is the first project of this kind undertaken by EScience Associates (PTY) LTD. Much progress was made in terms of model set up and knowhow for simulating rainfall. Furthermore, this project served as a good learning experience and capacity building for the project leader, Michael Weston.

ACKNOWLEDGEMENTS

The authors would like to thank the Reference Group of the WRC Project K5-2162 for the assistance and the constructive discussions during the duration of the project:

Dr Francois Engelbrecht : CSIR (fengelbrecht@csir.co.za)

Dr Scott Sinclair : UKZN (sinclaird@ukzn.ac.za)

Ms Mary-Jane Bopape : CSIR (mbopape@csir.co.za)

Prof Stuart Piketh : NWU (stuart.piketh@nwu.ac.za)

The Project team for all their efforts in producing meaningful model results;

Mr Michael Weston : EScience Associates (michael@escience.co.za)

Mr Paulo Kagoda : EScience Associates (pkagoda@gmail.com)

Mr Sintu Mhlonyane : EScience Associates (sintu@escience.co.za)

Mr Theo Fischer : EScience Associates (theo@escience.co.za)

EScience Associates for providing the machines on which to run the model simulations.

The WRC staff, Research Manager Mr Wandile Nomquphu for coordinating the project and Charmain Smit for keeping the paperwork up to date.

TABLE OF CONTENTS

LIST OF FIGURES

LIST OF TABLES

LIST OF ABBREVIATIONS

ARC	Agricultural Research Council
BMJ	Betts-Miller Janjic WRF cumulus scheme
CSI	Critical Success Index
Cu_physics	Cumulus parameterisation
CUDT	Time interval for calling cumulus physics in WRF
ECMWF	European Centre for Medium Range Forecasts
FAR	False alarm ratio
HR	Hit rate
Hr	Hit ratio
Ks	Soil Saturation
L	Soil Depth
Mp_physics	Micro physics parameterisation scheme
n_c	Manning’s channel roughness coefficient
n_o	Manning’s overland roughness coefficient
POD	Probability of detection
RADT	Time interval for calling radiation physics in WRF
RAINC	Convective rainfall from WRF
RAINNC	Non-convective rainfall from WRF
SAWS	South African Weather Service
TOPKAPI	Hydrological model: TOPographic Kinematic APproximation and Integration
WRF	Weather Research and Forecast Model
WSM3	WRF single moment 3-class microphysics scheme

1 INTRODUCTION AND OBJECTIVES

1.1 Background

Numerical weather prediction models (NWPs) are a tool used to forecast rainfall based on current meteorological conditions and how they are expected to develop. They simulate the atmosphere by solving finite difference equations that represent the physical processes that drive atmospheric circulation and transport of moisture. This provides some challenges which include; it is impossible to solve all atmospheric processes explicitly as they are too numerous and often involve more unknown variables than those known and; a single process may be driven by multiple forces, which are represented to a greater or lesser extent in the model. As such, parameterisation schemes are implemented to solve sub grid scale processes in the model, for example cloud formation. The aim of this work is to simulate rainfall using a NWP, and determine which parameterisation schemes within the model produce the best results.

1.2 Rationale

The Weather Research and Forecast (WRF) model is a numerical weather prediction model that simulates grid scale saturation and convective rainfall, which is a sub grid scale process. Several parameterisation schemes are available for each of these processes, which perform with varying degrees of success. Grid scale saturation is when water vapour in an air mass is forced to condense and form clouds, typically due to large scale uplift like a frontal system. While some areas experience this type of rainfall and it is best simulated using a certain parameterisation scheme, other areas may experience rainfall from convective storm cells which occur on a sub grid scale. Such rainfall may be best simulated using a different parameterisation scheme. Thus, when running a forecast which may cover a large area like the whole of South Africa, that experiences both rainfall types, only a single combination of schemes is applied. This may then favour one rainfall type, like convective rainfall, to the detriment of non-convective rainfall forecasts.

1.3 Aims and Objectives

The aim of this research is to determine the most suitable parameterisation of WRF to represent observed rainfall events in both convective and non-convective rainfall areas in South Africa and to create institutional and professional capacity in:

- Numerical weather prediction models in simulating and verifying rainfall using the WRF model (v3.4.1).
- Hydrological modelling using the PyTopkapi model
- WRFChem modelling and its effects on rainfall

These aims were achieved through simulation of rainfall over two catchments in South Africa, the Berg River catchment in the Western Cape Province and the Liebenbergsvlei catchment in the Free State Province. The objective was to identify the combination of model parameterisation schemes in the WRF model that best simulate the rainfall in each catchment, paying special attention to the convective schemes employed. Verification of rainfall was achieved through;

1. WRF to rain gauge comparison and
2. WRF rainfall entered into a hydrological model, PyTopkapi and compared to stream flow data.

The motivation for using the hydrological model as part of WRF rainfall verification is that WRF may at times model rainfall quantity correctly but not in the exact location as the observed rain gauge data. Thus, by aggregating WRF output over a larger area of a catchment, may better capture the rainfall from WRF.

The final objective was achieved through running WRFChem over the industrialised Highveld of South Africa, where emissions are expected to change the concentration of cloud condensation nuclei and therefor cloud droplet physics and rainfall patterns.

2 WRF LITERATURE REVIEW

2.1 Numerical Weather Prediction Models

Numerical weather prediction models (NWPs) simulate the atmosphere by solving physical processes that drive atmospheric circulation. This is achieved by dividing the atmosphere into cubes of air using a regular horizontal grid (Figure 2-1) and terrain following vertical coordinate system (Figure 2-2). Finite difference approximations are then applied to each grid point to solve the simplified atmospheric equations of motion (Stull, 2000). The spatial scale of the horizontal grids range between about 120 km (~1 degree) for global models, 3 km for operational forecasts to hundreds of meters for storm tracking and forecasting. The vertical grid is terrain following, also known as a sigma co-ordinate, and the distance between layers increases with height, as the grids try preserve mass and air density decreases with height.

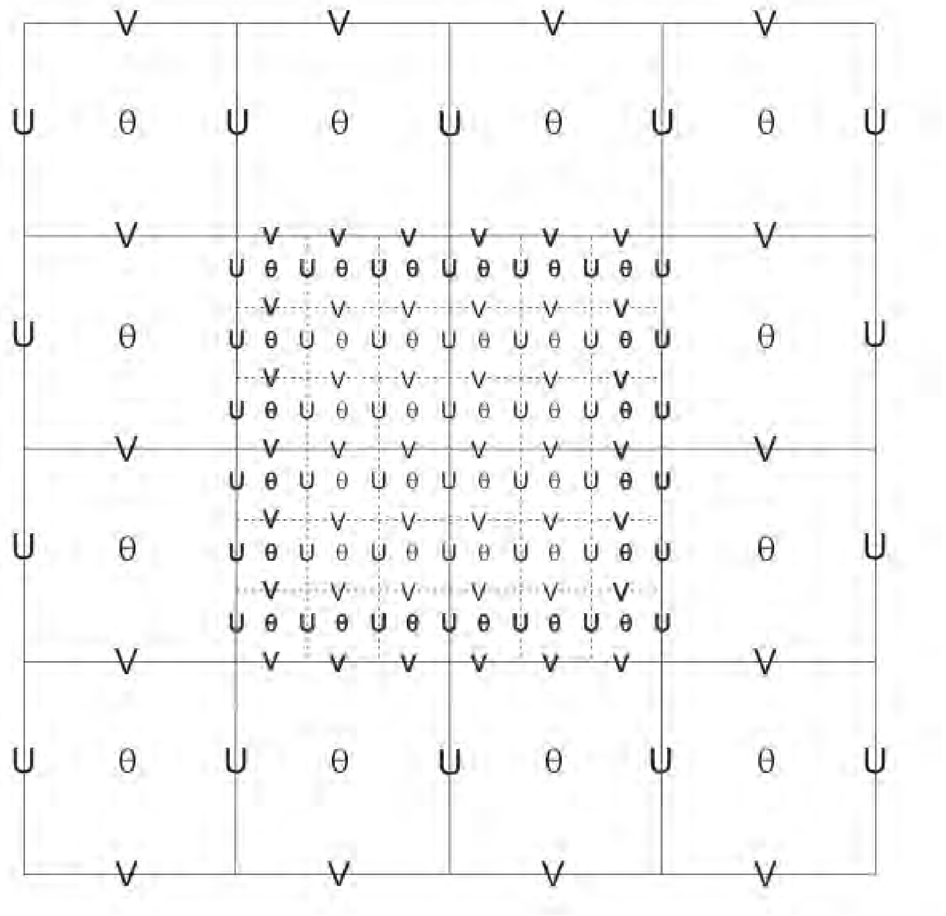

Figure 2-1: Staggered Arakawa-C horizontal grid of parent domain used in WRF (large cells) and nest or child domain (smaller cells). The U (V) wind component is calculated at the east (north) and west (south) face of each cell (Skamarock et al., 2008).

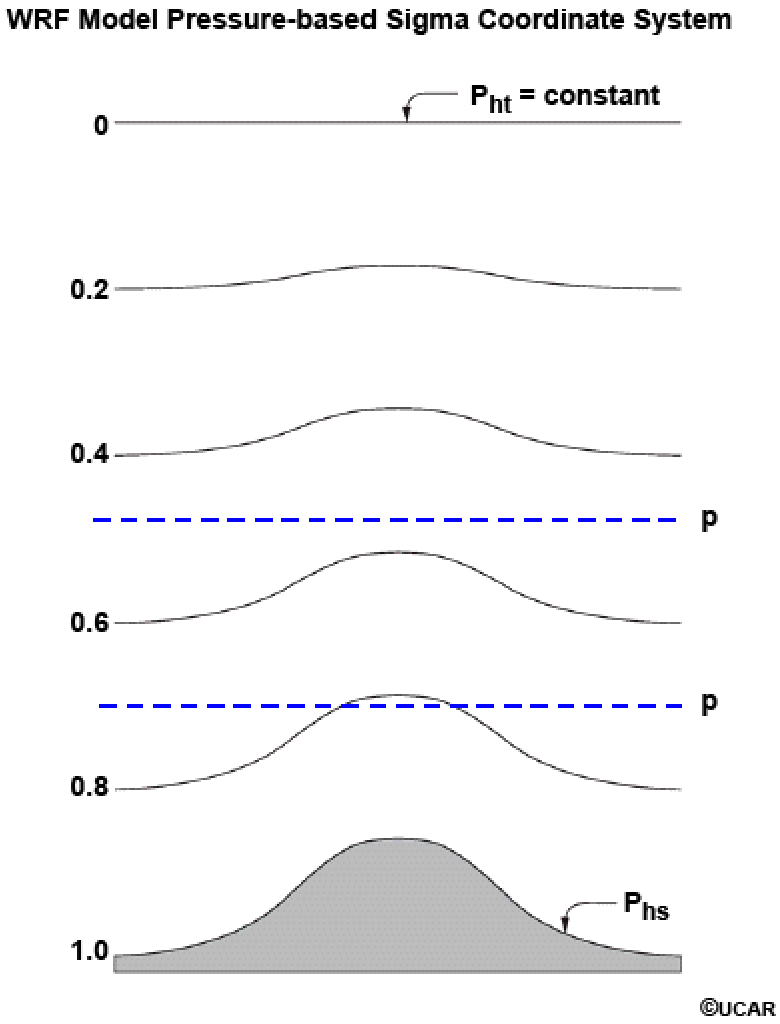

Figure 2-2: The vertical co-ordinate system is a terrain following, sigma co-ordinate system. Vertical grid spacing can vary with height, generally becoming more compressed closer to ground level over mountains (source: UCAR, 2006).

2.2 Model Parameterisation

Atmospheric processes occur on spatial scales that are much smaller than what can be represented in numerical weather prediction models. For example, to represent the small eddies associated with flow over obstacles using equations would result in more unknown variables than equations (Stull, 2000 pg 471) Parameterisation schemes are used to solve these sub-grid scale processes in the model. Schemes represent conceptual physical processes in the atmosphere to varying degrees of mathematical accuracy. This approach is computationally efficient as it emulates the net effect of sub-grid scale processes for a single model grid cell instead of solving each sub-grid scale process individually. Although this can be thought of as a trade-off, even the most basic of parameterisation schemes have been shown to improve model skill.

2.3 The WRF Model

The Weather Research and Forecast (WRF) model is a non-hydrostatic mesoscale meteorological model used for both operational forecasting and research purposes (MMM, NCAR, 2010). It is the successor to the 5th generation Mesoscale Model (MM5). WRF is a community based model with the largest collaborators being North American academic and governmental organisations (National Center for Atmospheric Research (NCAR), the National Oceanic and Atmospheric Administration (the National Centers for Environmental Prediction (NCEP) and the Forecast Systems Laboratory (FSL), the Air Force Weather Agency (AFWA), the Naval Research Laboratory, the University of Oklahoma, and the Federal Aviation Administration (FAA)) (www.wrf-model.org, 2012).

WRF solves the non-hydrostatic equations for each time step using a terrain-following mass vertical coordinate (Skamarock *et al.,* 2008) and an arakawa-C grid (staggered grid) in the horizontal. A nested grid is used with the option for one- or two-way nesting. Typically, a parent domain is used to determine atmospheric boundary conditions for an inner grid that covers the area of interest with two-way nesting activated. Two model cores are available for solving the model equations, the non-hydrostatic mesoscale model (NMM) core and the Advanced Research WRF (ARW) core. The ARW core is used in this study.

2.4 WRF Parameterisation Schemes

Atmospheric processes are divided into the following main categories (Figure 2-3). An introduction to these schemes is given here followed by more detailed explanations of the schemes available in WRF.

Planetary boundary layer (PBL)

Solves physics for the largest part of the atmosphere, including the region where clouds form. It is important to verify that the PBL scheme is working well before testing microphysics and cumulus schemes.

Microphysics

This is a rainfall scheme that solves cloud microphysics. These schemes determine if saturation occurs on a grid scale and calculates associated changes in temperature and relative humidity.

Cumulus

This is a rainfall scheme that solves cloud convection on a sub-grid scale. These schemes determine in convection is triggered and whether rainfall occurs. Generally, these schemes calculate vertical profiles of moister and temperature.

Surface

This category can be divided into two sections: 1- the land surface and 2- the surface layer of the atmosphere. The land surface scheme controls exchanges of heat and moisture between the lower atmosphere and the land surface. The surface layer of the atmosphere behaves differently to the planetary boundary layer. As such it has a separate scheme that controls flow in this layer as an intermediate step of heat and moister transfer between the land surface and planetary boundary layer.

Radiation

These schemes calculate the incoming long wave and outgoing short wave radiation. Long wave and short wave radiation is generally divided into multiple bands and the effects of scattering due to clouds and trace gases is taken into account.

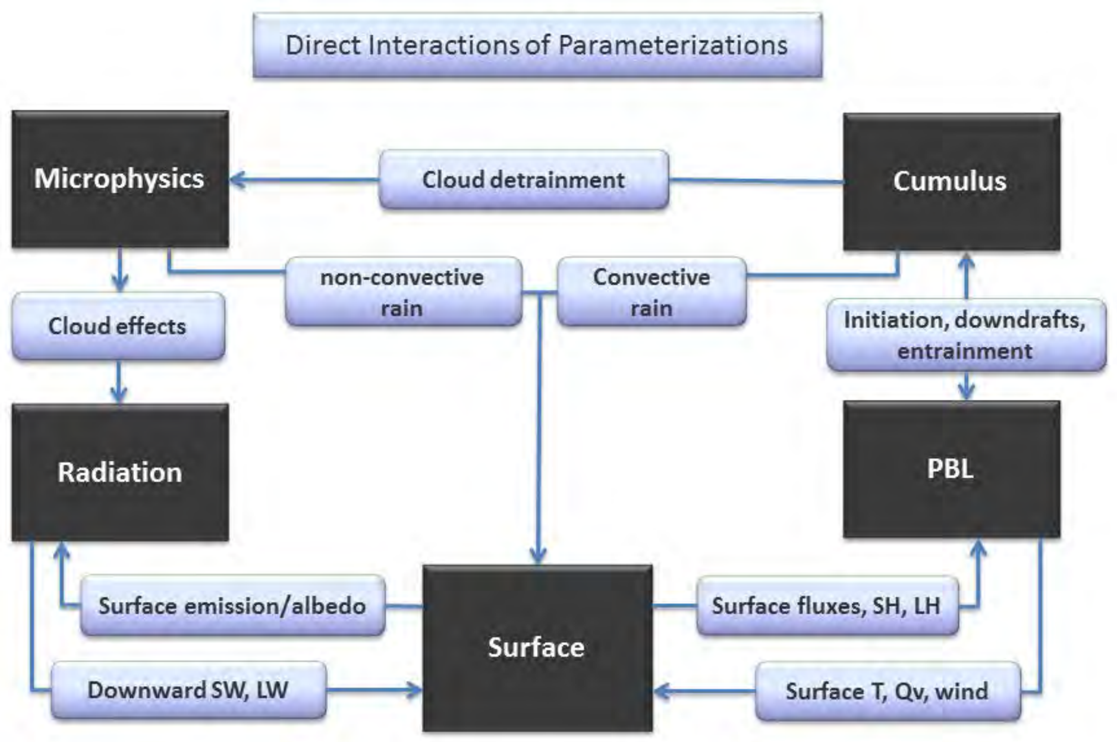

Figure 2-3: Parameterisation schemes and their interactions in WRFr)

Planetary boundary layer schemes

Planetary boundary layers (PBL) are driven by surface forcing and determine how the atmosphere develops during the course of the day (Stensrud, 2007). This is achieved by solving the mixing of different air masses due to turbulence. The choice of PBL scheme in the model will affect how stable layers are broken up and consequently the vertical temperature, vapour mixing ratio and wind speed profiles (Shin and Hong 2011). These variables are all crucial in modelling cloud processes, whether it is grid scale saturation related to vapour and temperature or convective processes related to wind speed.

There are many PBL schemes available in WRF and several comparative studies have been published. A selection of schemes will be described below including a discussion on how well the scheme performs.

<u>Yonsei State University (YSU)</u>

The Yonsei State University (YSU) PBL solves turbulence using a nonlocal closure approach (Hong et al., 2006). A nonlocal closure approach allows for vertical mixing to occur via large eddies and small eddies (Stull, 2000). The scheme allows for explicit entrainment at the top of the PBL associated with large eddy circulation from the surface (Hong et al., 2006, Skamarock et al., 2008). This scheme is the best performing scheme and is the most widely used. It includes many improvements compared to previous schemes but still has some draw backs, as will be discussed.

<u>Advantages/Improvements</u>

Shin and Hong (2011) compared surface and PBL variables from 5 different PBL schemes against observed data from a field campaign. The five schemes compared were the YSU PBL, Asymmetric Convective Model version 2 (ACM2), Mellor-Yamada-Janji (MYJ), quasi-normal scale elimination (QNSE), and Bougeault-Lacarrére (BouLac) PBL. The following surface variables were verified: surface temperature, 2 m temperature, sensible heat flux, latent heat flux, surface frictional velocity and 10 m wind speed.

The YSU PBL out-performed the other schemes for all surface variables except surface temperature, which it performed worst in. However, the over prediction in surface temperature does not cause adverse effects on PBL development as it is compensated by more realistic sensible and latent heat fluxes and, therefore, more realistic 2 m temperatures. Despite representing observed data more closely than the other schemes, the YSU PBL does over predict for all variables.

PBL profiles were verified against observed potential temperature, vapour mixing ratio, wind speed and wind direction. The YSU PBL performed well for all variables during the day when the atmosphere was unstable. However, during stable conditions at night, the YSU PBL scheme under predicts the vapour mixing ratio.

Disadvantages/inadequacies

The current issue with the YSU scheme is this: There is a systematic bias in over predicting surface winds (10 m a.g.l) under stable/night time conditions (Cheng and Steenburgh, 2005, Hong, 2010, Mass, 2012, Jimenez and Dudhia, 2011). This over prediction is in the order of 1 to 5 ms^{-1} and can adversely affect cloud formation by creating more turbulence that artificially breaks down stable layers. Furthermore, excess surface wind speeds can cause stronger convection over mountains and thus over estimate cloud formation. However, this trait is not unique to YSU PBL, as it has been shown to occur for other WRF PBL schemes (Shin and Hong, 2009, Kwum et al., 2009, Borge et al., 2008, Mohan and Bhati, 2011) and for other meso-scale models (Svennson and Holstag, 2006). In these studies, the YSU PBL scheme has been shown to out-perform other PBL physics options in WRF.

Mellanor-Yamada-Janjic (myj)

The MYJ PBL scheme is a local, total kinetic energy (TKE) closure scheme which means it essentially solves turbulence for small eddies only (Skamarock, 2008, Stull, 2000). This scheme was the first PBL implemented in WRF and, as discussed under the YSU PBL scheme, has more or less been replaced by the YSU scheme. However, the TKE schemes have been shown to perform more favourably than YSU under stable conditions only, but overall produce less favourable results when forecasting (Shin and Hong, 2009).

Large Eddy Simulation (LES)

Initially we considered running Large-eddy simulations as part of this study. However, the functionality of the LES in WRF is very much still a research development tool and is less tested than the microphysics and convection schemes. As such, we feel that it will not add to the science and later application of this work and so no LES simulations will be run.

Microphysics Schemes

Microphysics schemes solve precipitation processes when grid scale saturation occurs. These schemes explicitly solve processes related to water vapour, clouds and precipitation (Skamarock et al., 2008). These processes are well resolved at fine model resolution (<10 km) as grid scale saturation is more likely to occur. Updrafts are generally well represented at these scales promoting lifting and cooling. At even finer resolutions (<1 km) the microphysics scheme can be used without convective parameterisation to solve cloud processes because the microphysics solution is explicit (Stensrud, 2007). At coarse grid resolutions (~50 km) some of the processes like mixed phase (water and ice) are not well resolved by the microphysics and convective schemes are required to solve for sub grid scale processes.

Bulk microphysics schemes

Microphysics schemes operate by calculating the conversion between a maximum of six different classes of water in the cloud. These classes are water vapour, cloud water, rain, cloud ice, snow and graupel (Skamarock *et al.,* 2008, Stensrud, 2007). These classes, except for water vapour, are sometimes referred to as hydrometeors. The number concentration of each particle is required before calculating conversion between particles. There are two options when calculating number concentration of each particle class, namely “bin” or “bulk” distribution. Bin distributions empirically solve the number concentration for each size class of particle in the cloud. This is computationally expensive and is generally not applied in operational meso-scale modelling. The bulk approach assumes a size distribution based on empirical values. This can be in the form of an inverse exponential function as described by Marshal and Palmer (1948) or as a gamma distribution where greater diversity is included for smaller particles (Stensrud, 2007). For the most part, bulk distributions are applied in the meso-scale models using an inverse exponential function described as follows:

$$n(D) = n_0 e^{-\lambda D}$$

Where:

D = particle diameter (m)

n = number of particle per unit volume (m^{-4})

λ = slope parameter (fall off of particles as diameter increases)

n_0 = intercept parameter

Thus, bulk microphysics schemes assume the size distribution and then estimate particle mixing ratio and particle concentration (Thompson *et al.,* 2004). Schemes generally predict the particle mixing ratio (single-moment scheme) while some also predict the total particle concentration (double-moment scheme). As model rain clouds develop or grow the size distribution shifts towards larger cloud particles due to the conversion to rain drops from the previous model time step.

Below follows a short description of key microphysics schemes available in the WRF and a few case studies testing the performance of the different schemes.

WRF microphysics schemes

Reviews that verified microphysics schemes point to a general theme that WRF over predicts rainfall amounts, and often initiates early rainfall by one or two hours (Weisman *et al.,* 2008, Gallus and Pfeifer, 2008, Rajeevan *et al.,* 2010, Gallus and Breish, 2002). Each scheme is discussed here separately.

Lin

The Lin microphysics scheme is a sophisticated 6 class scheme that includes water vapour, cloud water, rain, cloud ice, snow and graupel (Skamarock *et al.,* 2008). Five WRF microphysics schemes (including Lin, Two versions of Thompson, WSM6 and WSM5) were assessed for a rainfall event of a squall line in Germany (Gallus and Pfeifer, 2008). Lin was found to perform worst for placement of rain events compared to the other schemes. It also over predicted the rainfall amounts to a greater degree than other schemes due to the production of excess rain clouds.

The Lin scheme predates the WRF model and is a sophisticated microphysics scheme. However, many improvements have been made on modelling microphysics and the Lin scheme is being used less frequently as a result.

Thompson

The Thompson microphysics scheme is a single moment bulk parameterisation scheme that uses 6-classes (Skamarock *et al.,* 2008, Thompson *et al.,* 2004). Generally, gamma size distributions (refer to section “Bulk microphysics schemes”) are used to assume particle size, except for snow particles where a combination of inverse exponential and gamma distribution is used.

Case study results vary for the Thompson scheme. In the study of the squall line in Germany, the Thompson scheme overestimated rainfall and produced rain in the wrong place (Gallus and Pfeifer, 2008). Weisman *et al.* (2008) also showed that Thompson microphysics overestimated rainfall, although to a lesser degree than the WSM6 scheme which is discussed later. The placement may be a timing issue as other studies have shown early rainfall events (Rajeevan *et al.,* 2010). This latter study was of a severe thunderstorm over India and showed that the Thompson scheme performed best in forecasting accumulated rainfall amounts compared to the Lin, WSM6 and Morrison schemes.

Morrison

The Morrison microphysics scheme is a sophisticated double moment, 6-class, bulk scheme. The double moment calculates particle mixing ratio and total particle number concentration which allows for rigorous particle size distributions by using gamma distributions with an adjusted y-intercept and gradient based on the mixing ratio and number concentration (Morrison, *et al.,* 2008, Skamarock *et al.,* 2008). The six classes of water are: vapour, cloud droplets, cloud ice, rain, snow, and graupel/hail.

In a comparative study of microphysics schemes over the Californian coast the Morrison, along with WSM6, scheme were shown to best represent cloud cover (Jankov *et al.,* 2010). Unfortunately, rainfall was not verified in this study as only cloud cover and brightness temperature of the cloud was verified. In a separate study over Ontario, Canada, several microphysics schemes were tested, including the WSM6 and Thompson scheme, and compared to observed and satellite data (Molthan, 2011). The Morrison scheme was shown to best represent accumulated and hourly rainfall for a rainfall event that lasted 6 hours. Furthermore, the Morrison, along with the Thompson scheme, best represented observed relative humidity vertical profiles from aircraft data.

ETA (Ferrier)

The Eta model scheme is less complex than the 6-class schemes as it groups separate classes of some hydrometeors into one class. As a result, some complexity is lost but the scheme is computationally more efficient. This scheme is only really applicable to warm cloud processes and so may not be applicable to this study.

The Eta model scheme essentially has four classes of hydrometeors (Rogers, *et al.,* 2001):

• Suspended cloud liquid water droplets

• Rain

• Large ice (includes snow, graupel, sleet, etc.)

• Small ice (generally suspended cloud ice, evaporates quickly in air subsaturated with respect to ice)

There are some limitations as a result of this grouping, for example, large ice includes snow and graupel and both precipitate out at the same time. The trade-off of this approach is that the scheme is computationally less intensive. Another feature and limitation is that advection accounts for total condensate of all classes, instead of for each hydrometeor type separately. However, this only applies to advection and makes the scheme computationally more efficient. For non-advection, i.e. when the hydrometeors remain in a grid cell, the classes are distinguishable. Thus, this limitation is highlighted in high resolution runs where transport between grid cells occurs more frequently. The scheme does not take into account the effect of varying cloud condensation nuclei and associated concentration and size distribution of cloud droplets.

A verification study of warm season rainfall using the Ferrier microphysics scheme showed that the scheme over predicts rainfall. This study was at high resolution (8 km) and covered 15 rainfall events in the rainfall season. The Ferrier scheme appears to model heavy rainfall events on an hourly timescale (Efstathiou *et al.,* 2012 and Pytharoulis *et al.,* 2010).

WSM 3 and 6 (WRF Single-moment 6-class)

There is a family of WRF single moment microphysics schemes that vary in the number of classes used to solve cloud processes. The schemes with fewer classes, like WRF single moment 3-class (WSM3), can be used when running domains with coarse resolution (>12 km). As model resolution becomes finer the model moves towards solving cloud processes explicitly, in which case a 6-class scheme is required. The 6-class scheme is suitable for cloud resolving scales but perhaps not required for coarser levels as WSM3 or 5 perform equally well.

In the study of the squall line in Germany (Gallus and Pfeifer, 2008) the WSM6 scheme performed well showing the least spatial displacement of the rainfall event as well as showing the most realistic rainfall reflectivity. However, WSM6 did over predicted rainfall, as did all the microphysics schemes. Similar results were found for the WSM6 scheme at high resolution (4 km) by Weisman *et al.* (2008).

Cumulus convection schemes

Cumulus convection schemes solve cloud formation that occurs on a sub-grid scale process, as opposed to microphysics schemes which solve grid scale processes. Cumulus schemes keep track of the vertical transfer of heat and moisture that result in cloud formation before grid scale saturation occurs (Stensrud, 2007). Variables from the planetary boundary layer need to be verified before choosing an appropriate cumulus scheme, as wind speeds, temperature and vertical velocity will effect cumulus performance.

Limitations of Cumulus schemes

A simplified conceptual model of processes that are simulated in cumulus parameterisation is show in Figure 2-4. At coarse model resolution (> 10 km) the cumulus scheme is trying to represent updrafts, down drafts, entrainment and detrainment of several cumulus clouds that may be present in the single model grid cell. A limitation of this by example of the downdraft is as follows. As the downdraft of each cloud is represented by a sub grid scale eddy, and in reality a single model grid may contain cumulus clouds of different types or stages, the model can only represent a single fractional area downdraft to represent all could types (Grell, 2012).

Nevertheless, although the parameterisation may not fully resolve the physical process, it achieves its task by simulating downdrafts and producing rain.

At higher model resolution (<10 km), the updraft in one model cell may have a reciprocal downdraft in a different grid cell. Cumulus schemes generally assume that the feedback is within the same grid cell (Grell, 2012). As such, there is much debate on whether cumulus schemes should be used at certain model resolutions, sometime referred to as gray scales. These scales are suggested to be between 5 and 15 km by Stensrud (2007). However, the uses of cumulus schemes at these resolutions still produce improved forecasts compared to no cumulus forecasts, and as such are being used at these scales (Hong and Dudhia, 2012). Once the model resolution is much finer, i.e. cloud resolving, which is normally less than 1 km, the cumulus scheme is no longer needed as all cloud processes can be solved explicitly by the microphysics scheme.

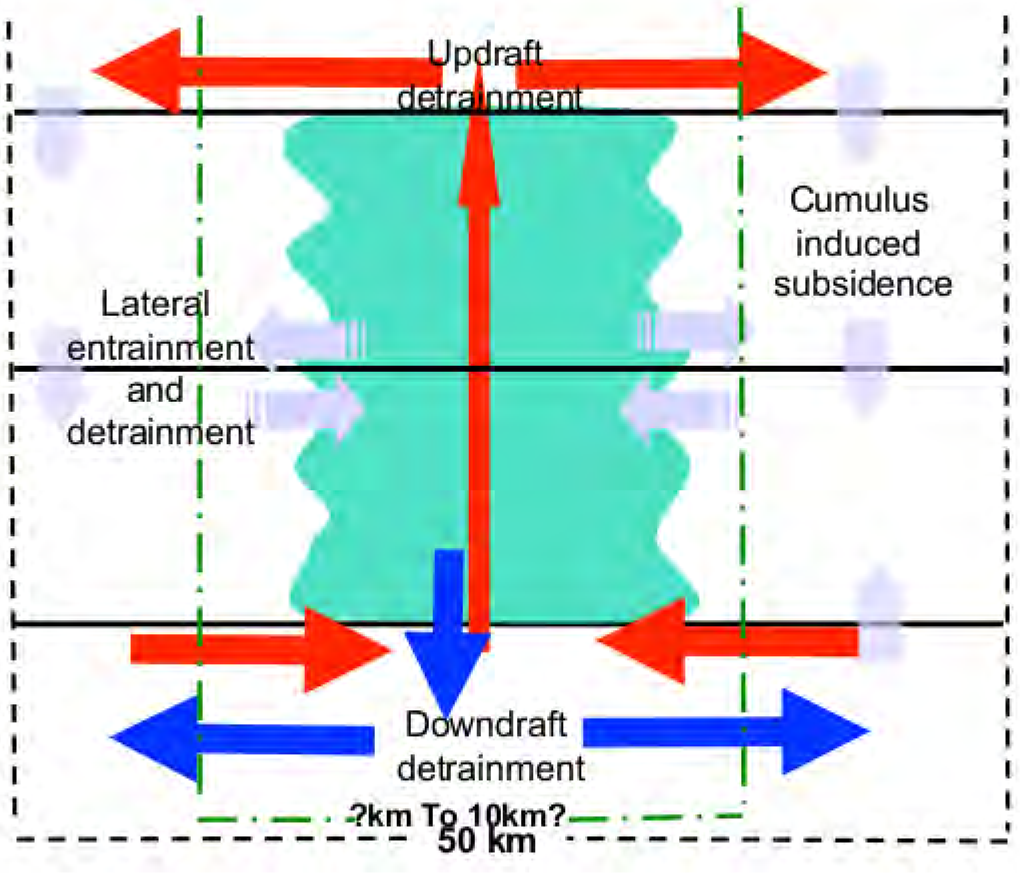

Figure 2-4: Simplified conceptual picture of statistically averaged cloud convection (Grell, 2012).

A further limitation is the link between convective and microphysics schemes. Subsidence by the convective scheme can cause artificial heating and drying which may prevent the microphysics schemes from triggering. Nevertheless, cumulus schemes have been shown to be advantageous. Forecasts that exclude cumulus schemes have been shown to prolong rainfall development and overestimate rainfall once it has developed. Thus, although the assumptions of the cumulus schemes may be violated at these “gray” scales, the cumulus schemes are still improving model results.

WRF CUMULUS schemes

Betts-Miller-Janjic (BMJ)

This scheme aims to solve deep convection first before switching to solving for shallow convection (Stensrud, 2007). Deep convection allows for vertical transport of moisture and heat through most of the troposphere while shallow convection only occurs in the lower parts of the troposphere. This scheme uses a moisture line based on empirical studies of tropical convection. Saturation points between condensation level and cloud top are used to plot a moisture line which is essentially a vertical profile of moisture availability. Moisture lines are empirically smooth lines and the saturation point approach is efficient because it only requires two variables to calculate the saturation point.

To solve deep convection it is first established whether the convective available potential energy (CAPE) is greater than zero. CAPE is basically the maximum amount of energy available to an ascending parcel of air. Once CAPE is established to be greater than zero, the cloud base and cloud top from the most unstable parcel in the lowest 200 mb is calculated. This allows for the reference moisture line to be calculated by solving the saturation points between cloud base and cloud top. Once the reference moisture line is determined, the temperature and mixing ratio profiles can be determined using "saturation pressure departure". This reference profile is then adjusted for each time step until enthalpy is conserved. Once enthalpy is conserved precipitation is judged to occur and the precipitation rate is calculated.

If precipitation is triggered then the BMJ scheme activates and vertical profiles move towards the reference profile over a period of 1 hour. If no rainfall occurs then the scheme does not activate. If the scheme activates then the shallow convection warms and dries the lower half of cloud and cools and moistens upper half of cloud, unlike the Kain-Fritsh scheme, which cools the bottom half of the cloud and causes warming and drying in the troposphere.

Kain-Fritsh (KF)

The Kain-Fritsh (KF) convection scheme is a low-level control scheme. The scheme aims to remove convective inhibition (CIN) through forced convection (as opposed to free convection) before accessing the convective available potential energy (CAPE) (Kain-Fritsch 1990, Gallus 1999, Stensrud 2007). The Kain-Fritsh scheme is a mass flux scheme that includes the updraft mass flux and an equivalent downdraft mass flux which accounts for evaporation. The downdraft component makes this scheme unique as other mass flux schemes only represent the updraft component.

Although this is a low-level control scheme it does produce deep convection as it aims to use the CAPE. However, there is also a shallow convection mechanism that is activated when all deep convection triggers are met, except for minimum cloud depth. Minimum cloud depth for deep convection is typically between 2000-4000 m (Kain-Fritsch 1990, Stensrud 2007).

This cumulus scheme links with the microphysics scheme as it supplies moisture through evaporation in the downdraft component. This is a physical based approach and produces cold outflow at the bottom of the cloud, while warming and drying the top half of the cloud. The link with the microphysics scheme also helps produce realistic stratiform cloud formation in the lee of a convective line (Kain-Fritsch 1990, Stensrud 2007). Due to the physical based approach and the link with the microphysics, this scheme often produces realistic rainfall totals. However, the rainfall is not always spatially accurate, as that depends on accurate triggering due to local features like upper air divergence related to a front or orographic uplift which can be affected by grid scale. Some of these issues can be overcome by decreasing the grid size, as the scheme responds to the advective time step in the model. However, as discussed in section “Bulk microphysics schemes”, this is only useful to a point before the cumulus scheme becomes redundant and cloud microphysics can be solved empirically.

Grell-Devenyi (GD)/Grell 3d (G3d)

The Grell-Devenyi (GD) cumulus scheme is an ensemble scheme where several cumulus schemes are run and an ensemble average is returned. The Grell-3 scheme is similar to the GD scheme with the exception that it can be used at grid resolutions less than 10 km. Subsidence, as depicted in Figure 2-4, is not restricted to a single grid column but is allowed to occur in adjacent grid columns.

Tiedtke

The Tiedtke cumulus scheme is a mass flux scheme, meaning it simulates updrafts and downdrafts as well as compensating subsidence outside of the convective cell. It is triggered by large scale convergence of moisture and closes through removal of convective available potential energy (Stensrud, 2007, Zhang *et al.,* 2011).

Land-Surface schemes

Land-surface schemes, or the land-surface model (LSM), control the transfer of radiation and moisture to the surface layer of the atmosphere. Essentially, these fluxes provide a lower boundary condition for vertical transport in the PBL (Skamarock *et al.,* 2008). There are two major schemes that will be considered here: The Noah LSM and Rapid Update Cycle (RUC) LSM. Typically, land-surface models divide the surface soil into different layers for which temperature and moisture transfer is calculated and then transferred to the atmosphere. The degree of sophistication of these layers differs between schemes, as will be discussed here.

<u>Noah and Rapid Update Cycle Land Surface Model</u>

The Noah LSM calculates temperature and moisture for 4-levels of soil up to 1 m deep. The model allows for time varying vegetation cover, soil variables and fractional snow cover.

The RUC LSM uses 6-layers of soil up to 3 m deep. Like the Noah LSM, time varying vegetation and soil is accommodated. Extra to the Noah LSM is a multi-layer snow scheme.

Some problems identified with surface-models is that they require a spin up time that can be substantially longer than spin up times typically associated with atmospheric models. The problem is when moisture forcing that is fed into the LSM is too wet and, consequently, causes the atmosphere to become too wet and too warm. The solution is to let the LSM spin up to allow time for the reserve moisture in the deeper soil layers to be removed from the LSM into the atmosphere (Romine *et al.,* 2012). A study that compares Noah and RUC LSM showed that surface temperature at 2 m is most sensitive to the type LSM used rather than the type of PBL (Mooney e*t al.*, 2012).

WRF Summary

There are often trade-offs when selecting a parameterisation scheme. For example, some microphysics schemes are superior when simulating heavy rain fall events while others will simulate the timing of a non-heavy event more realistically. Nevertheless, the discussion presented above is a starting point for testing schemes that will perform well under South African conditions.

3 PYTOPKAPI LITERATURE REVIEW

TOPKAPI is an acronym which stands for **TO**Pographic **K**inematic **AP**proximation and **I**ntegration, and is a physically-based distributed rainfall-runoff model originally proposed by Liu and Todini (2002), following a critical analysis of the ARNO (Todini, 1996) and the TOPMODEL (Beven and Kirby, 1979; Beven *et al.,* 1984) hydrological rainfall-runoff models. The ARNO and the TOPMODEL are both variable contributing area models with ARNO being a semi-distributed conceptual model controlled by the total soil moisture storage, and widely used for real-time flood forecasting. The critical analysis of ARNO revealed that the lack of physical grounds for establishing some of ARNO's parameter values reduces on its possible extension to ungauged catchments. The TOPMODEL on the other hand is formulated in a manner that allows for runoff formation to be determined predominantly by factors represented by the topography, the transmissivity of the soil and its vertical delay. It was revealed, from the analysis, however, that the model preserves its physical meaning only at the hill slope scale (Franchini *et al.,* 1996), degrading into a conceptual model at larger scales, and thus suffers the same drawback as ARNO at larger scales with respect to extension to ungauged catchments.

Unlike these two models, TOPKAPI's parameters preserve their physical basis even at larger scales owing to its basis on the lumping of a kinematic wave assumption in the soil, on the surface and in the drainage network. In the formulation, the rainfall-runoff and runoff routing processes are transformed into three nonlinear reservoir differential equations which can be solved analytically (Liu and Todini, 2002) with the consequence that TOPKAPI model parameter values are scale independent and obtainable from a digital elevation map (describing the topography of the catchment), soil map and vegetation or land-use map in terms of slope, soil permeability, roughness and topology.

3.1 TOPKAPI Model Description

TOPKAPI consists of 5 main modules comprising soil, overland, channel, evapotranspiration and snow modules (Figure 3-1). The first 3 modules take the form of non-linear reservoirs controlling the horizontal flows. Its implementation is mainly based on elevation data (provided by a Digital Elevation Model) and also requires information about catchment surface properties and land use.

TOPKAPI considers the catchment as a tree-like network of cells with water flowing from one to another in a down slope direction, as shown on Figure 3-2. Since it is assumed the water always flow in the direction of the arrow, downstream effects such as backwater or due to ponding are not modelled (Bruen and Parmentier, 2005).

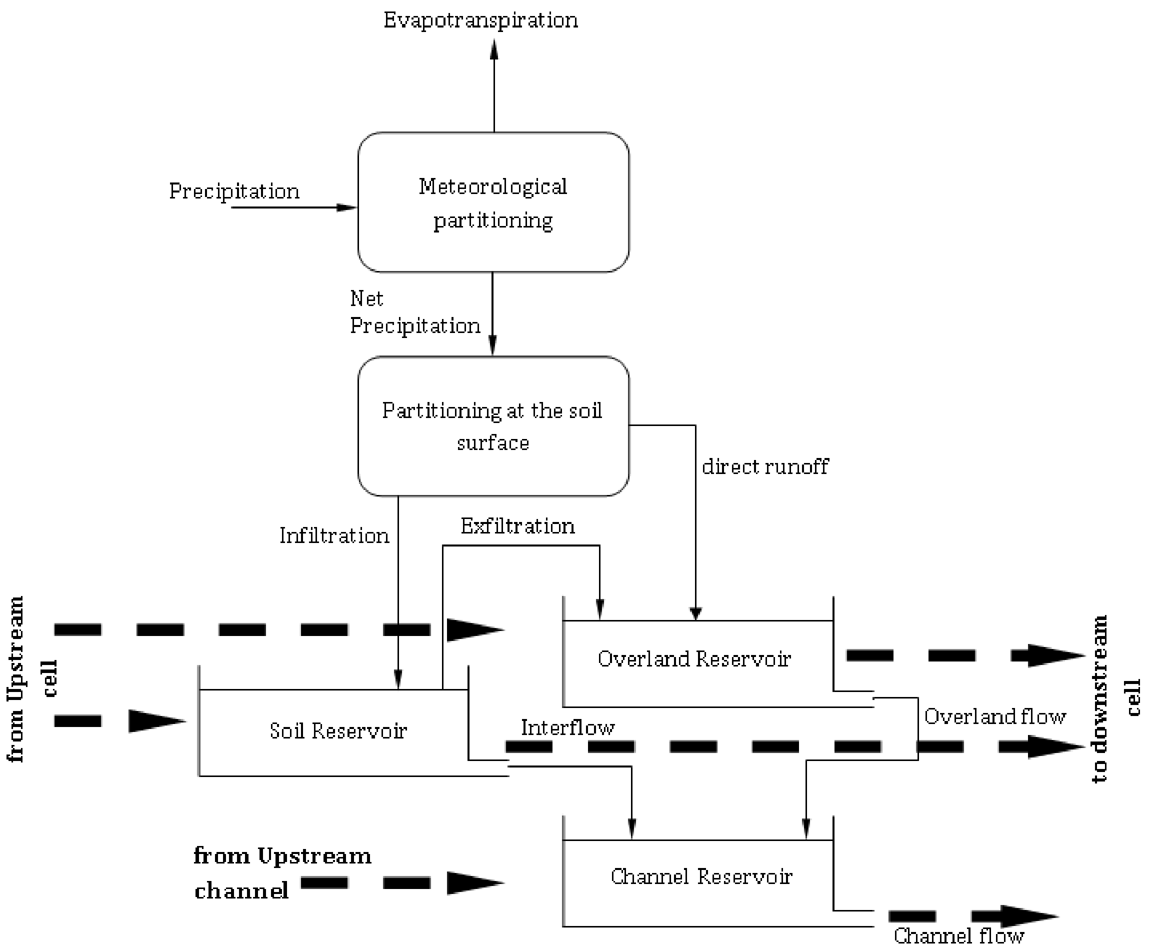

Figure 3-1: Unit of distributed TOPKAPI model, one for each grid cell (Bruen and Parmentier, 2005).

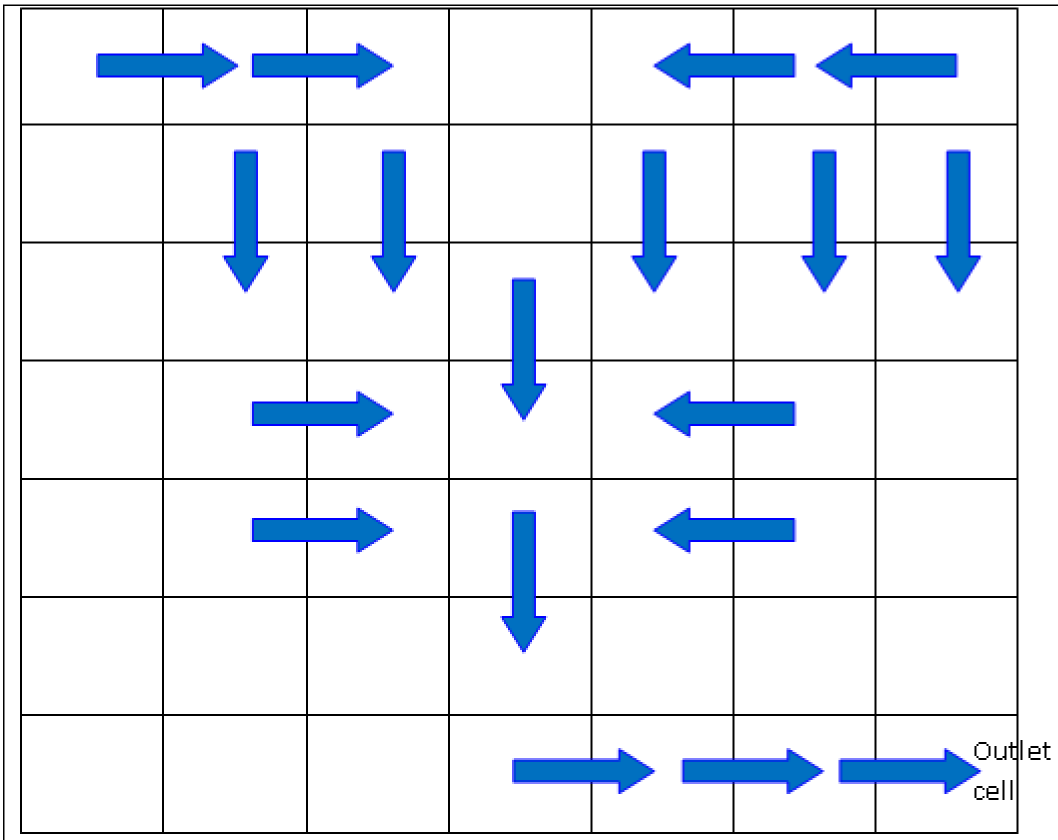

Figure 3-2: DEM-based tree showing water flow direction (Source: Bruen and Parmentier, 2005).

3.2 Model Assumptions

The TOPKAPI model is based on 6 fundamental assumptions (Liu and Todini, 2002):

- Precipitation is constant in space and time over the integration domain (namely the single grid cell or pixel and the basic time interval, usually a few hours). This assumption simply means that the model is lumped at the grid scale.
- All precipitation falling on the soil infiltrates, unless the soil is already saturated (Dunne, 1978)
- The slope of the groundwater table coincides with the slope of the ground
- Local transmissivity, like horizontal subsurface flow in a cell, depends on the integral of the total water content of the soil in the vertical plane
- In the soil surface layer, the saturated hydraulic conductivity is constant with depth and, due to macro-porosity, is much larger than in deeper layers
- During the transition phase, the variation of water content in time is constant in space.

3.3 TOPKAPI Model Equations

The equations controlling the level of the three main reservoirs that comprise a cell (soil, overland and channel reservoirs) are obtained by combining the physically-based continuity and mass equations under the approximation of the kinematic wave model. The kinematic wave assumption is based on the simplification of the Saint-Venant Equation describing one-dimensional unsteady open channel flow (Pegram et al., 2007). For this simplification it is assumed that the effects of local acceleration, convective acceleration and pressure acting on a control volume are negligible when compared to the effects of gravity and friction. The well-known point-scale differential equations obtained are then analytically integrated in space to the finite dimension of a grid cell, which is taken to be the pixel of the digital elevation model (DEM) that describes the topography of the catchment.

An overview of the relationship between the equations (adapted from Vischel *et al.* (2008)) is provided below.

The equation of mass continuity of each of the three reservoirs that compose a cell *i* can be written as a classical differential equation of continuity

$$\boldsymbol{\frac{dV_i}{dt} = Q_i^{in} - Q_i^{out}} \tag{1}$$

where:

all the variables are observed at time t

V_i is the total volume stored in the reservoir

$\frac{dV_i}{dt}$ is the rate of change of water storage

Q_i^{in} is the total inflow rate to the reservoir

Q_i^{out} is the total outflow rate from the reservoir

On resolving the continuity and the mass balance using the kinematic wave approach, it can be shown that there is a nonlinear relationship Q_i^{out} between and V_i . This allows (1 to be transformed into an ordinary differential equation (ODE) of the form:

$$\boldsymbol{\frac{dV_i}{dt} = Q_i^{in} - b_i V_i^{\alpha}} \tag{2}$$

where:

Q_i^{in} is a combination of the input variables dependent on whether the reservoir in question is the soil, overland or channel reservoir (Figure 3-1), and may consist of interconnecting flows between the elemental storage reservoirs within the cell and from upstream connected cells, including rainfall and evapotranspiration.

b_i is constant in time and is a function of the geometrical and physical characteristics of the reservoir. It may vary spatially.

α is a constant in both space and time and together with b_i are dependent on each type of reservoir. This is discussed below.

Soil Reservoir

For the soil reservoir, the coefficient b_i is expressed as:

$$\boldsymbol{b_i = \frac{C_{s_i} X}{X^{2\alpha_s}} \; with \; C_{s_i} = \frac{L_i K_{s_i} \tan(\beta_i)}{\left(\theta_{s_i} - \theta_{r_i}\right)^{\alpha_s} L_i^{\alpha_s}}} \qquad (3)$$

where:

X is the lateral dimension of the grid-cell

L_i is the soil depth

K_{s_i} is the saturated hydraulic conductivity

$\tan(\beta_i)$ is the tangent of the ground slope angle β_i

θ_s is the saturated soil moisture content

θ_r is the residual soil moisture content

α_s is a dimensionless pore-size distribution parameter that usually takes on values between 2 and 4 (Vischel *et al.,* 2008).

Overland Reservoir

For the overland flow reservoir b_i is expressed as

$$\boldsymbol{b_i = \frac{C_{o_i} X}{X^{2\alpha_o}} \; \text{with} \; C_{o_i} = \frac{1}{n_{o_i}} \sqrt{\tan(\beta_i)}} \qquad (4)$$

where:

$\boldsymbol{n_{o_i}}$ is Manning's roughness coefficient for overland flow

$\tan(\beta_i)$ is the tangent of the ground slope angle β_i

α_o is the dimensionless power coefficient equal to 5/3 originating from Manning's equation

Channel Reservoir

$$\boldsymbol{b_i} = \frac{\boldsymbol{C_{c_i} W_i}}{(\boldsymbol{X_c W_i})^{\alpha_c}} \; \boldsymbol{with} \; \boldsymbol{C_{c_i}} = \frac{\mathbf{1}}{\boldsymbol{n_{c_i}}} \sqrt{\mathbf{tan}(\boldsymbol{\beta_{ci}})} \qquad (5)$$

where:

$\boldsymbol{X_c}$ is the channel length ($\boldsymbol{X_c}$ =X or $\boldsymbol{X_c}$ = $\sqrt{2}$X)

$\boldsymbol{W_i}$ is the width of the channel

$\boldsymbol{n_{c_i}}$ is Manning's roughness coefficient for channel flow

$\mathbf{tan}(\boldsymbol{\beta_{ci}})$ is the tangent of the channel slope ($\boldsymbol{\beta_{ci}}$)

$\boldsymbol{\alpha_c}$ is the dimensionless power coefficient equal to 5/3 again originating from Manning's equation.

Evapotranspiration

The literature reviewed (e.g. Vischel et al., 2008) suggests that evapotranspiration can be introduced directly as an input to the model or computed externally or estimated internally by a radiation method (Doorembos *et al.,* 1984) starting from the temperature and from other topographic, geographic and climatic information.

Ciarapica and Todini (2002) for their application of TOPKAPI, adopt the same method used to calculate evapotranspiration in the ARNO model (Todini, 1996). In this approach, the effects of the vapour pressure and wind speed, that are otherwise fully accounted for by the rigorous Penman-Monteith equation, are explicitly ignored and evapotranspiration is calculated starting from a simplified equation known as the radiation method (Doorembos et al., 1984).

$$ET_r = C_v W_{ta} R_s = C_v W_{ta} \left(0.25 + 0.5\frac{n}{N}\right) R_a \qquad (6)$$

where:

ET_r is the reference evapotranspiration, i.e. evapotranspiration in soil saturation conditions caused by a reference crop

$\mathrm{C_v}$ is an adjustment factor obtainable from tables as a function of the mean wind speed

$\boldsymbol{W_{ta}}$ is a compensation factor that depends on the temperature and altitude;

$\boldsymbol{R_s}$ is the short-wave radiation measured or expressed as a function of $\boldsymbol{R_a}$ in equivalent evaporation;

$\boldsymbol{R_a}$ is the extraterrestrial radiation expressed in equivalent evaporation;

$\boldsymbol{n/N}$ is the ratio of actual hours of sunshine to maximum hours of sunshine.

Observing that R_s requires both Ra and *n/N* to be known, an empirical equation relating the reference potential evapotranspiration ET_r to the compensation factor $\boldsymbol{W_{ta}}$, temperature of the month ***T*** and the maximum number of hours of sunshine *N,* was developed for use in the absence of the measured short-wave radiation values R_s or of the actual number of sunshine hours otherwise needed to calculate R_s.

$$ET_r = \alpha + \beta N W_{ta} T_m \tag{7}$$

where:

ET_r is the reference evapotranspiration for a specified time step $\triangle t$

α and β are regression coefficients to be estimated for each sub-basin;

$\boldsymbol{T_m}$ is the area mean air temperature averaged over $\triangle t$;

$\boldsymbol{W_{ta}}$ for a given sub-basin can be either obtained from tables or approximated by a fitted parabola:

$$\boldsymbol{W_{ta}} = A\bar{T}^2 + B\bar{T} + C \text{ where } \begin{matrix} A, B \text{ and } C \text{ are coefficients to be estimated;} \\ \bar{T} \text{ is the long term mean monthly sub} - \text{basin temperature} \end{matrix}$$

N is the monthly mean of the maximum number of daily hours of sunshine (tabulated as a function of latitude).

The developed relationship is linear in temperature (and hence additive), and permits the disaggregation of the monthly results on a daily or even on an hourly basis, whereas most other empirical equations are ill-suited for time intervals shorter than 1 month (Todini, 1996).

For the pyTopkapi implementation, however, the evapotranspiration module has been slightly modified, making it more elaborate. In the channel, the evaporation is extracted at the rate of the potential evaporation from a free water surface. On each cell *i*, the actual evapotranspiration Et_a is computed as a proportion of the reference crop evapotranspiration Et_r using, as a first approximation, a constant crop factor k_c and the current saturation of the reservoir computed at each time-step *t* as the ratio between the effective and maximum soil water content (respectively $V_s(t)$ and V_{smax}), as shown in (8

$$ET_{ai} = k_{c_i} \frac{V_{s_i}(t)}{V_{s\,\max i}}\ ET_{ri} \qquad (8)$$

For each cell, at each simulation time-step *t*, the inflow rate is computed, assumed to be a constant over the interval Δt, then the ODE equation is solved by numerical integration. At $t+\Delta t$, the evapotranspiration losses are then either extracted from the channel as well as from the overland flows if the cell is saturated or from the soil store alone if the demand is not satisfied by the overland storage.

3.4 Derivation of TOPKAPI model parameter values from catchment information

Implementing the model to simulate flow in a catchment requires data sets that can be obtained from field measurements or remotely sensed observations. From the elevation data, the geomorphological features of the catchment that assist in determining the grid cell size, the cells composing the stream network and how the cells are connected, are extracted. This is followed by the determination of adequate model parameter values in order to obtain realistic modelling of the catchment hydrology through a process of establishing links between the data describing the elevation, soil and surface characteristics of the catchment and the physical parameters displayed in the TOPKAPI model equations.

From catchment DEM to cell connection

The automation of the TOPKAPI model, as is the case of its implementation using pyTopkapi, requires the definition of a numerical grid dividing the catchment space into squared cells (see Figure 3-2) that must be connected in order to model the transfer of flow (surface and subsurface) within the catchment. For this, a Digital Elevation Model (DEM) is used as the base map to:

- Define the grid and thus the spatial resolution of the model
- Delineate the stream network.

These two steps can be achieved by using GIS software and the reader is referred to ***WRC Report No: 1429/1/06*** for a thorough discussion on how this is done.

In practice, the occurrence of sinks is a common problem associated with the use of DEMs. A sink is a cell or area that is surrounded on all sides by higher elevation values (Vischel et al 2008) and thus prevents the down-slope routing of water. Unless it is in fact a depression such as a lake or swamp, the occurrence of a sink is an error. These errors often arise due to the sampling techniques used in processing a DEM or due to the rounding off of elevation values to integers (Mark, 1988).

From catchment data to physical model parameters

TOPKAPI model parameters can be estimated *a priori* from the elevation data, soil and surface properties.

A total of 15 parameters have to be assigned in the TOPKAPI model. Among them, 11 are cell specific, meaning that they are potentially spatially variable (depending on the detail of the information available), and they mainly refer to physical characteristics ($\tan(\beta)$, $\tan(\beta_c)$, L, K_s, θ_r, θ_s, n_o, n_c, α_s, k_c, W. The 4 others are constant and refer to geometrical characteristics of the channel or grid cell (X, $A_{threshold}$, the minimum width of channel W_{min}, the maximum width of channel W_{max}).

3.5 Application of TOPKAPI

While TOPKAPI model is considered a physically based model, with all its parameters having physical meaning and which can be measured directly through fieldwork, it, like every physically-distributed model, is subject to several uncertainties associated with the data (Vischel eta al 2008) on:

- The information on topography, soil characteristics and land cover,
- The approximate methods and tables used to infer physical parameters from the data
- The approximations introduced by the scale of the parameter representations.

For these reasons, implementing a calibration scheme for the parameters is still necessary. The calibration approach implemented in PyTOPKAPI consists of calibrating a dissociated calibration of the parameter responsible for the production of the runoff, from those responsible for the routing of runoff. The most sensitive parameters controlling the runoff production are the soil depth (L) and the soil conductivity (Ks), while the Manning roughness of channel (n_c) and overland (n_o) are the main routing parameters (Vischel et al., 2007).

Essentially, the method consists of:

1. Defining range of values for the factor and initial soil moisture to be simulated.
2. Discretizing the ranges of values obtained
3. Running the model for all the combinations of values
4. Order the simulations according to the objective functions

4 WRFCHEM LITERATURE REVIEW

It is proposed that WRF/Chem is used to simulate aerosol emissions from industries and other sources over the industrial Highveld of South Africa and to quantify the effect of these aerosols on rainfall amounts.

WRF/Chem is the chemistry component of The Weather Research and Forecast (WRF) model and includes many options for representing chemical reaction pathways and conversions of trace gases and aerosols. Aerosols are of more interest when considering rainfall formation as they act as cloud condensation nuclei and excessive loading of aerosols of the appropriate size can affect rainfall processes. Major sources of aerosols over South Africa include industries, biomass burning, marine aerosols and windblown dust. Research campaigns over Southern Africa like Aerosol Recirculation and Rainfall Experiment (ARREX) and the Southern African Regional Science Initiative (SAFARI-2000) identified biomass burning and industry as major sources of cloud condensation nuclei over the Highveld region. Biomass burning and windblown dust are most prevalent during the dry season of the Highveld. However, biomass burning may affect the first rains of the season due to a build-up of aerosol concentrations in late winter. As such, biomass burning will be considered for the Highveld of South Africa, but more focus will be placed on industrial emissions as they contribute during the wet season.

5 WRF METHODOLOGY

This section includes a description of the WRF model input, model configuration and verification. An overview of the WRF modelling process is presented in Figure 5-1.

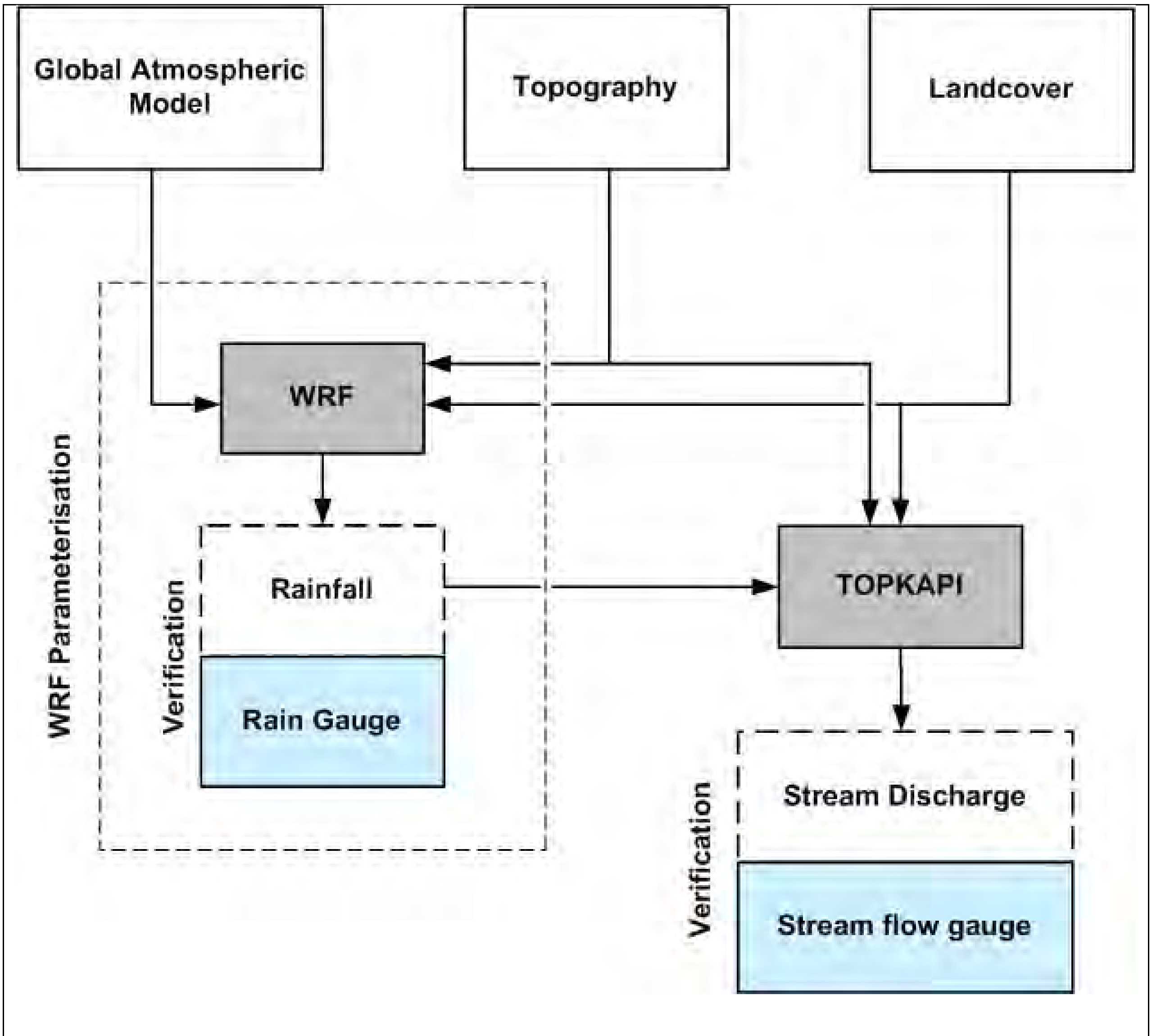

Figure 5-1: Proposed WRF verification methodology.

5.1 Synoptic Data

The WRF model will be run in “hindcast” or reanalysis mode as it is being run for events that have already occurred and data is available. This is in contrast to typical forecasting applications of WRF.

Meso-scale meteorological models typically require coarse resolution global forecast model data as input which is then downscaled dynamically by the meso-scale model. The European Centre for Medium-range Forecasting (ECMWF) provides global data at a high resolution (0.7 ˚) which will be used to initialise WRF. ECMWF ERA-interim global reanalysis data is available for the periods of the measurement campaigns. Time steps of 12 and 6 hours will be used to initialise WRF, i.e. atmospheric boundary conditions are fed from ECMWF data every 12 or 6 hours into WRF.

5.2 Study Catchments

Liebenbergsvlei

The Liebenbergsvlei catchment is located near Bethlehem in the eastern Free State of South Africa. A rain gauge network consisting of 43 gauges was established in this catchment as part of a summer rainfall campaign from 1993-2001. Rainfall was measured during the months of October to December and January to March. Data from these gauges was acquired from the South African Weather Service to verify the WRF model. The catchment is approximately 120 km long and 60 km wide with a total area of 4 625 km^2 and receives a total annual rainfall between 600 and 700 mm (Vischel *et al.,* 2008).

The high density of gauges in the catchment is ideal for model verification purposes. Additionally, much research involving the PyTopkapi model has been performed for this area and will aid in parameterising the hydrological model (Vischel *et al.,* 2008a, Vischel *et al.,* 2008b). The 2000/2001 season will be used initially for modelling.

Berg River

The Berg River catchment falls in the Western Cape winter rainfall region of South Africa, receiving most of its rainfall from passing frontal systems. Further to the frontals systems, orographic rain can form due to the complex terrain of the surrounding area. Rain fall gauge data is available for about 7 stations from the Agricultural Research Council (ARC) and the South African Weather Service. Stream flow gauge data is available for one station and is supplied by the Department of Water Affairs. The extent of the area is approximately 80 km long and 30 km wide. The season modelled will depend on data availability from the various stations where the year of most data overlap will be used.

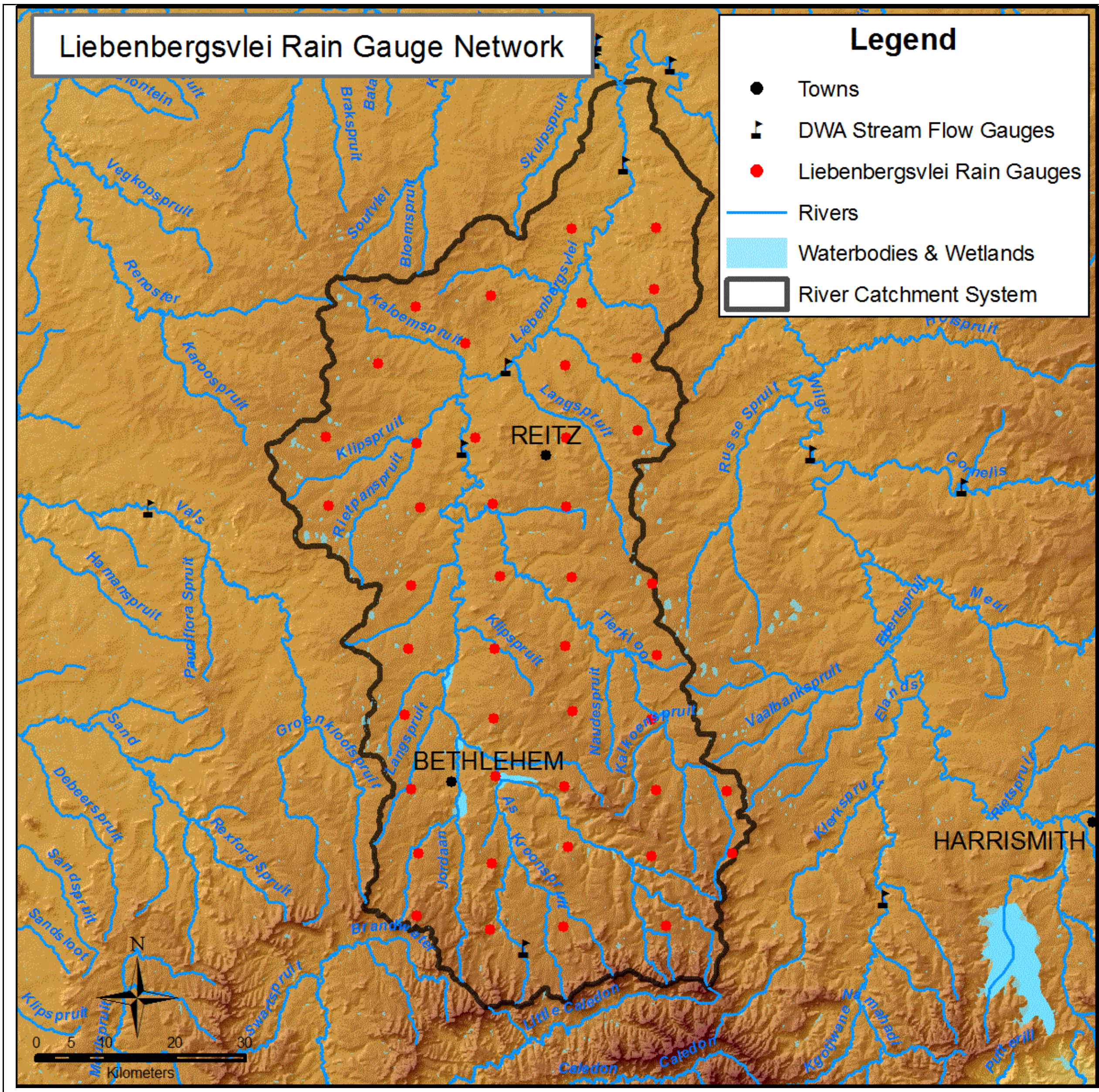

Figure 5-2: Liebenbergsvlei catchment showing rain gauge and stream flow gauge locations.

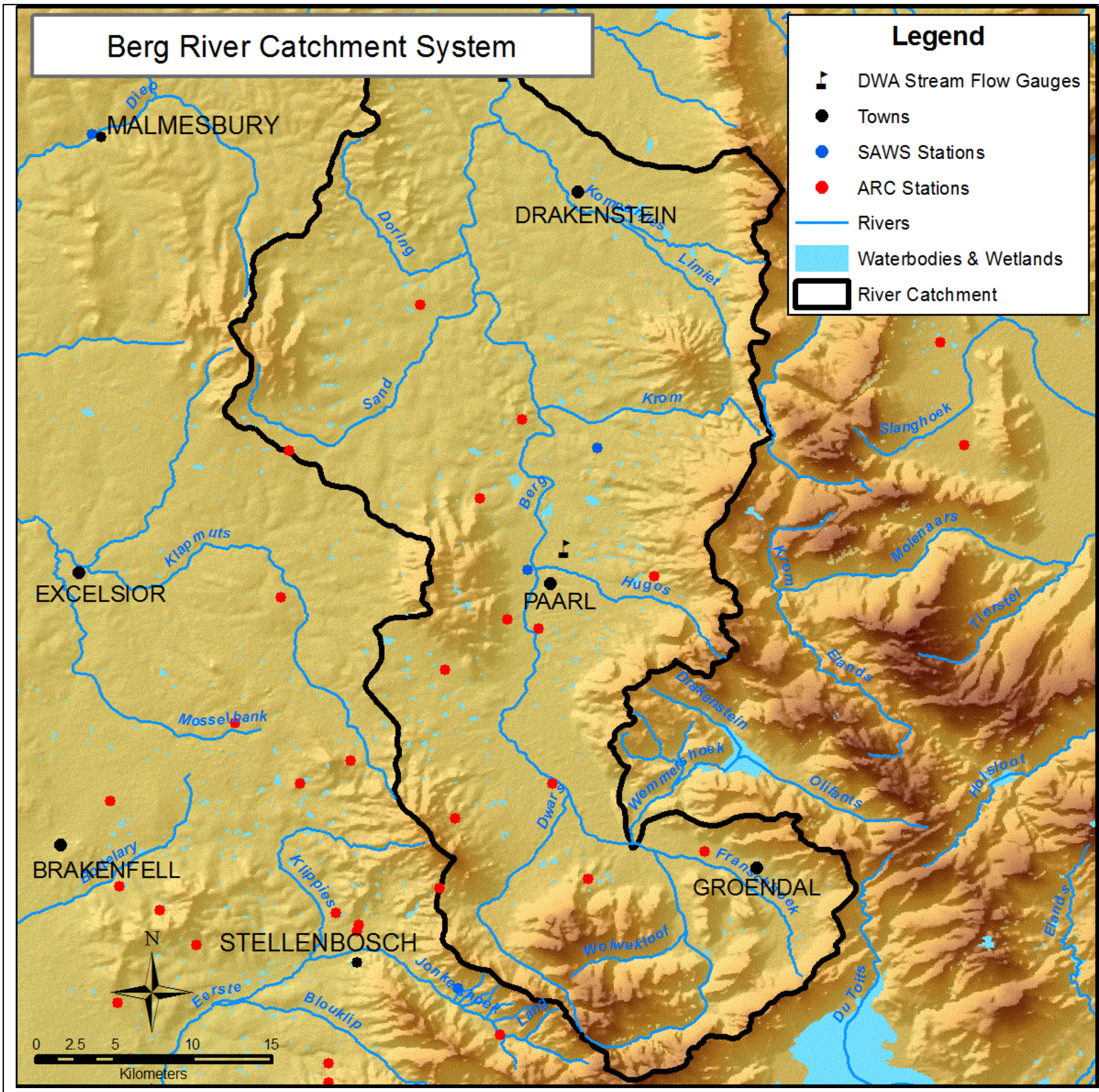

Figure 5-3: catchment showing rain gauge and stream flow gauge locations.

5.3 WRF Domains

Nested domains were used in WRF covering resolutions of 36-12-4 km, with the parent domain covering Africa South of the equator to 40 degrees south (Figure 5-4). The 12 km domain covers South Africa with all 4 corners of the domain falling over the oceans, allowing for favourable forcing at the lateral boundary. The 4 km domains covered each catchment and were utilised for model scenarios that excluded convective physics options.

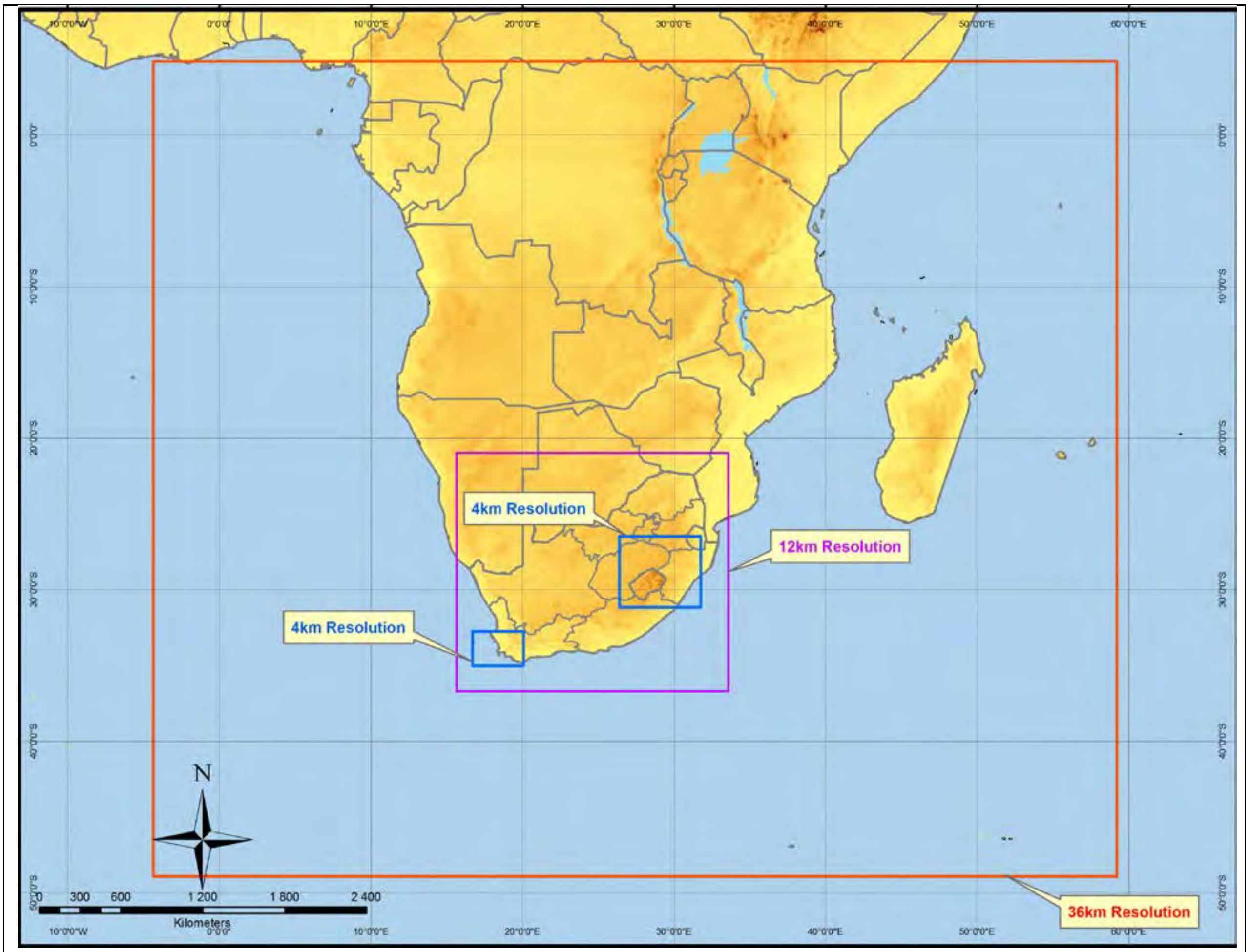

Figure 5-4: WRF model domains

5.4 WRF Configuration

Thirteen configurations of WRF were used for the Liebenbergsvlei 12 km domain (Table). These covered various combinations of microphysics and cumulus physics schemes. Further improvements were subsequently made to the best performing configurations by calling the cumulus (cudt) and radiation (radt) schemes more frequently. This means that the solvers for these schemes are run more often, e.g. when radt = 30 radiation is solved every 30 minutes in a 1 hour simulation, so the solver is only called twice. Some comparisons were conducted by changing the frequency with which the lateral boundary conditions were forced (e.g. every 12 hours or 6 hours, referred to as 6hr and 12hr). This means that reanalysis data of the synoptic conditions are introduces every 12 or 6 hours.

Table 5-1: Configuration of WRF 12 km domain over Liebenbergsvlei

Referred to in this document as:	Forcing Interval	Mp_physics	Cu_physics	RADT (minutes between calls to solver)	CUDT (minutes between calls to solver)
BMJ-12hr	12 hr	WSM3	BMJ	30	5
BMJ-6hr	6 hr	WSM3	BMJ	30	5
BMJ-radt12	6 hr	WSM3	BMJ	12	5
Kain	6 hr	WSM3	Kain-Fritcsh	30	5
WSM3-Tiedtke	6 hr	WSM3	Tiedtke	30	5
Tiedtke-radt12	6 hr	WSM3	Tiedtke	12	5
Tiedtke-cudt0	6 hr	WSM3	Tiedtke	12	0
Lin-BMJ	6 hr	Lin	BMJ	30	5
Lin-Tiedtke	6 hr	Lin	Tiedtke	12	5
Lin-Tiedtke-cudt0	6 hr	Lin	Tiedtke	12	0
Lin-noconv	6 hr	Lin	None	12	n/a
Wsm3-noconv	6 hr	WSM3	None	12	n/a
Lin-BMJ-cudt0	6 hr	Lin	BMJ	12	0

Table 5-2: Configuration of WRF 12 km domain over Berg River

Referred to in this document as:	Forcing Interval	Mp_physics	Cu_physics	RADT	CUDT
BMJ-6hr	6 hr	WSM3	BMJ	30	5
Kain	6 hr	WSM3	Kain-Fritcsh	30	5
WSM3-Tiedtke	6 hr	WSM3	Tiedtke	30	5
Lin-BMJ	6 hr	Lin	BMJ	30	5

Table 5-3: Configuration of WRF 4 km domain over Liebenbergsvlei

Referred to in this document as:	Forcing Interval	Mp_physics	Cu_physics	RADT	CUDT
Thompson	6 hr	Thompson	none	10	n/a
Grell3d	6 hr	WSM3	Grell-3D	10	5
WSM3-noconv	6 hr	WSM3	none	10	n/a
WSM6	6 hr	WSM6	none	10	n/a

5.5 WRF Rain Gauge Verification

Point-to-grid verification was implemented, where the observed point is verified against the closest model grid point (Figure 5-5). This methodology was preferred to grid-to-point, where model results have to be interpolated to match the observed location, as interpolation can cause further room for error when processing the data set.

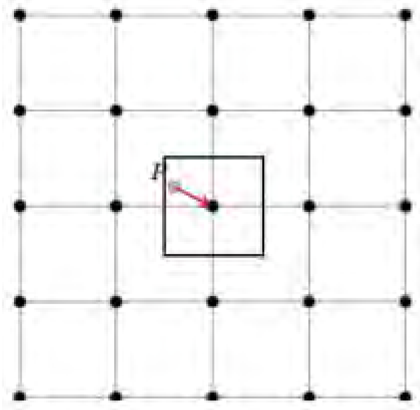

Figure 5-5: Point-to-grid verification method. Observed data (P) is verified against the closest model grid cell.

One method for evaluating model performance involves the compiling of a contingency table (GAW, 2008). Once observed data is matched to a model grid cell, a contingency table can be created. Model results are allocated into four possible categories: hits (event exists in observed and model data sets), misses (event occurs in reality but not in the model), false alarms (simulated, but not observed) and correct negatives (does not occur in model or observations, e.g. No rainfall). Quantitative and comparable metrics can be derived from these categories in evaluating mode performance.

Table 5-4: Typical contingency table

	Observed event yes	**Observed event no**
Forecast event yes	Hits	False alarms
Forecast event no	Misses	Correct neg.

From these categories the following metrics are derived;

Hit Rate, which is the ratio of correct forecasts to all modelled rainfall, where a value of 1 is ideal.

$$HR = \frac{hits}{hits + false\ alarms} \tag{9}$$

Probability of detection, which represents the ratio of correctly forecast events to all observed rainfall. A result of 1 is ideal.

$$POD = \frac{hits}{hits + misses} \tag{10}$$

False alarm ratio (FAR), which represents the ratio of false alarms against all model rainfall. Values range from 0 to 1 where 0 is ideal.

$$FAR = \frac{false\ alarms}{hits + false\ alarms} \tag{11}$$

Systematic bias is defined as:

$$Sytemnatic\ Bias = \ FAR + POD \tag{12}$$

Where a value of 1 means no bias, >1 = positive bias and <1 = negative bias.

Critical Success Index, or threat score, which is similar to hits, but includes the number of missed forecasts.

$$CSI = \frac{hits}{hits + false\ alarms + misses} \tag{13}$$

Hit ratio, which is the ratio of the total correct forecasts, both rain and non-rain, to total modelled rain.

$$Hr = \frac{hits + correct\ neg}{hits + false\ alarms} \tag{14}$$

Individually, these metrics cannot adequately assess model performance. However, when considered together, along with 24 hours bias, model performance can be evaluated qualitatively.

6 PYTOPKAPI METHODOLOGY

Modelled rainfall from WRF will be used as input into a hydrological model, TOPKAPI that has already been successfully applied in several countries around the world (Liu and Todini, 2002; Bartholomes and Todini, 2005; Martina et al., 2006; Vischel et al., 2008), to model stream and river channel discharge from the selected catchments. In this study, PyTOPKAPI (Vischel et al., 2007), a BSD licensed Python library, will be used to implement TOPKAPI in order to simulate the hydrology of the selected catchments. The simulated streamflow data that will be output by TOPKAPI will then be verified against observed stream flow data.

PyTopkapi will be parameterised using observed rainfall as input prior to using modelled rainfall from WRF (Figure 7-1). This process will establish that PyTopkapi is performing within a certain level of certainty using observed rainfall, thus decreasing the uncertainty when using modelled rainfall from WRF as input.

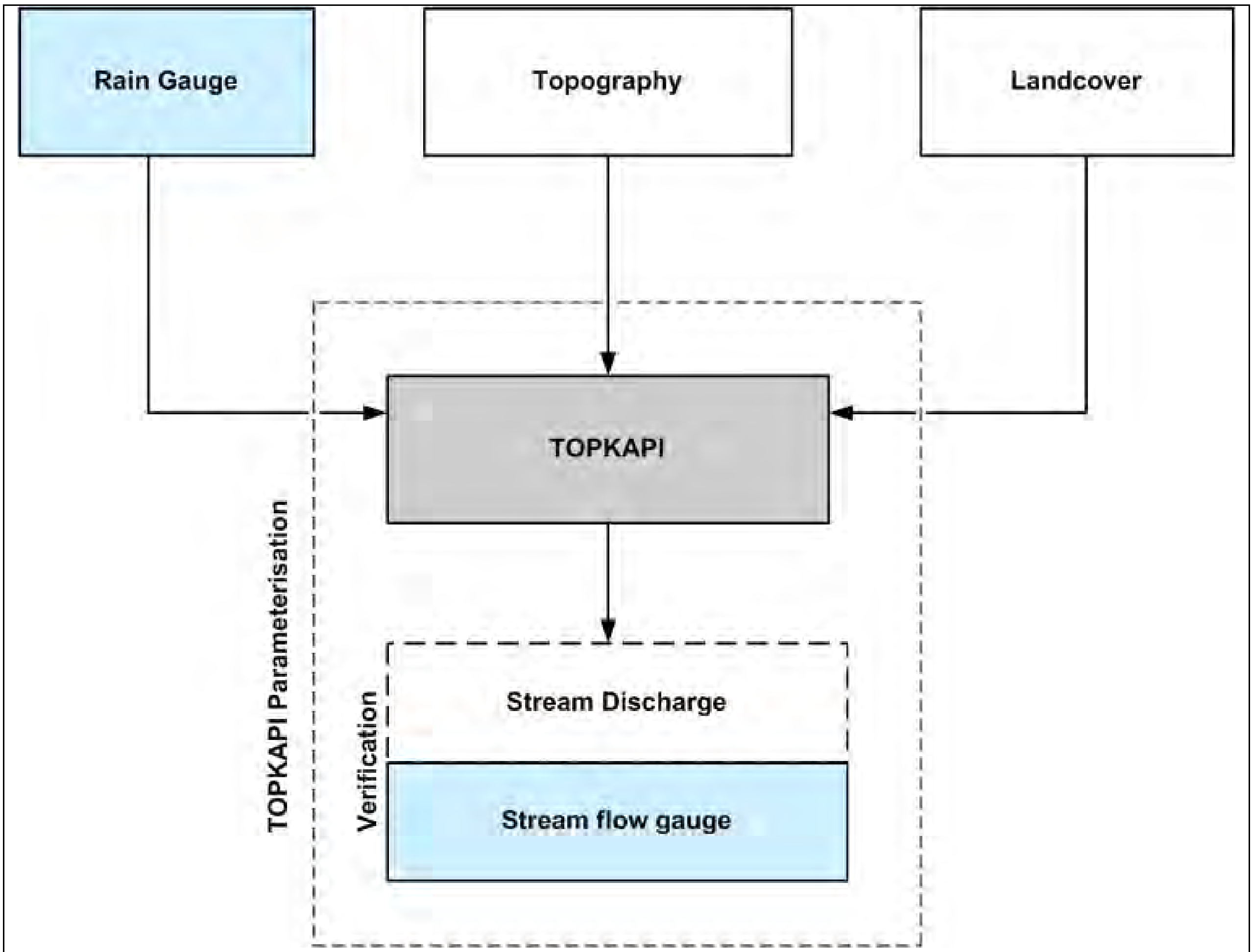

Figure 6-1: Proposed PyTopkapi verification methodology.

6.1 Data – Sources and Description

Rainfall

TOPKAPI hydrological model requires that rainfall data is derived for every grid cell of the respective catchment for every time-step. The PyTOPKAPI implementation of this model accepts rainfall data in HDF5 format owing to the convenience this format provides in compressing such an extensive set of data. Estimation of rainfall data for each grid cell was achieved through a GIS routine in ARCGIS employing the Thiessen polygons to estimate rainfall for each cell. Thiessen polygons are created in two steps:

Step 1: Triangles are created between rain gauges by connecting one rain gauge to the next two closest gauges.

Step 2: Once the irregular triangle network is created, a perpendicular bisector is drawn from each side of a triangle. Each intersection of these bisectors serves as a vertex of the Thiessen polygon, which surrounds a single rain gauge. Rainfall from that gauge is then designated to all raster cells that fall inside the polygon.

The polygons were then clipped to the catchment boundary. In the case of the Berg River, some segments of polygons were assigned to rain gauges outside of the catchment. These segments were reassigned to the closest gauges that fall inside the catchment.

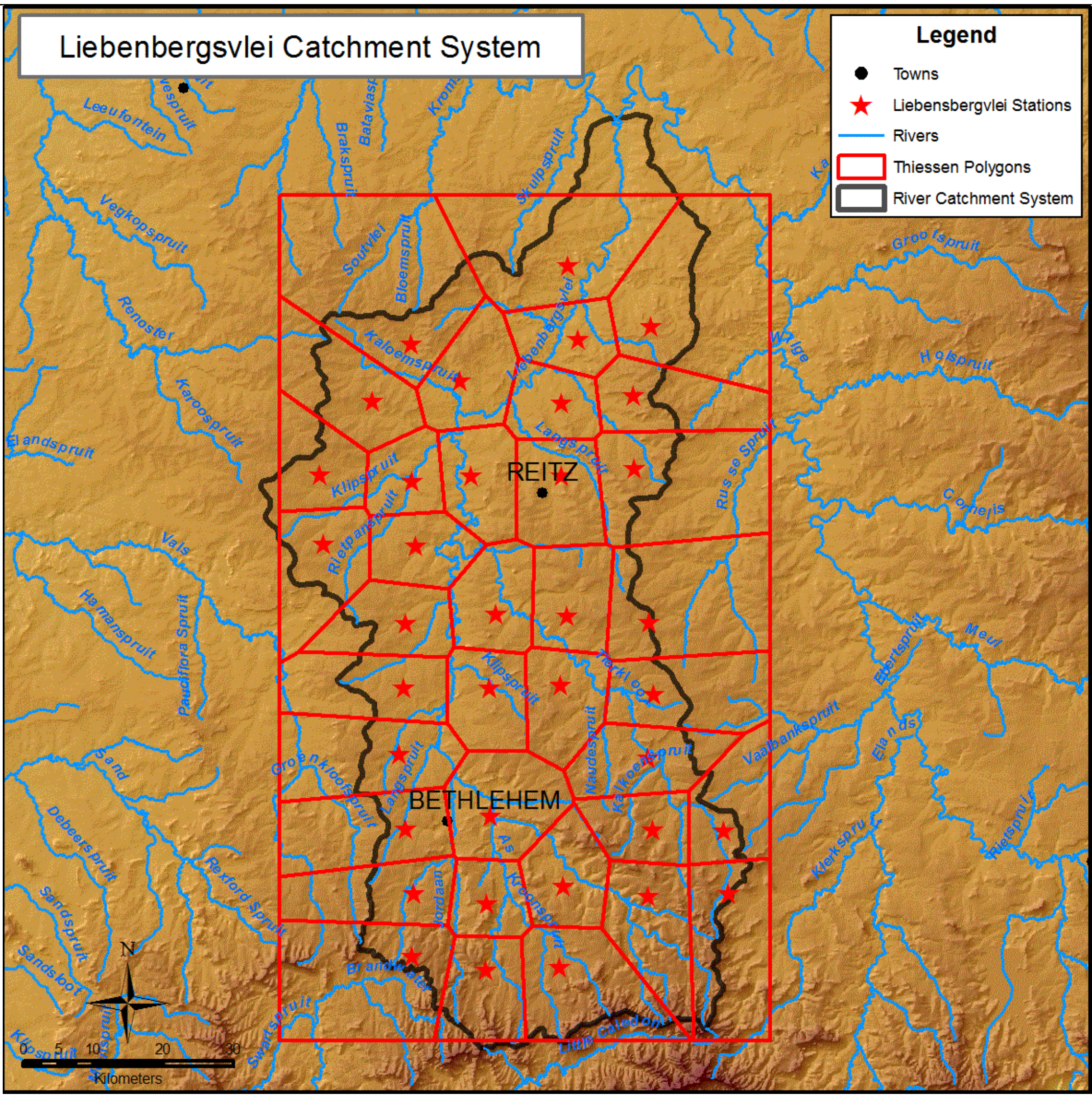

Figure 6-2: Thiessen Polygons for Liebenbergsvlei catchment

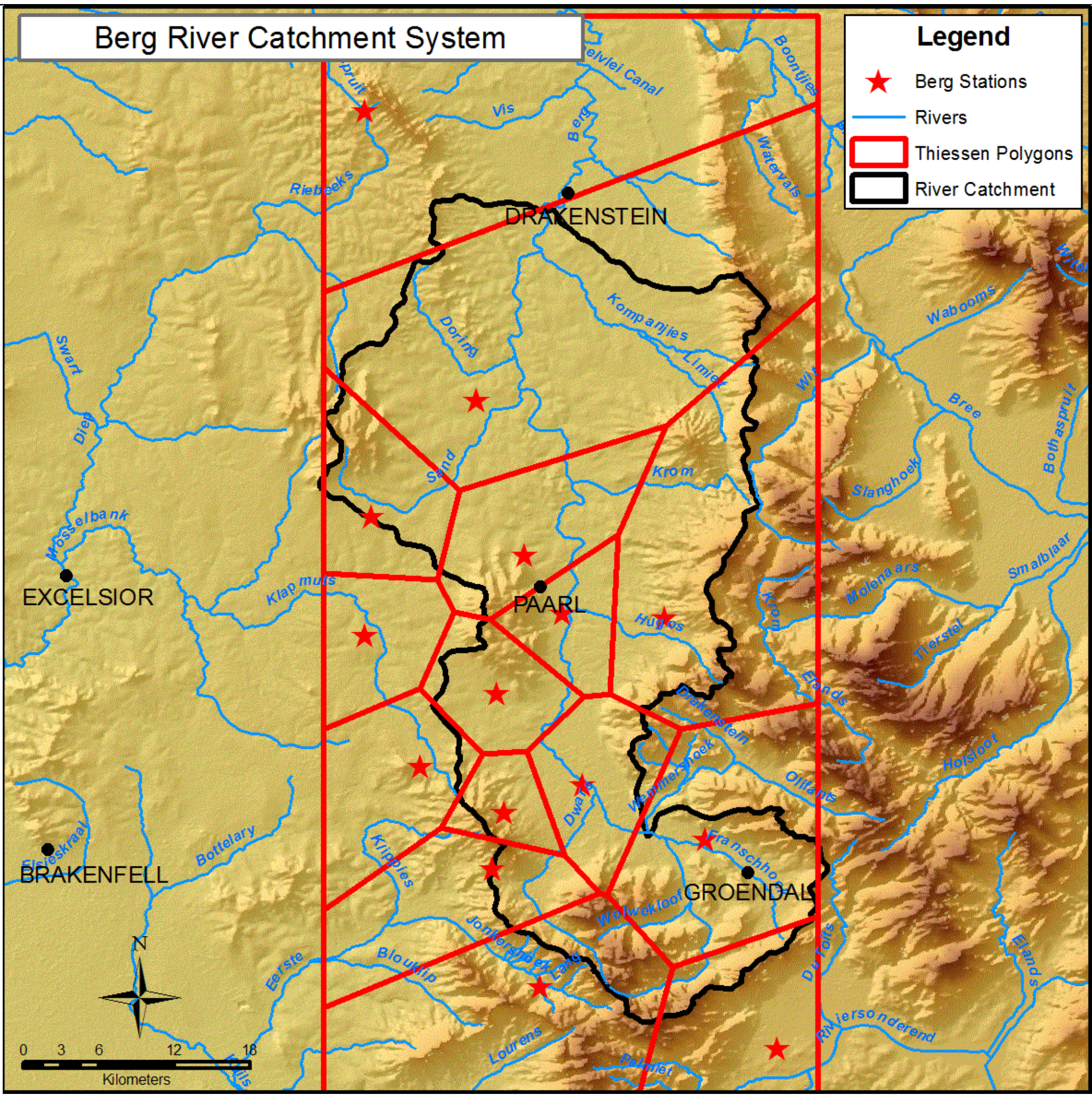

Figure 6-3: Thiessen polygons for Berg River catchment.

<u>Liebenbergsvlei Catchment</u>

A rain gauge network consisting of 43 gauges was established in this catchment as part of a summer rainfall campaign from 1993-2001. Rainfall was measured during the months of October to December and January to March. Data from these gauges was acquired from the South African Weather Service to verify the WRF model. The high density of gauges in the catchment was considered ideal for model verification purposes.

Berg Catchment

Rain fall gauge data is available for about 15 stations from the Agricultural Research Council (ARC) and the South African Weather Service. Stream flow gauge data is available for one station and is supplied by the Department of Water Affairs.

Streamflow Data

The streamflow data was obtained from a database maintained by the Department of Water Affairs (DWA). DWA has a network of flow measurement weirs across the country that it maintains and has set up a database into which this flow data is stored.

Two gauges were used for Liebenbergsvlei, one for verification of stream discharge and another as a source of flow from the Lesotho Highlands Water project. Gauge C8H037 was used for stream flow verification while gauge C8H036 was used for input flow from the Ash River fallout. In the Berg River, the stream gauge at Paarl was used for verification (G1H020). There is a gauge further downstream at Vleesbank (G1H036), however, the ratings table is out dated and stream flow beyond 25 m^3/s are not recorded.

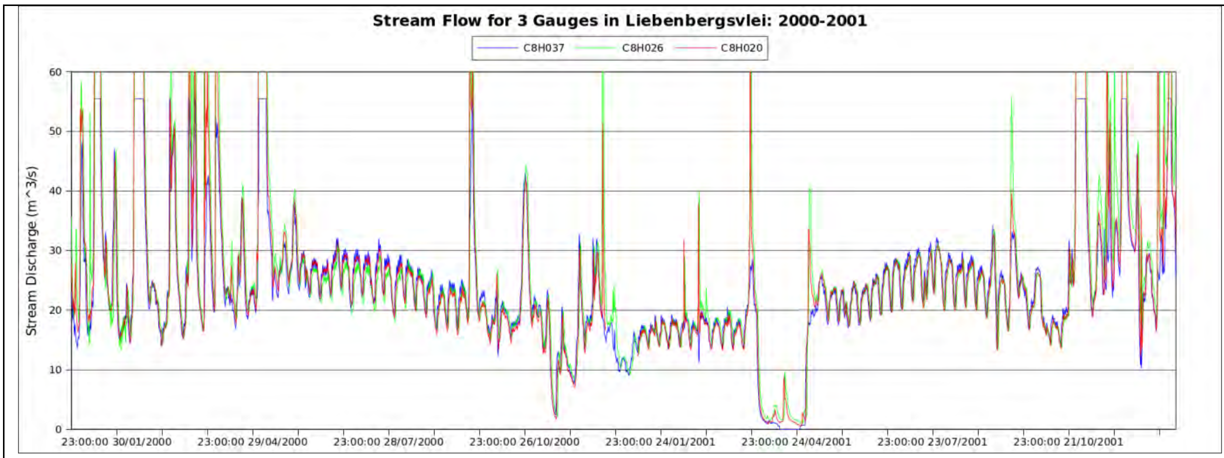

Figure 6-4: Liebenbergsvlei: Three downstream gauges suitable for model verification. Gauge C8H020 was missing data for part of Dec 2000- Jan 2001. Gauge C8H037 had a full data record and was used for model calibration.

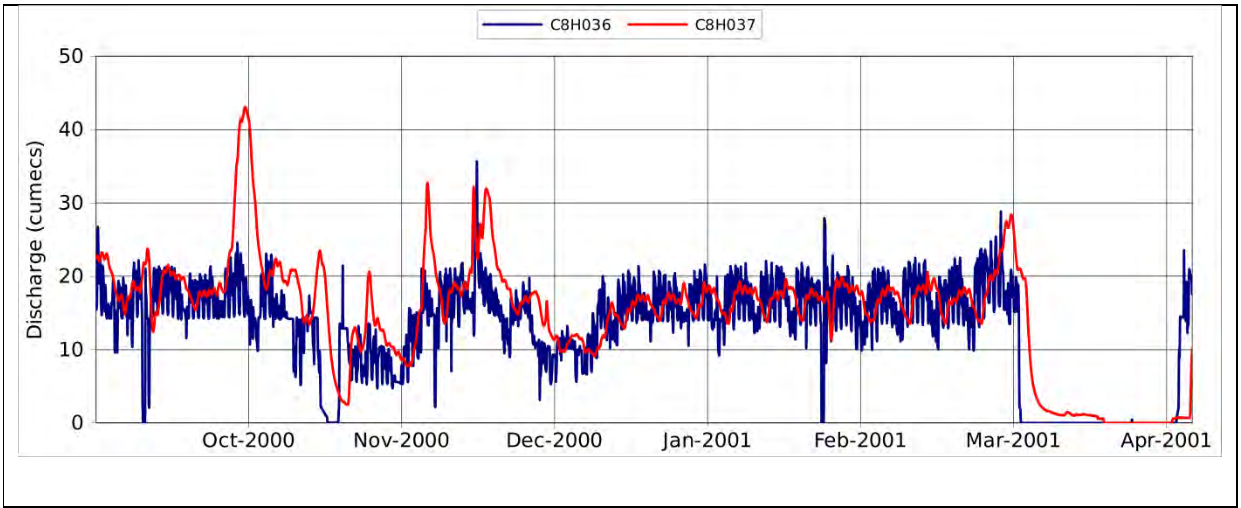

Figure 6-5: Liebenbergsvlei – External flow from the Ash River fallout (C8H036) and corresponding observed flow further downstream at gauge C8H037 during modelling period.

Evapotranspiration Data

Like rainfall data, PyTOPKAPI hydrological model requires that evapotranspiration data is derived for every grid cell of the respective catchment for every time-step. As such the PyTOPKAPI implementation of this model has been set to accept this data in HDF5 format.

For the simulation periods used in this study, Evapotranspiration data was not readily available, it was decided that the data would be derived from available monthly values of S-pan evaporation data for the study catchments for the period. By applying the same monthly S-pan-to-catchment evapo-transpiration conversion factors as used in the WR90 publications (Midgley et al., 1994), the Evapotranspiration data used in this study was derived. This methodology was applied for the Berg River catchment as S-pan data was available, however, for Liebenbergsvlei, no S-Pan data was available. Instead, satellite derived data from the Satellite Applications and Hydrology Group (SAHG) was used. Daily averages were calculated from observed satellite data measured from 2007-2012 (sahg.ukzn.ac.za). This created spatially varying values for each time step as opposed to constant values using the S-pan methodology.

6.2 PyTOPKAPI Parameterisation

With PyTOPKAPI being a semi-distributed model, it consists of a total of 15 parameters which have to be estimated *a priori* from the elevation data, soil and surface properties. Among them, 11 are cell specific, meaning that they are potentially spatially variable and they mainly refer to physical characteristics. The 4 others are constant and refer to geometrical characteristics of the channel or grid cells and are referred to as Global Parameters. The source of the elevation, soil and surface information that was used to derive the model parameters is detailed in the Table 6-1 below.

Table 6-1: Physical parameters required for simulation of the hydrology (after Vischel et al., 2008).

Type of Data	Description	Source
Soil Type	Used to derive Soil Depth and saturated soil moisture	SIRI (1987)
Topography	SRTM derived digital elevation model (DEM)	DLSI (1996)
Land use/Land cover	Used to derive overland roughness	GLCC (1997)

The description of how the cell parameter data is extracted from the information in Table 6-1 is described in great detail by Vischel et al., (2008). However, for this study use was made of the PyTOPKAPI (Vischel et al., 2007) library as this contains scripts that utilized the information in the Table 6-1 above to create and modify the cell parameter files for the respective catchments. The User Manual provided with the above python library can be referred to for details on the manner this is undertaken.

6.3 Model Calibration

While the PyTOPKAPI model should require no calibration as it is a physically based model, in practice modification of some parameter values is done. This is what is referred to here as model calibration. This calibration exercise is, however, not undertaken at cell level as this would lead to an extreme over-parameterization of the model and to multiple and inconsistent combinations of parameter values (Vischel et al., (2007b).

Furthermore, the method used to calibrate the model on the selected study catchments consisted of a dissociated calibration of the parameters responsible for the production of the runoff and those responsible for the routing of runoff. It has been found that the most sensitive parameters controlling the runoff production are the soil depth and the soil conductivity, while the Manning roughness of both the channel and overland are the main routing parameters. As such multiplicative factors (contained within the TOPKAPI.ini file within the PyTOPKAPI library) associated with these parameters are adjusted as part of the calibration process with the aim of raising the Nash-Sutcliffe Efficiency (NSE) – the objective function comparing modelled and observed discharge volumes – to a value between 0 and 1. NSE ranges between $-\infty$ and 1 (1 inclusive), with NSE = 1 being the optimal value. According to Moriasi et al., (2007), values between 0 and 1 are generally viewed as acceptable levels of performance, whereas values less than 0 indicate that the mean observed value is a better predictor than the simulated value, thus indicating unacceptable performance.

6.4 External Flows

The Liebenbergsvlei catchment is part of the Lesotho Highlands Water Project and forms part of the upper Vaal River basin which supplies water to the Vaal Dam and Gauteng. As such, it receives water from a transfer tunnel from Katse Dam at the Ash River fallout (gauge C8H036).

These external flows are registered in gauges further downstream and are useful in the calibration process of the PyTopkapi model because they only affect one part of the model namely, channel flow. As such, by simulating flow using external flow only, one can suitably calibrate the Manning channel roughness parameter, before introducing more complex flow from rainfall.

The channel distance between the external flow and verification gauges is 88 km (Figure 6-6). The time delay between peak flows in the two corresponding observed data sets is 42 hours (Figure 6-7). These peaks are easy to identify due to a controlled diurnal cycle and a 5day/2day (week/weekend) cycle (Figure 6-7). In order to obtain the same delay in simulations, the Manning channel roughness was adjusted and results are presented in Section 9.

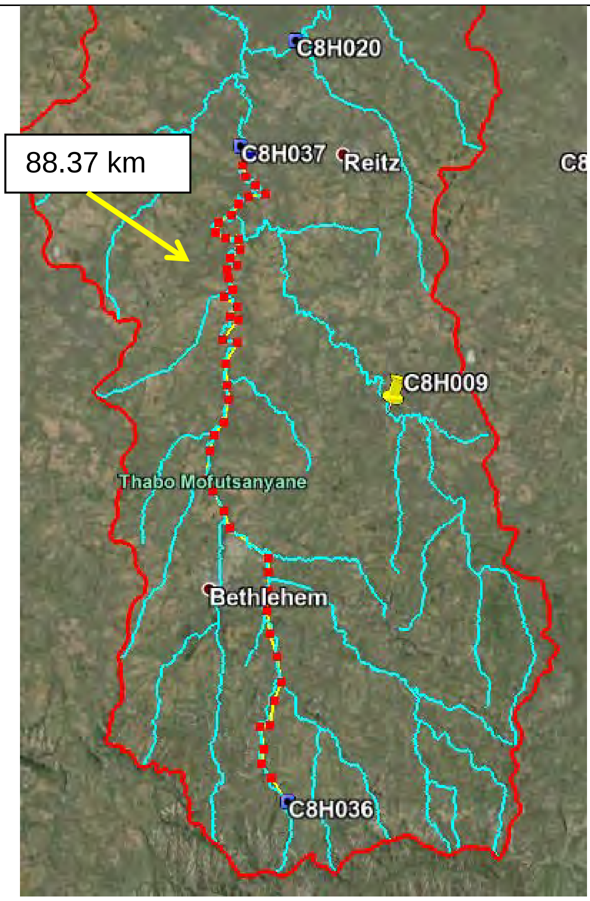

Figure 6-6: Liebenbergsvlei. Distance between external flow (C8H036) and verification gauge (C8H037) is 88 km.

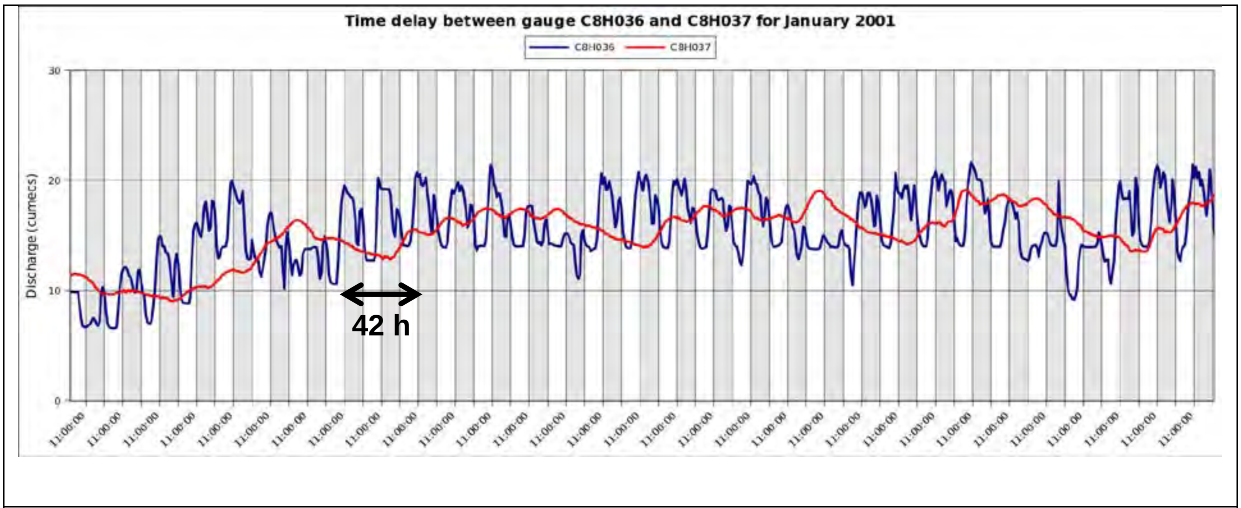

Figure 6-7: Liebenbergsvlei. Time delay between peak flow at external flow (C8H036) and verification gauge (C8H037) is 42 hours.

7 WRFCHEM METHODOLOGY

7.1 Area of Interest

The Highveld in situated in the elevated interior of South Africa at about 1500 m above sea level. It receives summer rainfall varying from 900 mm per annum in the east to 650 mm in the west. It is a large industrialised area mainly due to coal seams which are mined for power generation. However, there are many other industries including ferro-alloy, iron and steel, petrochemical and brick manufacturing. These sources are spread over an area covering about 31 000 km^2.

These industries contribute to the aerosol loading of the mixed layer of the atmosphere over the Highveld (Ross *et al.,* 2003) mainly due to emissions from tall stack which are required to decrease ground level concentrations. The relative contributions of each industry to aerosol emissions and sulphur dioxide emissions are shown in Figure 7-1and Figure 7-2. Sulphur dioxide is converted to sulphate aerosols through oxidation, either in-cloud or gas phase (Ross *et al.,* 2003). The gas-phase pathway is followed by condensation which results in a sulphate aerosol which acts as a cloud condensation nuclei. The interactions between emissions inventories, chemical pathways and cloud physics are demonstrated in Figure 7-3.

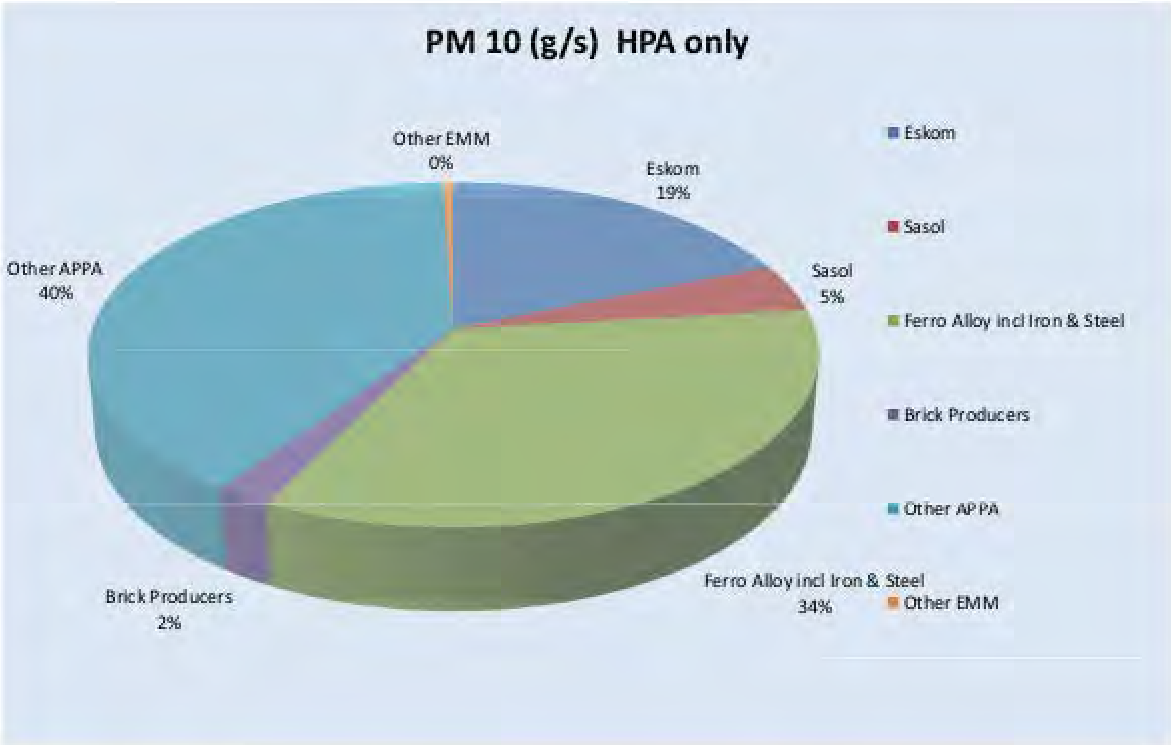

Figure 7-1: Industrial sources of PM10 in the Highveld

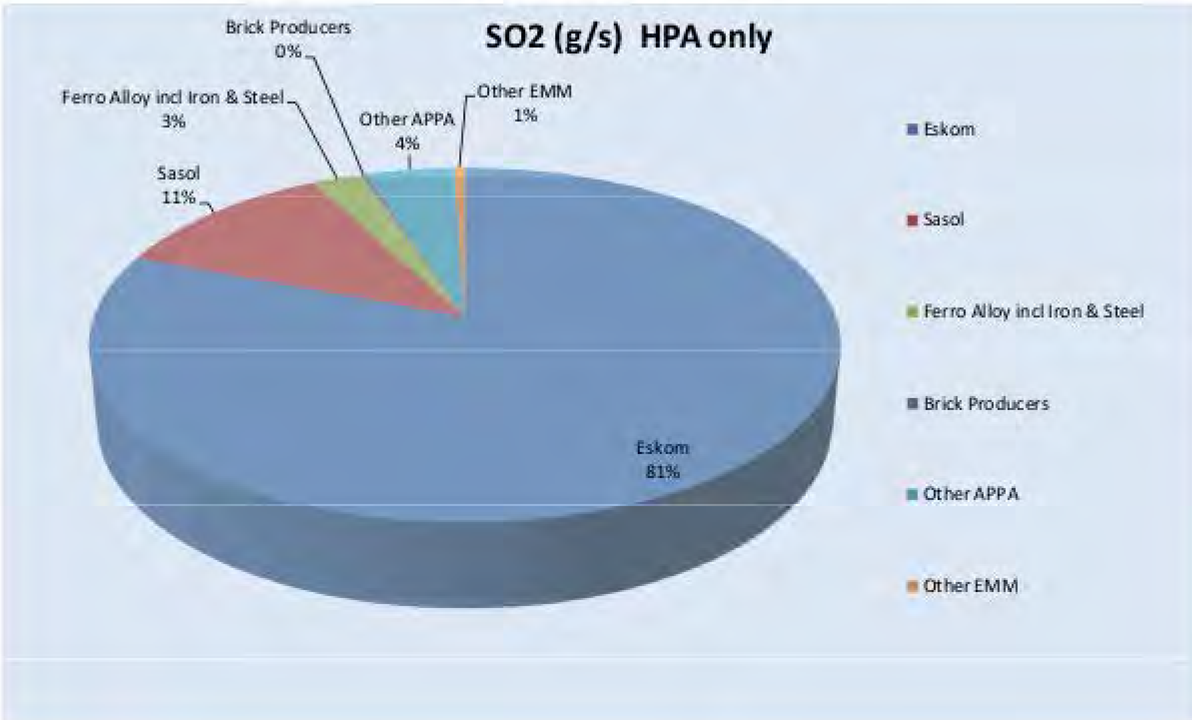

Figure 7-2: Industrial sources of SO2 in the Highveld

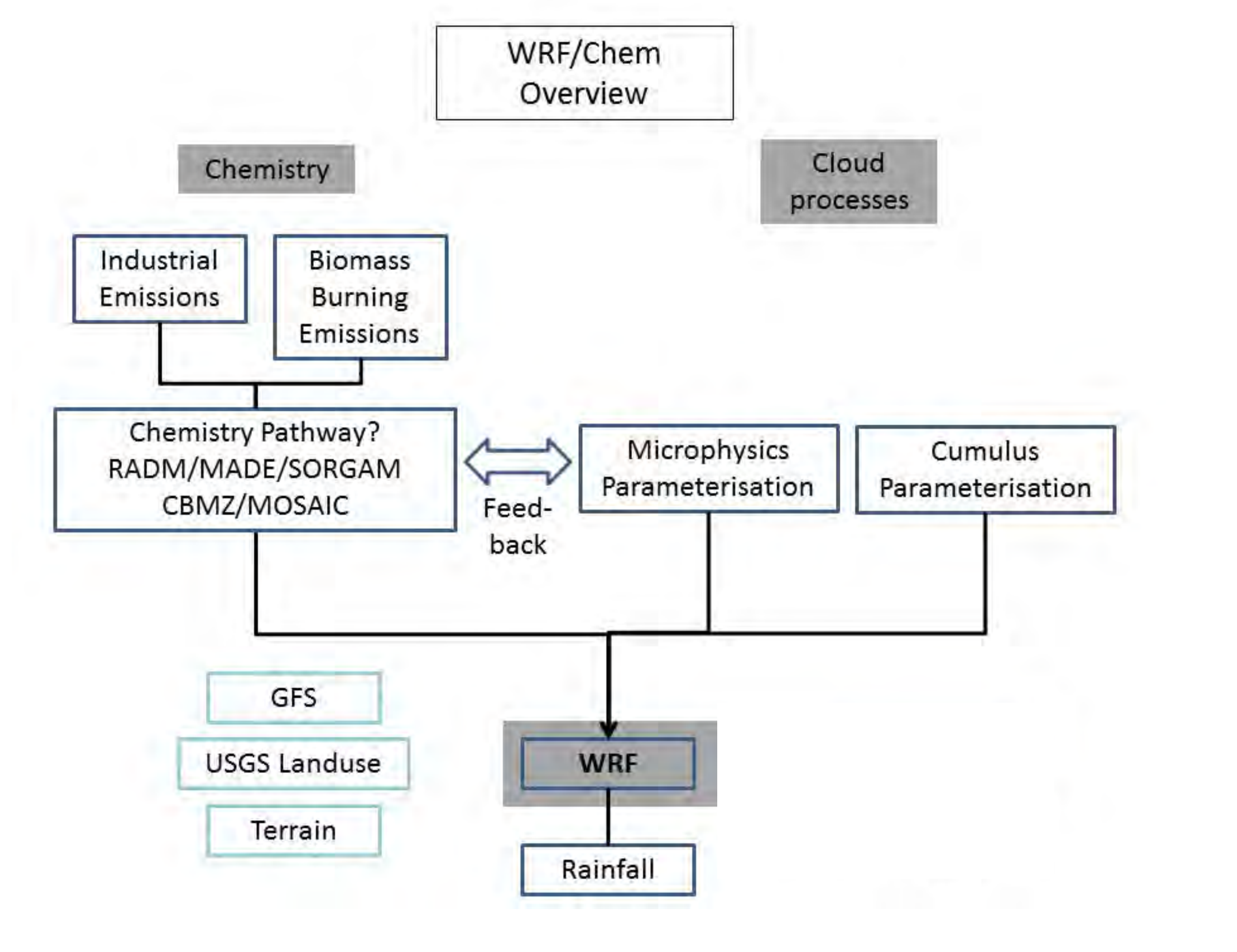

Figure 7-3: Overview of WRF/Chem modelling process as proposed for the Highveld area.

7.2 Emissions Inventories

Global emission inventories are available from two sources; the REanalysis of the TROpospheric (RETRO) chemical composition over the past 40 years (http://retro.enes.org/index.shtml) and Emission Database for Global Atmospheric Research (EDGAR) (http://www.mnp.nl/edgar/introduction) (Grell *et al.,* 2005). Both emissions inventories have a resolution of 0.5°. Examples of anthropogenic and biomass emissions are presented in Figure 7-1 and Figure 7-2.

A locally developed emissions inventory for South Africa, based on emissions information supplied by major industries, will be used for a WRFChem simulation. An example of SO_2 and PM10 emissions is given in Figure 7-6.

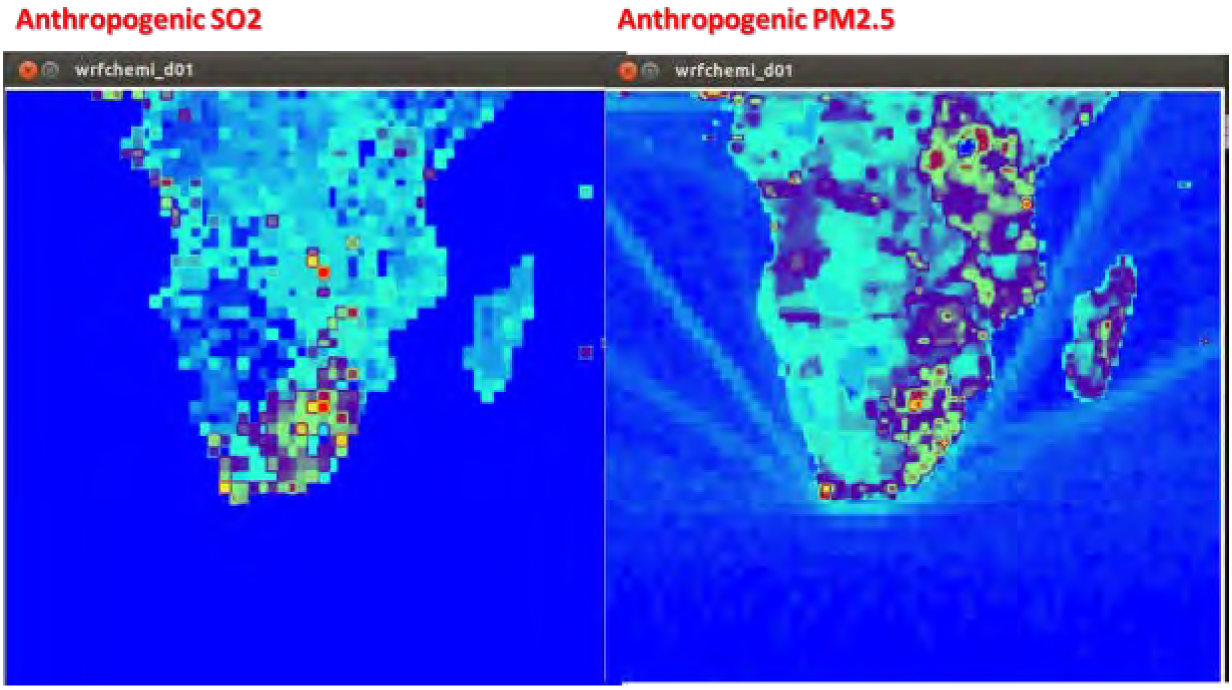

Figure 7-4: Anthropogenic global emissions inventories for SO_2 and PM2.5 at 0.5° resolution. Ship tracks are visible as a source of PM2.5 on the right.

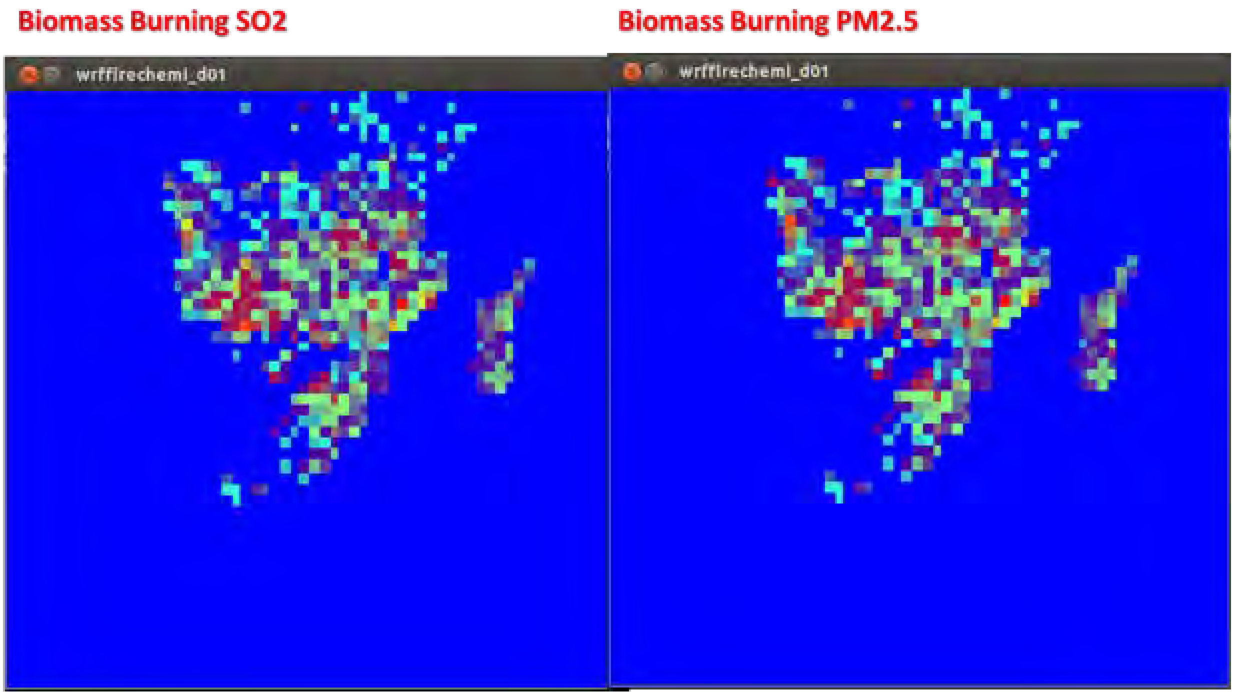

Figure 7-5: Biomass burning global emissions inventories for SO_2 and PM2.5 at 0.5° resolution.

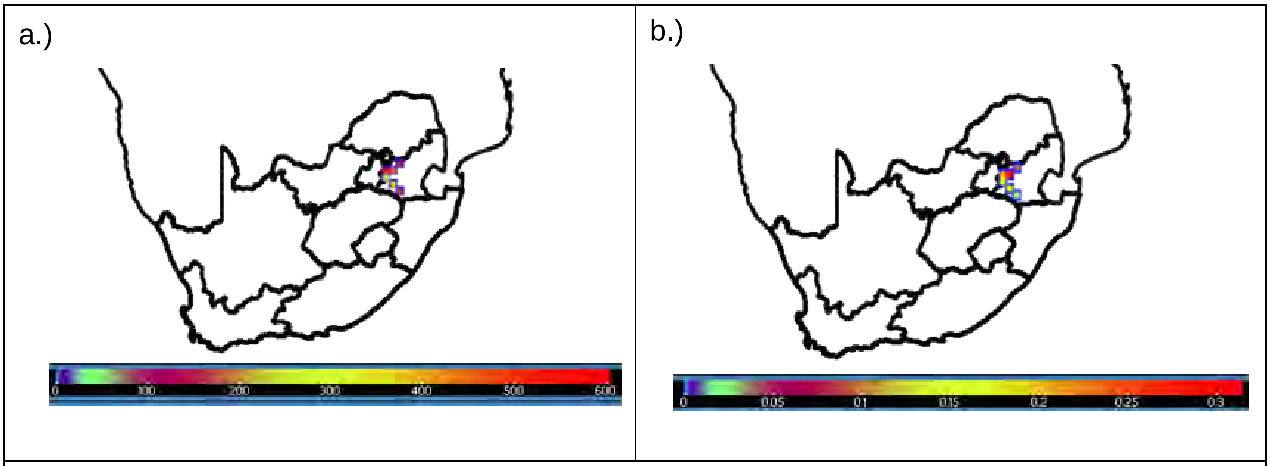

Figure 7-6: Industrial emissions inventories for a.)SO_2 and b.) PM10 at 36 km resolution. Units are mol/km^2/hr.

8 WRF RESULTS AND DISCUSSION

8.1 Overview

The WRF, and meso-scale models in general, tend to have a positive bias when forecasting rainfall over the Eastern half of South Africa. Three meso-scale models showed a positive daily bias of 1-2 mm over the Liebenbergsvlei catchment in South Africa for the summer rainfall season (Landman *et al.,* 2012). Results from WRF show higher biases of 7 mm for the same area, as presented by Ratna *et al.* (2011). We found that WRF had a positive daily bias for the Liebenbergsvlei catchment, ranging from < 1 mm to > 4 mm and will be presented in this section.

Model results from a 3 month period spanning from 28 September to 31 December 2000 are presented here for the Liebenbergsvlei catchment. All scenarios for Liebenbergsvlei show a positive 24hour bias and will be shown to be caused by 3 factors; 1) Surplus rain days in the model 2) Early triggering and formation of convective rainfall and 3)Excessive grid scale saturation and rainfall at night.

8.2 Liebenbergsvlei Rain days and Bias: WRF 12 KM

All scenarios show a positive 24hr bias ranging from 0.65 to 4.12 mm (wsm3-no convection and wsm3-kain respectively) as seen in Figure 8-1. Results represent rainfall overall rain gauges in the catchment from 28 September to 31 December 2000. Slight improvements in model bias were achieved by adjusting various timing controls in WRF such as updating lateral boundary conditions from 12 hours to 6 hours, as seen in (wsm3_bmj_12hr and wsm3_bmj) (Figure 8-1). Further, although slight, improvements were made by calling the radiation scheme (radt) more frequently (wsm3_bmj_radt12 in) as well as the cumulus physics calls (cudt).

Of the cumulus schemes used, the Kain-Fritsch scheme produced the worst bias, due mainly to overactive convective rain, as will be discussed in Section 8.3. The Betts-Miller-Janjic (BMJ) scheme produced positive bias between 2 and 3 mm, with either the WSM3 or Lin microphysics implemented. The Tiedtke convective scheme produced the lowest bias results of less than 2 mm when implemented with the WSM3 microphysics scheme. This increased when run with the Lin microphysics. However, the two schemes with the best model setup in terms of frequency of lateral boundary updates and calls to radiation and cumulus physics produced bias results of 1.22 (wsm3_tiedtke_cudt0) and 1.66 mm (lin_tiedtke_cudt0) respectively.

The positive bias results illustrated in Figure 8-1 are partly attributable to false alarms in the model; rain events that are simulated when there is no corresponding observed event. There are 36 observed rain days in the Liebenbergsvlei catchment out of a possible maximum of 94 days. However, some scenarios produce 50% more rain days, where individual false alarm days can produce 15 mm of rainfall (discussed later in Section 8.5). The total effect of false alarms is marginally offset by misses; observed rainfall events that the model fails to simulate (Figure 8-2). Scenarios that produced daily bias results greater than 2 mm (the BMJ scenarios) have a high hit count, and consequently score well in probability of detection (POD) (Figure 8-3), which does not account for false alarms. However, the number of false alarms is too high, resulting in a high daily bias. Thus, more favourable parameterisation is required to maintain the high hit count but decrease false alarms. The hit rate is the ratio of correctly modelled rainfall to all modelled rainfall and includes the false alarm ratio directly. For these model scenarios, the hit rate hovers around 0.5 (Figure 8-3). A hit rate of 0.5 translates to a false alarm count that is equal to the hits count, which loosely means the model is incorrect as often as it is correct. An ideal hit rate is 1 and thus a preferred score should be greater than 0.5 but less than or equal to 1.

The two scenarios that excluded convective parameterisation and used microphysics alone to simulate rainfall scored the lowest for POD. The POD is the ratio of modelled rain to all observed rainfall. The reason for the poor performance is due to a high count of missed events, lending weight to the argument that convective parameterisation improves model forecasts. However, although both the “no convection” scenarios produced the most realistic number of rain days, the rainfall totals were still too high resulting in a high daily bias.

The Tiedtke scenarios produced hit rates greater than 0.5 as well as favourable POD scores. The hit rate improved when increasing the frequency of calls to the cumulus physics solver when run with either the WSM3 or Lin microphysics scheme. The most defensible scenarios, in terms of physics and frequency of calls to the solvers, were WSM3 Tiedtke cudt0 and Lin Tiedtke cudt0 (radt=12 for both scenarios) and produced daily bias of less than 2 mm. Both schemes struck a balance between achieving hits, while minimising false alarms. Thus, considering all metrics presented in Figure 8-1, Figure 8-2 and Figure 8-3, these two scenarios performed most favourably across the board.

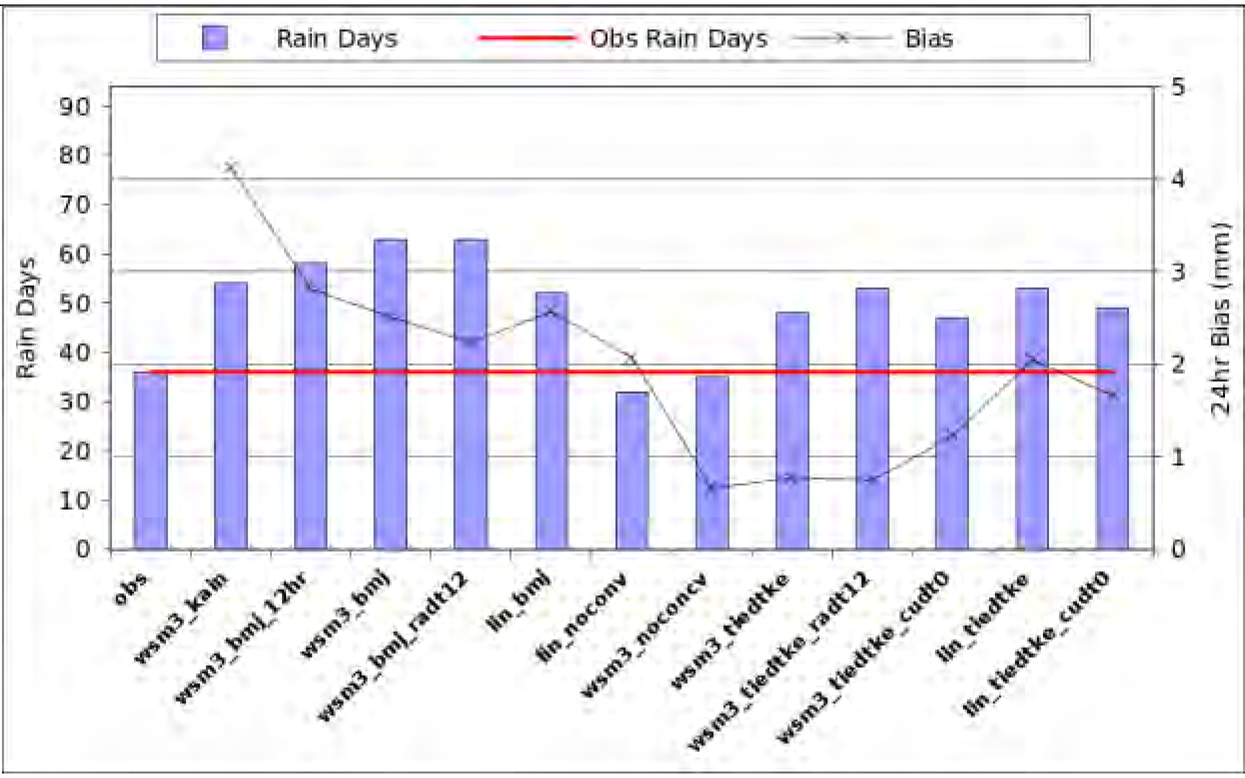

Figure 8-1: Rain days (>1 mm/d threshold) and 24hr bias for Liebenbergsvlei 12 km WRF domain. Results represent all rain gauges in the catchment from 28 September to 31 December 2000.

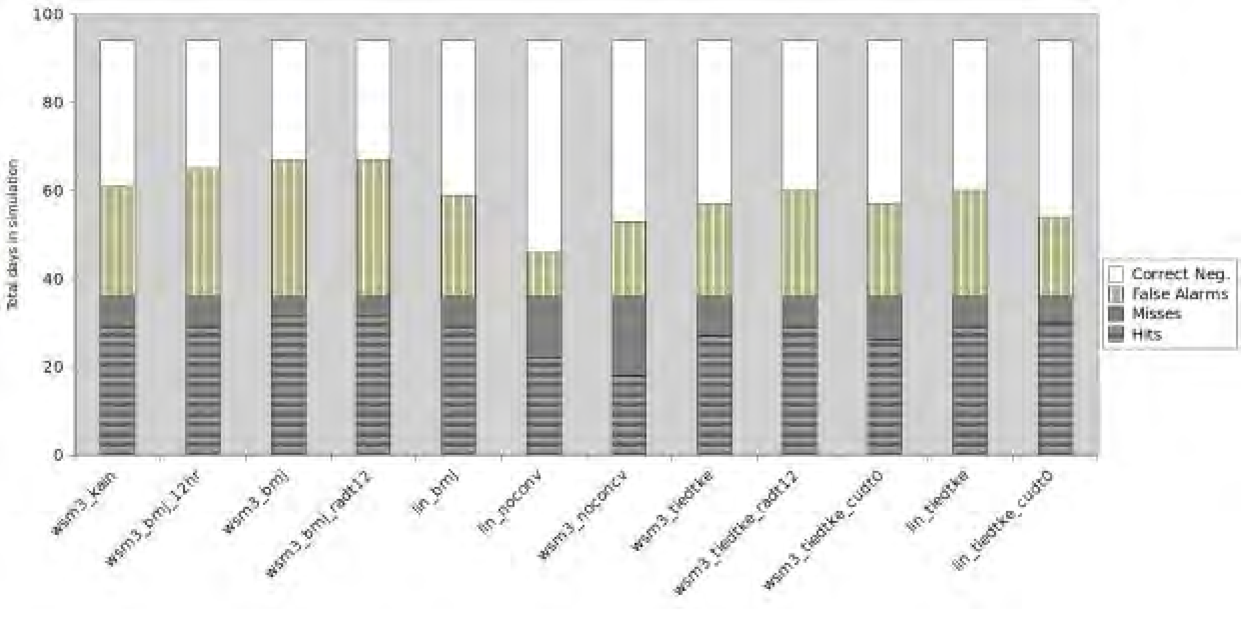

Figure 8-2: Contingency tables counts of hits, misses, false alarms and correct negative (no rainfall) for daily threshold of >1 mm/d for Liebenbergsvlei 12 km WRF domain. Results represent all rain gauges in the catchment from 28 September to 31 December 2000.

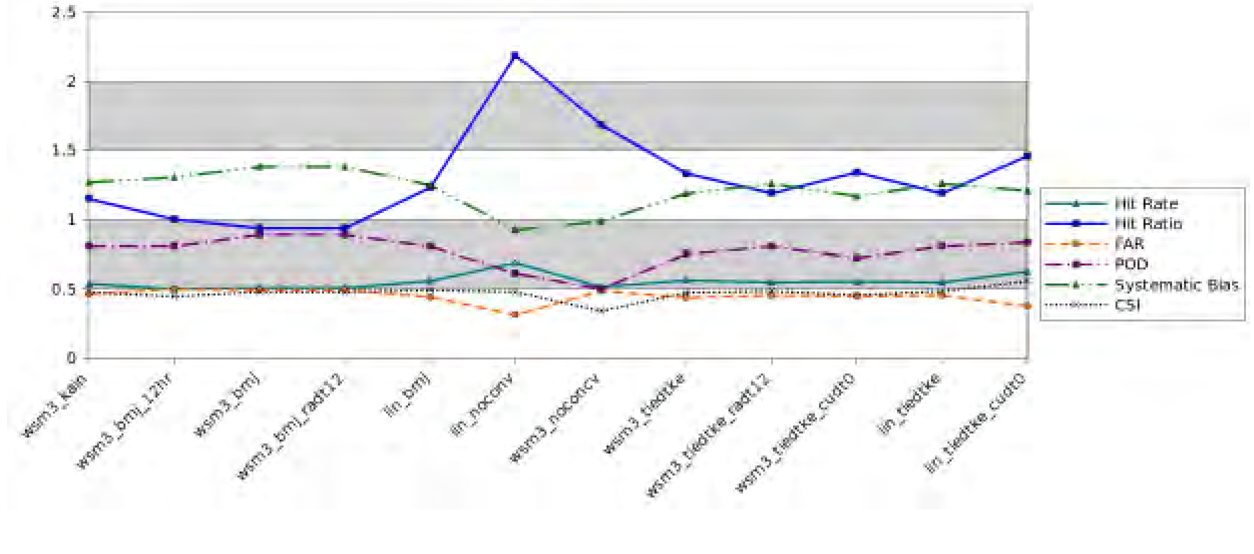

Figure 8-3: Scores derived from contingency table counts (>1 mm/d threshold) for Liebenbergsvlei 12 km WRF domain. Optimum score is 1 for Hit Rate, POD (probability of detection) and CSI (critical success index). Ideal score for FAR (false alarm ratio) is 0. Results represent all rain gauges in the catchment from 28 September to 31 December 2000.

8.3 Liebenbergsvlei Rainfall Maps

Total Rainfall

The observed total rainfall in Liebenbergsvlei varies from 110 mm to 290 mm and shows no particular geographic gradient or relationship with elevated terrain (Figure 8-6). As this only represents a three month period from 2000-09-28 to 2000-12-31, the geographic distribution of rainfall can be affected by single isolated events of convective rainfall that passed over the catchment. The 12 km WRF domain is too coarse to resolve the observed rainfall pattern; however, the WRF rainfall totals will be presented here in comparison with the observed data. Furthermore, the WRF results give a broader context of the role of terrain in modelled rainfall formation which can be compared to annual averages for the country.

Modelled rainfall over the catchment varied from 300 mm to 700 mm, the latter being produced by the Kain convective scheme (Figure 8-6a). A map of annual mean rainfall developed by the Agricultural Research Council indicates annual rainfall of 601-800 mm for the Liebenbergsvlei catchment, which is in line with observed data from the catchment (Figure 8-5). Thus, the total rainfall produced by the Kain schemes is producing annual rainfall results typically received over six months when only three months is simulated. The Kain scheme is overactive for areas over the escarpment producing >1000 mm in the three month simulation where annual mean rainfall is 801-1000 mm and >1000 mm for parts of the Drakensberg.

The improvement achieved by calling the lateral boundary conditions every 6-hours as opposed to every 12-hours was not obviously noticeable in the catchment (Figure 8-6b and Figure 8-6c), although improvements in bias and POD were noted in Section 8.2. However, obvious improvements are noted outside the catchment along the escarpment where BMJ-6hr produced much lower rainfall totals than BMJ-12hr. Catchment totals ranged between 400-500 mm for both scenarios, while escarpment rainfall ranged from 1000 mm, 600 mm and 600 mm for 6-hour nudging, compared to 1100 mm, 700 mm and 900 mm for 12-hour nudging. By introducing lateral conditions more frequently, the model is prevented from producing uninhibited convection and therefore dampens the rainfall totals. More frequent calls to the radiation scheme made improvements in the catchment, which now shows a larger area of 400 mm, and on the escarpment where contours showed the same values as BMJ-6hr, but were restricted to smaller areas (Figure 8-6d).

The Lin-BMJ scenario produced similar rainfall totals as WSM3-BMJ for the catchment area which explains why the daily bias results were similar (Section 8.2). However, rainfall totals over the escarpment were much higher (Figure 8-6e). Two scenarios were run without convective schemes where rainfall was produced by microphysics only, WSM3 and Lin in these cases. There are arguments for and against using convective schemes at a resolution of 12 km. Some argue that resolutions between 5 and 15 km are grey areas for convective schemes as they violate some of the assumptions inherent to the scheme (Stensrud, 2007). In spite of this, the inclusion of convective schemes has been shown to improve forecasts. We wanted to test the latter for our catchment area. The Lin scheme sans convection actually showed an improvement for the catchment in terms of rainfall total (Figure 8-6f). Yet, it produced some of the highest rainfall totals for the escarpment and lower lying areas below the escarpment, which are unrealistically high when compared to annual mean rainfall in Figure 8-5. Similarly, but slightly better than Lin, the WSM3 scenario produced good rainfall totals for the catchment, but over predicted rainfall compared to convective scenarios and annual mean rainfall (Figure 8-7a).

The WSM3-Tiedtke scenarios (Figure 8-7b-d) produced realistic totals, compared to the observed data, in the catchment evident by the location of the 300 mm rainfall contour. Furthermore, these scenarios produced lower totals, and therefore more realistic totals, over the escarpment and lower lying areas below the escarpment. Overall, in terms of contours of rainfall totals, these schemes performed the best. The Lin-Tiedtke schemes produced higher rainfall totals in the catchment, and totals outside the catchment were similar to the WSM3-BMJ scenarios.

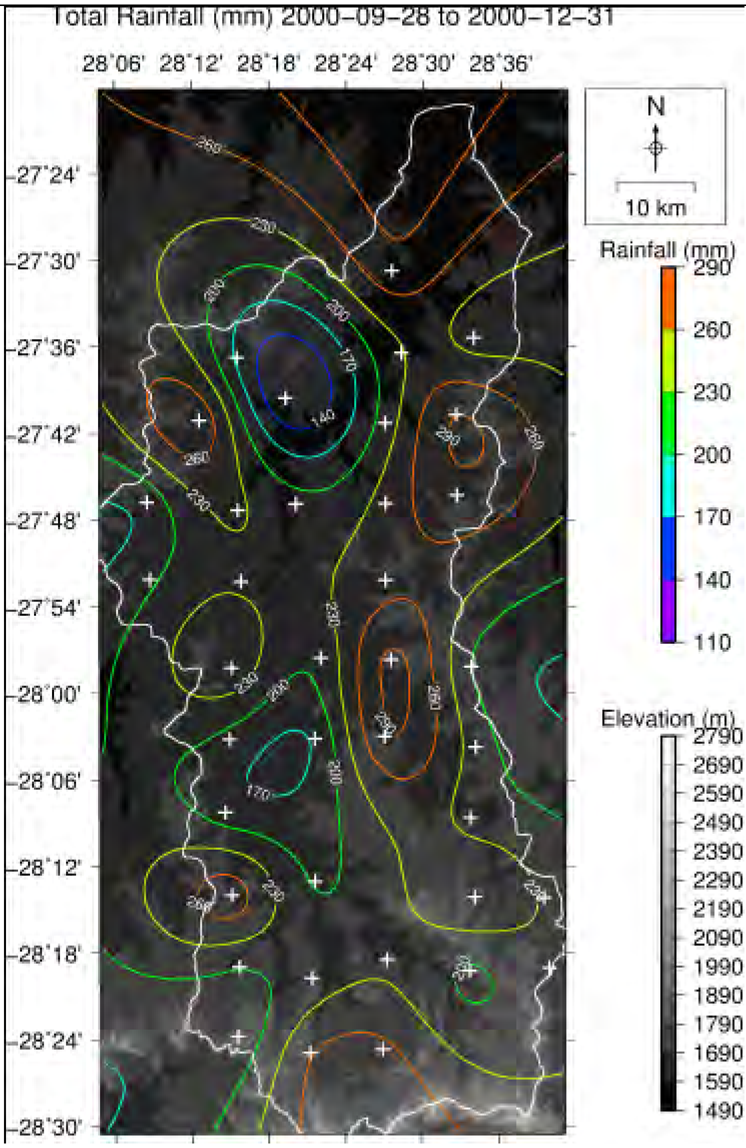

Figure 8-4: Observed total rainfall at Liebenbergsvlei from 2000-09-28 00:00:00 to 2000-12-31 23:00:00. Contours created using simple tracing of each contour through a grid.

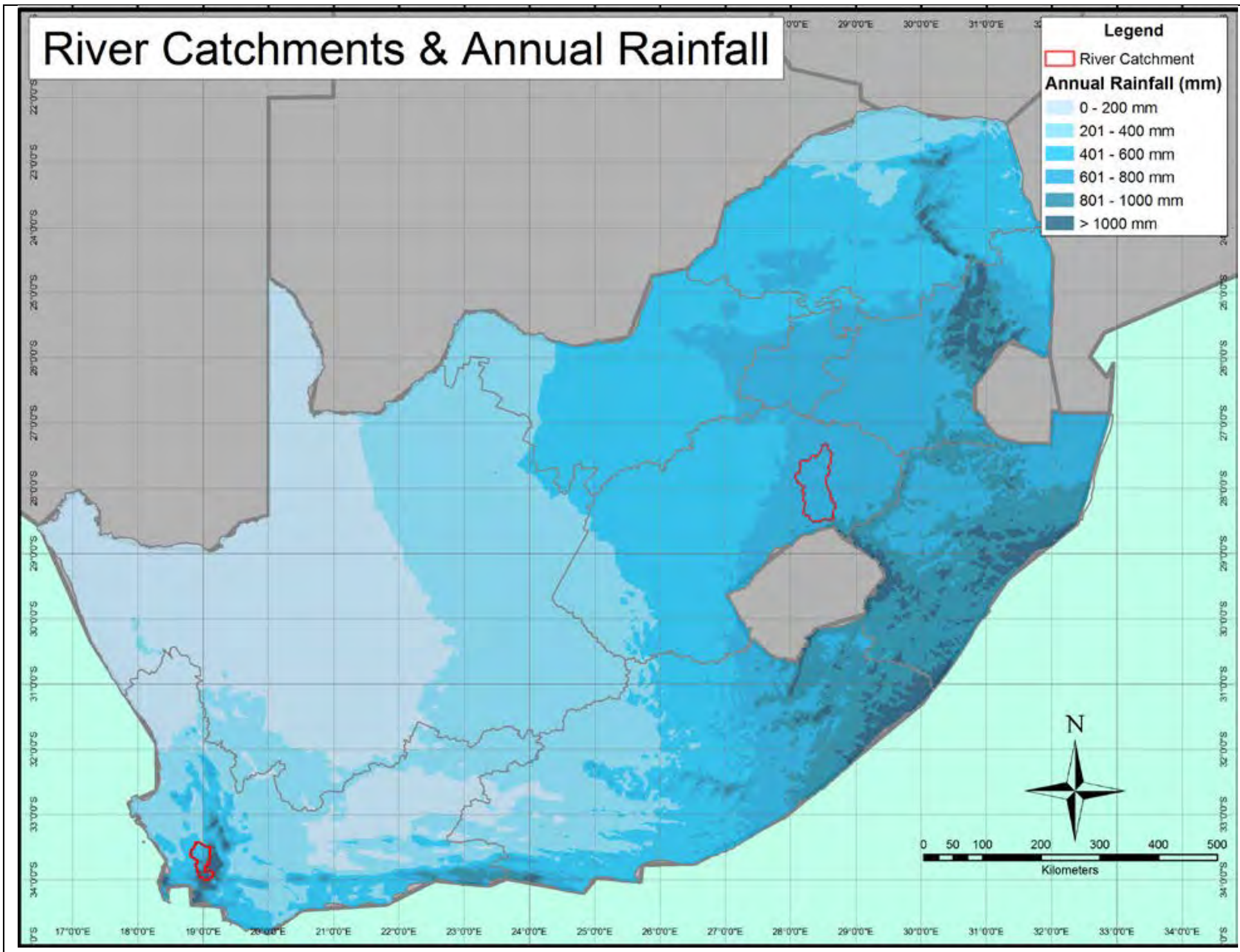

Figure 8-5: ARC annual rainfall map

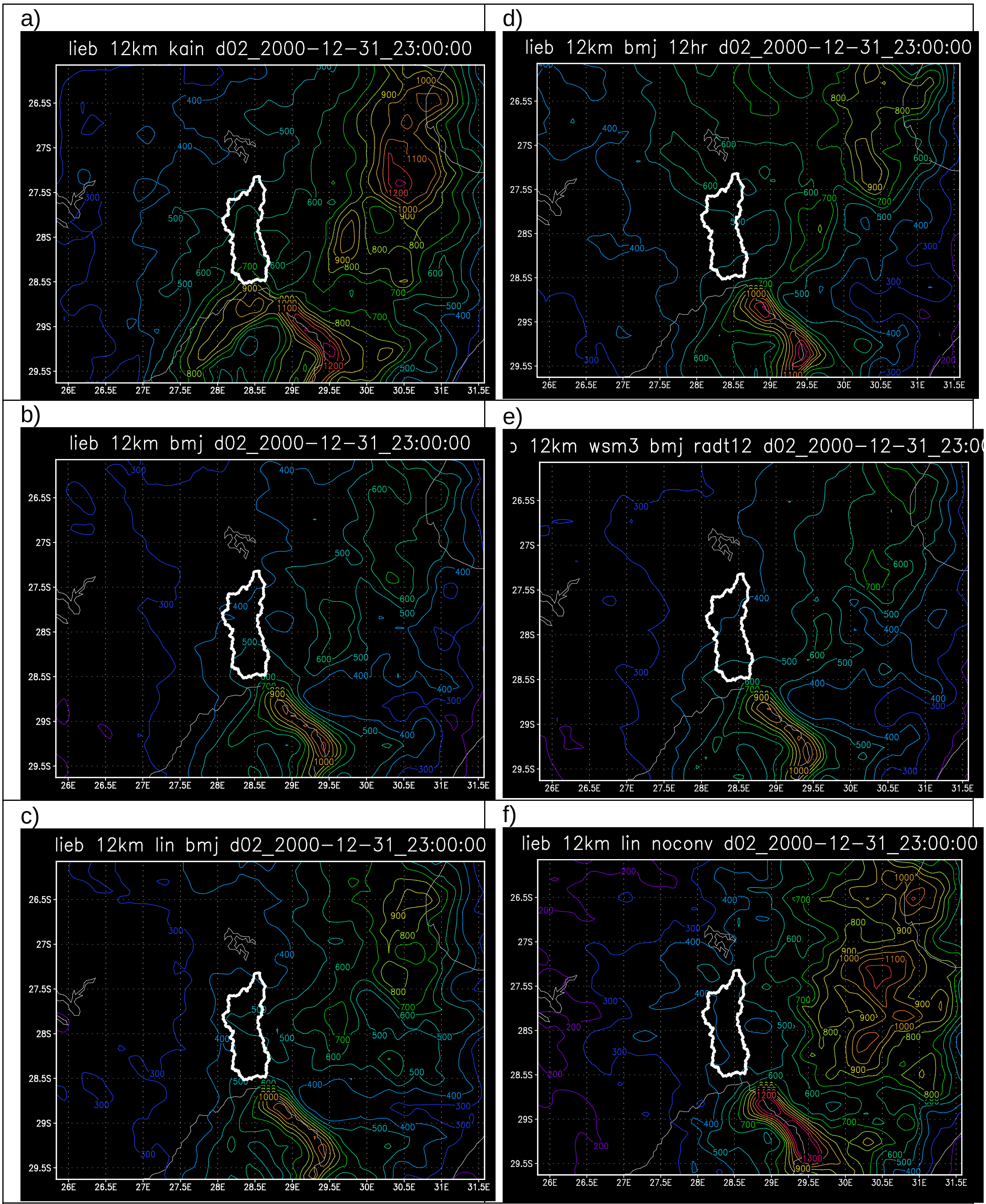

Figure 8-6: Total rainfall maps from WRF for 2000-09-28 00:00:00 to 2000-12-31 23:00:00 a) kain; b) bmj; c) lin bmj; d) bmj 12 hr; e) wsm3 bmj radt12; f) lin noconv

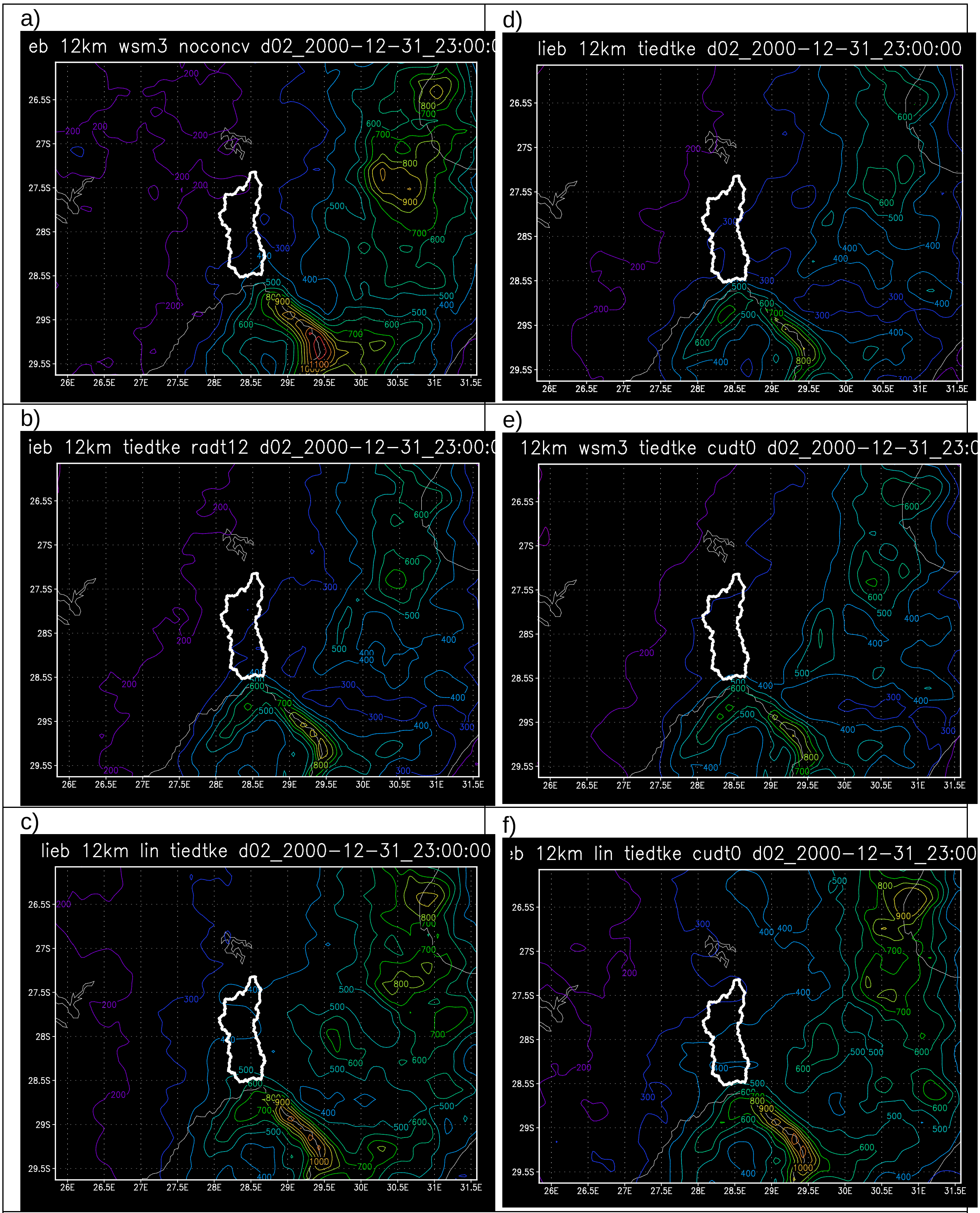

Figure 8-7: Total rainfall maps from WRF for 2000-09-28 00:00:00 to 2000-12-31 23:00:00 a) wsm3 noconcv; b) tiedtke radt12; c) llin tiedtke; d) tiedtke 12 hr; e) wsm3 tiedtke cud10; f) lin tiedtke cud10

Convective and Non-Convective Rainfall

The previous section dealt with rainfall totals from WRF. In this section, the rainfall totals are split into convective and non-convective components and presented alongside the total rainfall. This will demonstrate the relationship between the convective and microphysics schemes and the respective geographic influence of each.

Over the Liebenbergsvlei catchment, the majority of rainfall is expected to be convective, and the model should indicate this. However, the escarpment and lower lying areas are expected to experience rainfall from non-convective systems more frequently than the catchment. For the WSM3-Kain scheme, the majority of rainfall over the catchment was produced by convective rainfall (Figure 8-8). However, convective rainfall was predominant in the rest of the model domain, suggesting that the mechanism producing the rain is too sensitive, or easily triggered, producing overactive convective systems. This was the only scheme to show a much higher percentage contribution from convective rainfall.

For the BMJ scenarios it is shown that the progression of more frequent forcing of lateral boundary conditions and calls to radiation and cumulus physics solvers inhibits convective rainfall (Figure 8-8 and Figure 8-9). The relative contributions of convective and non-convective rainfall are more even, 300 mm and 200 mm respectively, than the Kain scenario. Additionally, non-convective rainfall is seen to produce the majority of rainfall over the escarpment, which is opposite to what was observed with the Kain scenario.

The Lin-BMJ schemes show similar results to the WSM3-BMJ schemes with the exception that the non-convective rainfall is more active over the escarpment and low lying areas. The WSM3-Tiedtke schemes effectively switch off non-convective rainfall over the catchment. The only notable non-convective rainfall is over the escarpment where topography forces water vapour to rise, cool and condense. Otherwise, convective rainfall contributes most of the precipitation for the remainder of the area displayed. The Lin-Tiedtke scenarios are interesting as there seems to be an equal battle for, or allocation of, moisture and consequently rainfall to convective and non-convective physics. This is in contrast to Lin-BMJ, where most rainfall is non-convective, and WSM3-Tiedtke, where non-convective rainfall is almost switched off for the catchment.

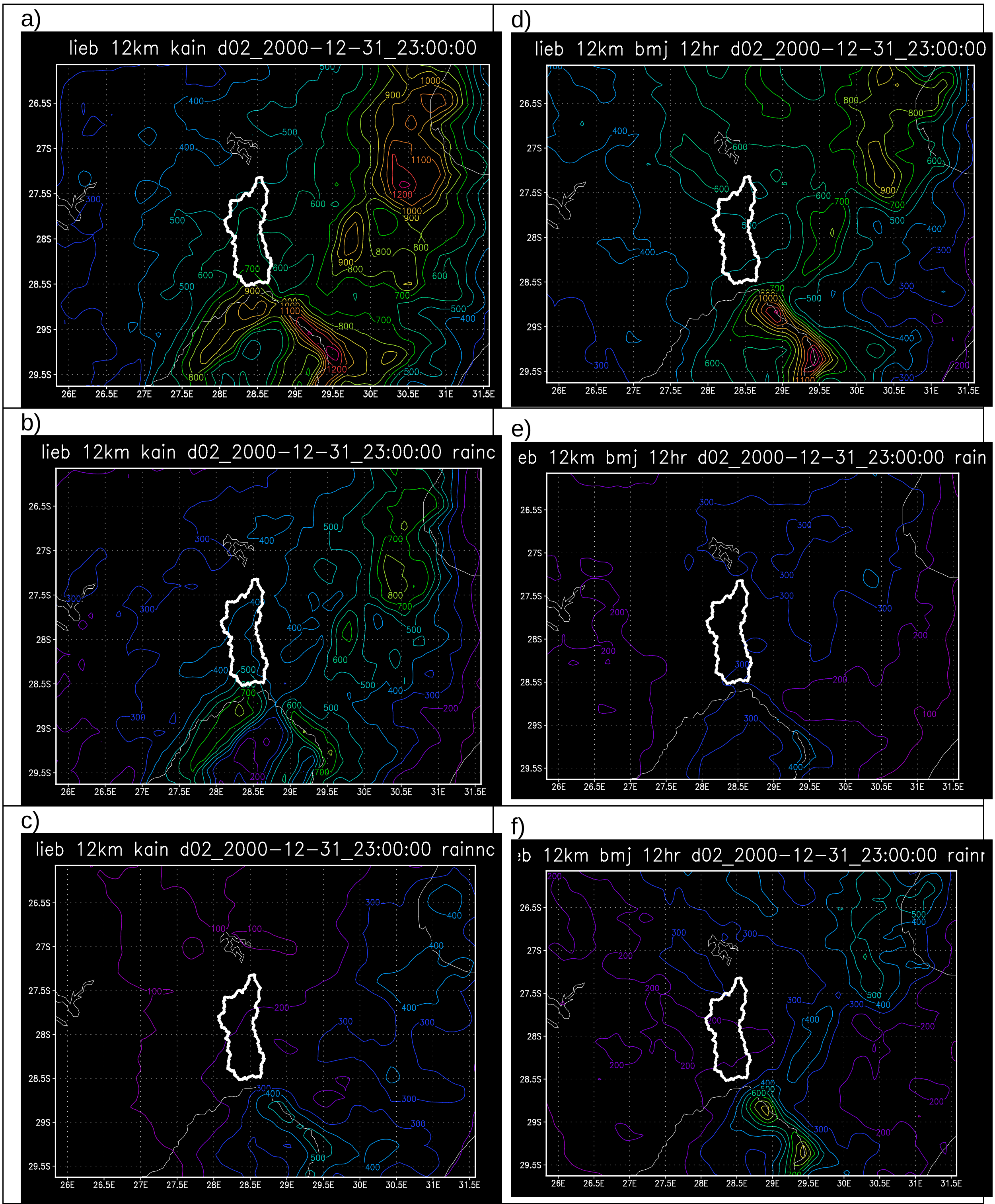

Figure 8-8: Rainfall maps of total rainfall, rainc and rainnc for
a) kain ; b) kain rainc; c) kain rainnc; d) bmj 12 hr rain total; e) bmj 12 hr rainc; f) bmj 12 hr rainnc

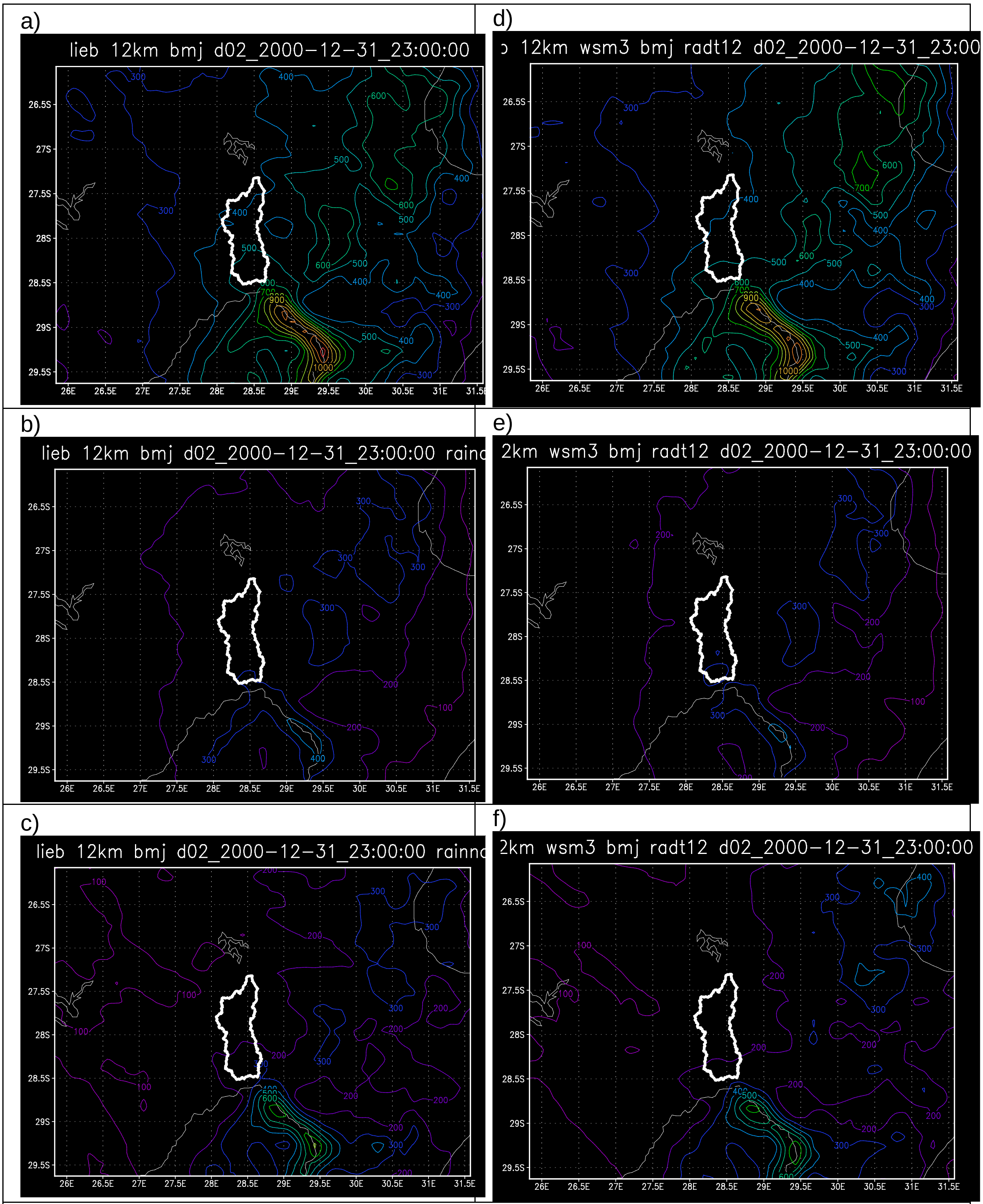

Figure 8-9: Rainfall maps of total rainfall, rainc and rainnc for
a) bmj ; b) bmj rainc ; c) bmj rainnc ; d)wsm3 bmj rad 12 ; e) wsm3 bmj rad 12 ; f) wsm3 bmj rad 12.

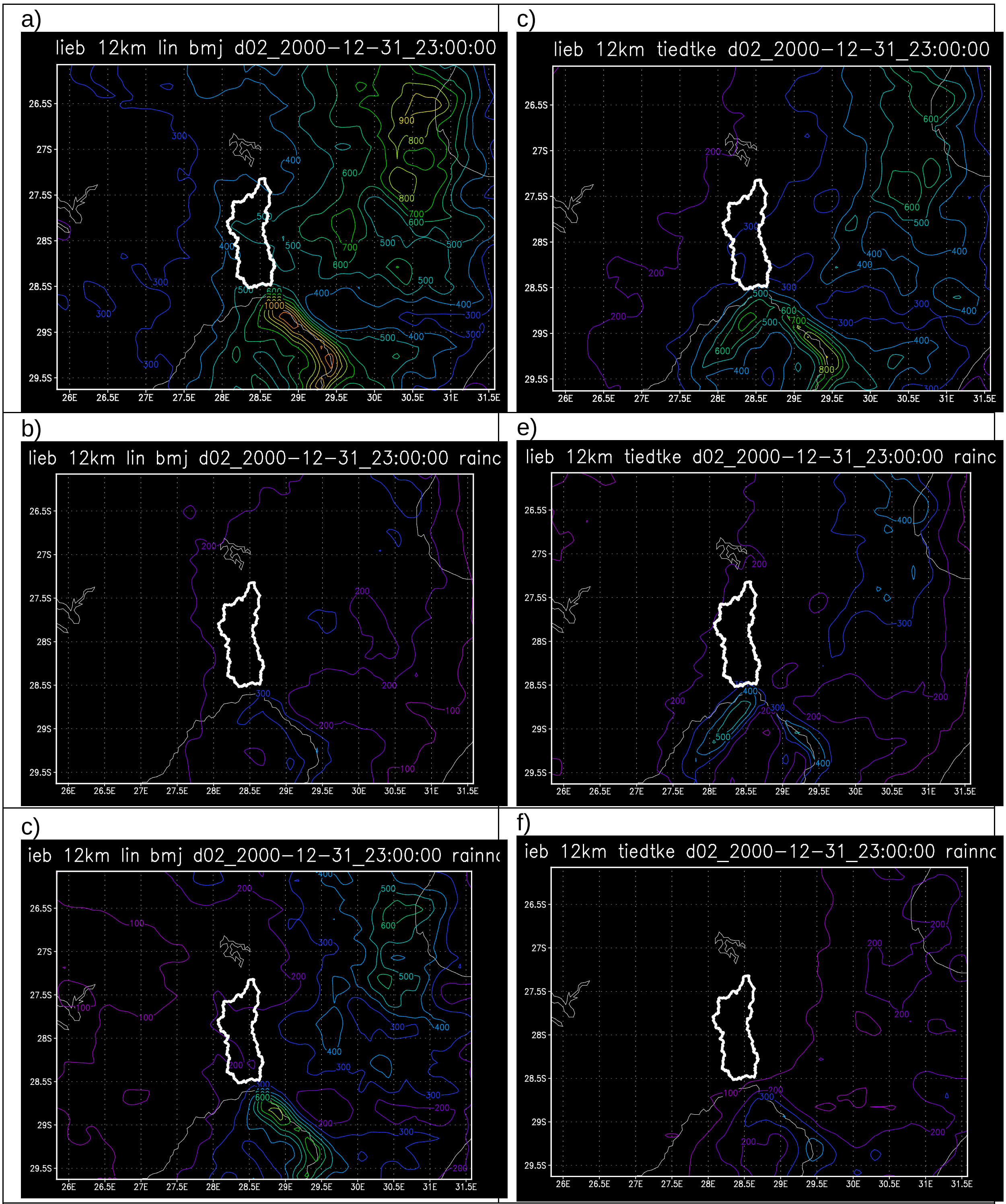

Figure 8-10: Rainfall maps of total rainfall, rainc and rainnc for a)bmj ; b) bmj rainc; c)lin bmj rainnc ; d)tiedtke ; e)tiedtke rainc ; f) tiedtke rainnc.

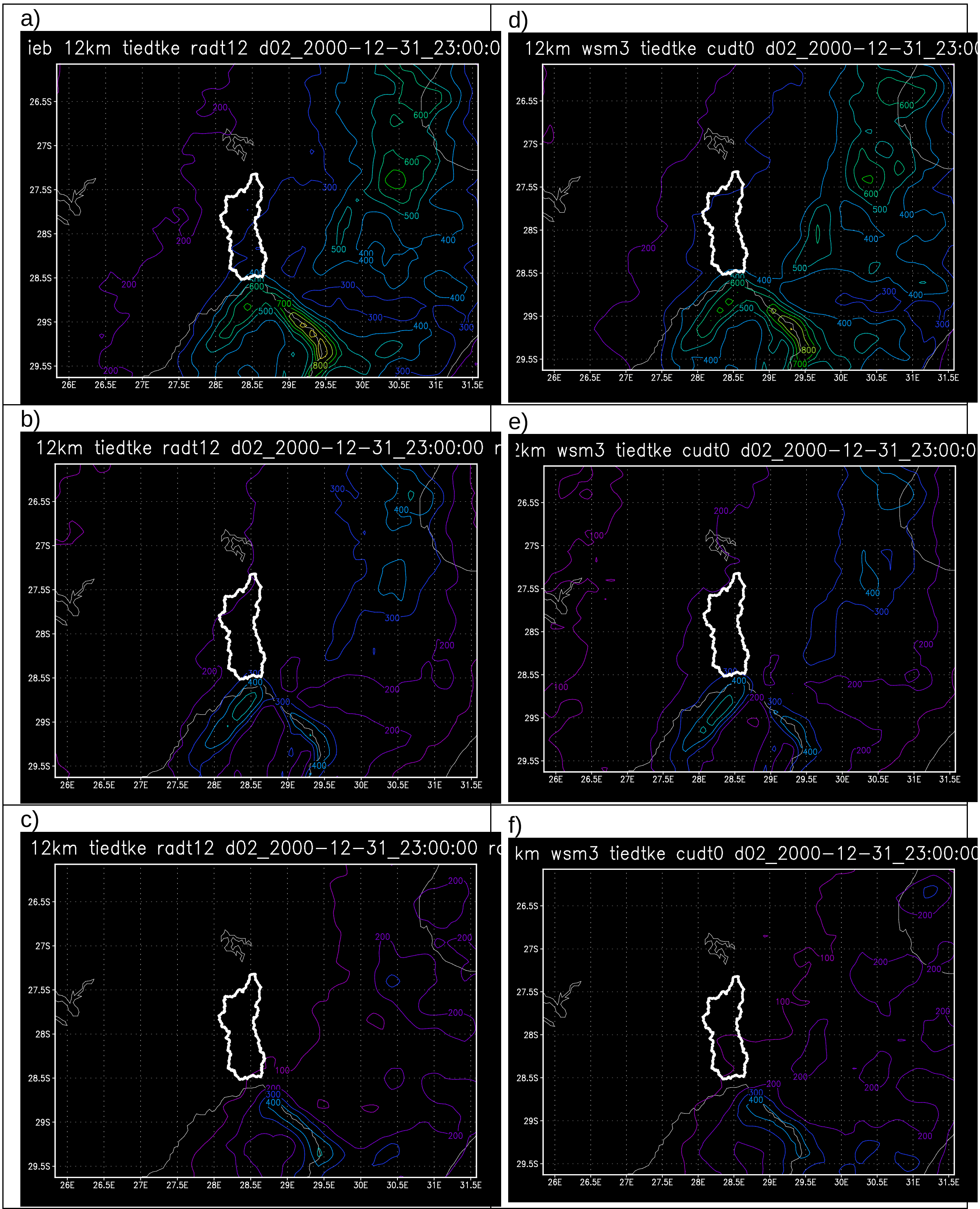

Figure 8-11: Rainfall maps of total rainfall, rainc and rainnc for
a) tiedtke radt12; b) tiedtke radt12 rainc ; c) tiedtke radt12 rainnc ;
d) tiedtke cudt0; e) tiedtke cudt0 rainc ; f) tiedtke cudt0 rainnc .

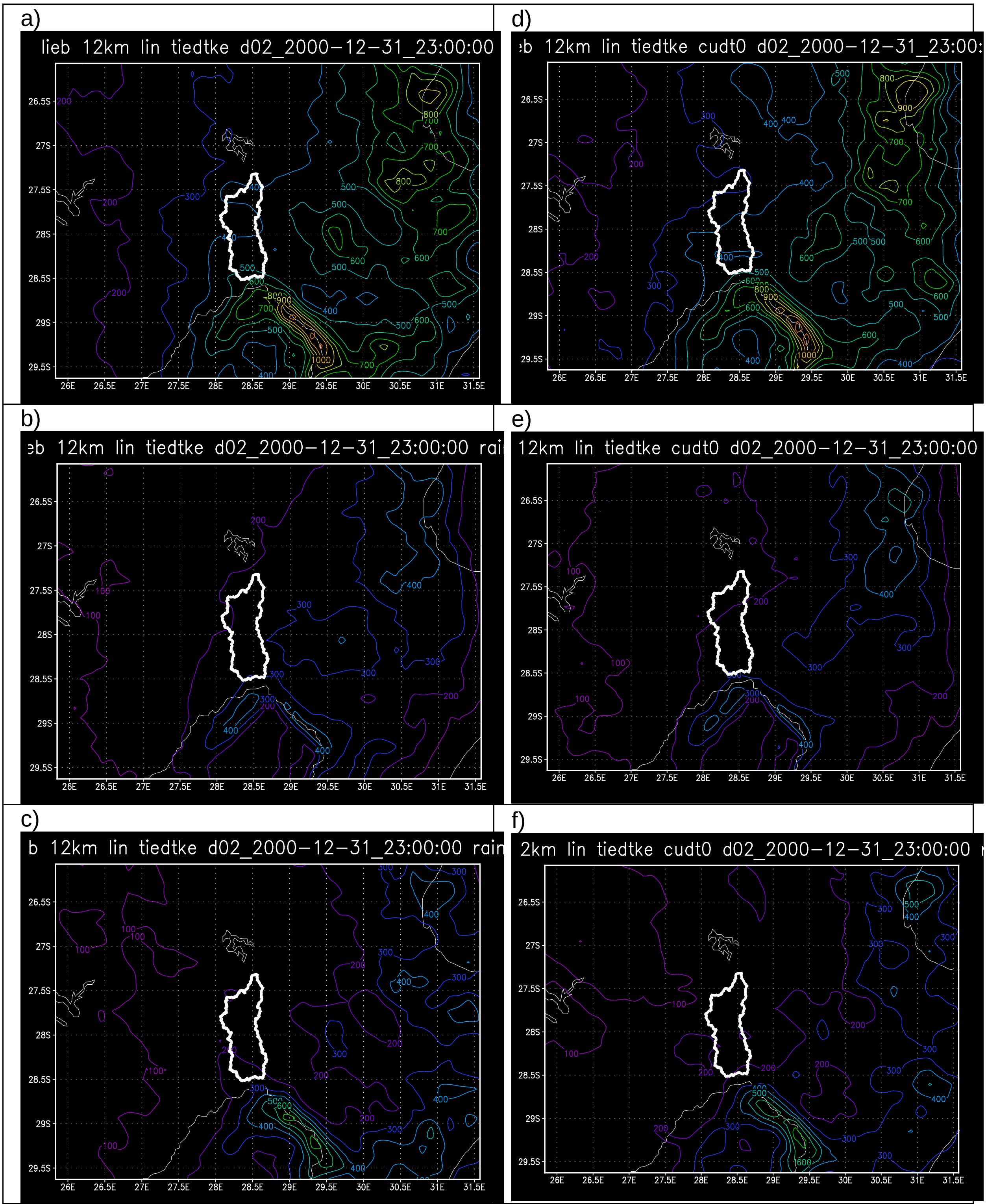

Figure 8-12: Rainfall maps of total rainfall, rainc and rainnc for
a) Lin-tiedtke ; b) Lin-tiedtke rainc; c) Lin-tiedtke rainnc;
d) Lin-tiedtke-cudt0 ; e) Lin-tiedtke-cudt0 rainc ; f) Lin-tiedtke-cudt0 rainnc.

8.4 Liebenbergsvlei River Catchment Diurnal Cycle

In this section, the diurnal cycle of rainfall is presented for the Liebenbergsvlei catchment with the intention to show when the model is over predicting, and why. Graphs represent the average rainfall of all observations from rain gauges within the catchment and the corresponding WRF model grid cells.

The observed rainfall (blue line; identical in all graphs) shows a clear diurnal cycle of low rainfall before 1200 UTC followed by larger rainfall totals until 2100 UTC. This is typically referred to as afternoon thundershowers over the Highveld. There was a smaller rain event recorded from 1000 to 1100 UTC. In general the modelled convective rainfall (green line) starts too early for all scenarios, starting at 0700 UTC and ending between 1600 and 1800 UTC. It must be noted that the Kain scheme produced convective rainfall about 2 hours later than the other schemes. Convective rainfall occurs during daylight hours and appears to be linked to surface heating in the model. The largest overestimation occurs during these hours and is due to convective rainfall.

Non-convective rainfall (cyan line) follows a different diurnal cycle to convective rainfall, producing most rainfall totals between 1500 and 2300 UTC. This coincides with observed totals from about 1700 UTC for some cases. Exceptions to this pattern are the WSM3-Kain and WSM3-Tiedtke, where most rainfall is produced by convective physics. Increased frequency of forcing lateral conditions and calls to the radiation scheme affected the timing and totals of non-convective rainfall. In the BMJ-12hr scenario, non-convective rainfall over estimated totals from 0000 to 0900 UTC. This was decreased with the BMJ-6hr and BMJ-radt12. Additionally, non-convective rainfall started later, moving from 1300 UTC to 1500 UTC for BMJ-12hr and BMJ-6hr respectively. For the WSM3-Tidetke schemes, the more frequent calls to physics solvers increased afternoon non-convective rainfall (1500 to 2300 UTC), resulting in more accurate simulations of observed totals.

It must be noted the scheme that produced the most realistic diurnal cycle was the Lin-Tiedtke-cudt0. Apart from peak early morning non-convective totals, which is not present in any other scheme, the remainder of the WRF rainfall totals follows the observed, albeit it an over estimate for day time hours.

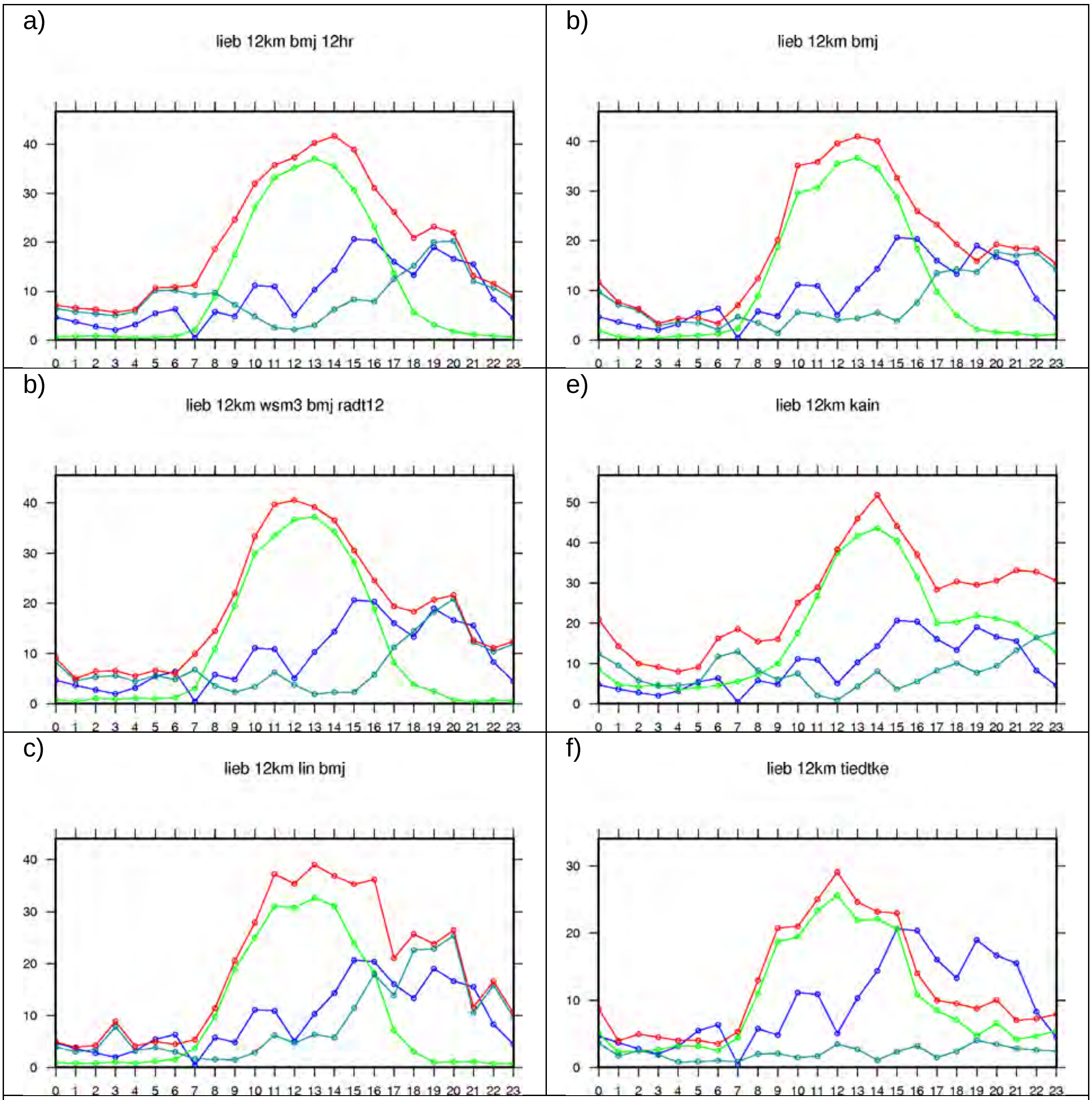

Figure 8-13: Diurnal cycle of average rainfall over the catchment. Blue=Observed, Red=WRF total, Green=WRF Convective, Cyan= WRF Non-convective.
Wsm3-Bmj 12hr ; b) wsm3-bmj ; c) Lin-bmj ; d)wsm3-bmj 6hr ; e)wsm3-kain ; f)wsm3-tiedtke
.

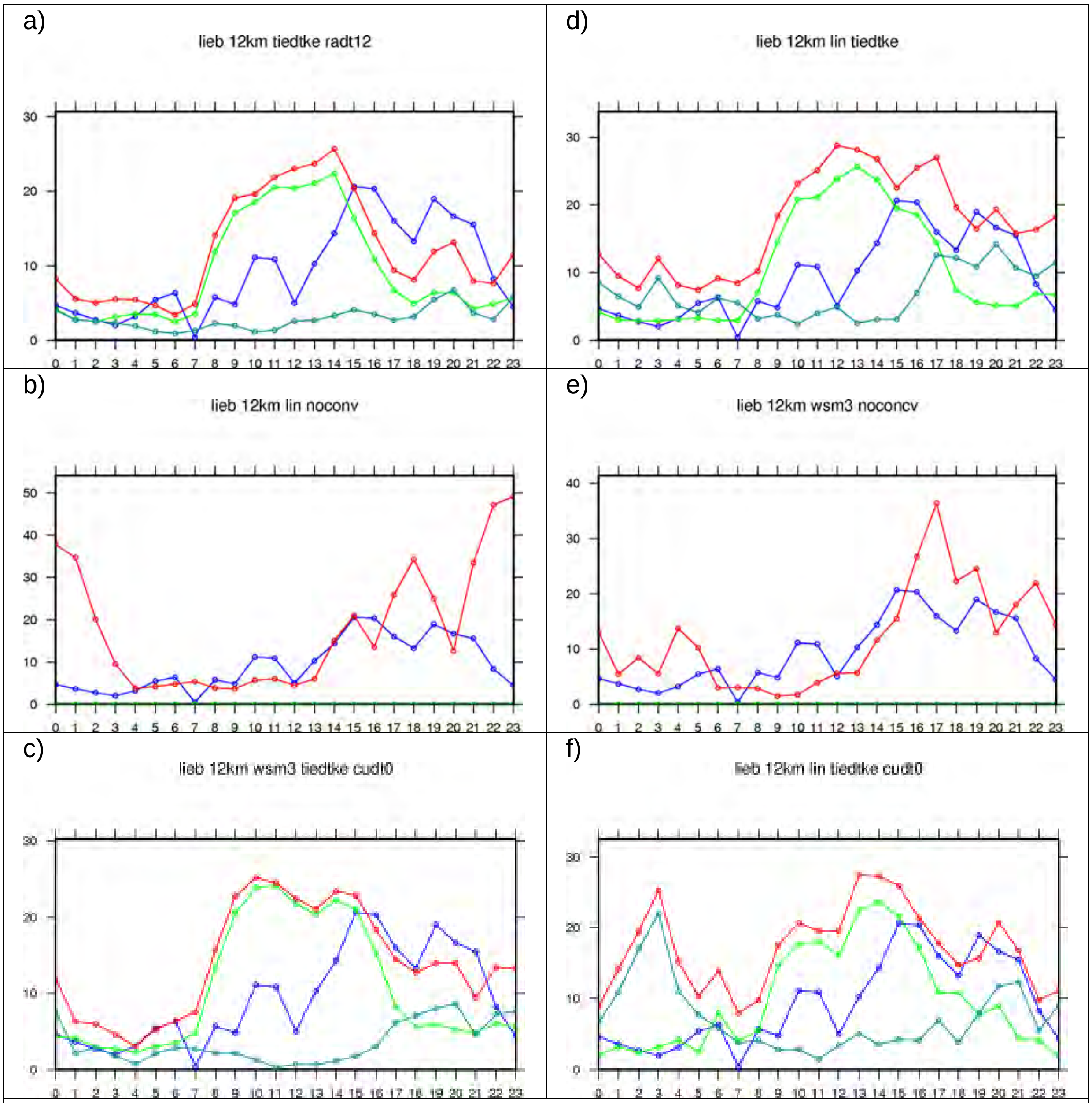

Figure 8-14: Diurnal cycle of average rainfall over the catchment. Blue=Observed, Red=WRF total, Green=WRF Convective, Cyan= WRF Non-convective. a)wsm3-tiedtke-radt12 ; b)lin noconv ; c) wsm3-tiedtke-cudt0 ; d)lin-tiedtke ; e) wsm3 noconv; f) lin-tiedtke-cudt0 .

8.5 Liebenbergsvlei River Catchment Scatter Plots

In this section we match model to observed rainfall events in time for 24 hour totals, where as previously we have looked at diurnal averages or rainfall totals over 3 months. This approach gives an indication of when the model is over predicting, and by how much. Rainfall totals are divided using thresholds of 1, 5, 10, 25 and >25 mm. Totals represent an average 24 hour total for the catchment.

The Kain scheme produces too much rainfall for event less than 5 mm, including false alarms of 15 mm or more. No other scheme produces false alarms of that magnitude. The WSM3-BMJ schemes produce a greater number of hits for the 5 mm threshold, but often produce results of 10 mm or greater where the observed is < 5 mm. The WSM3-Tiedtke schemes, on the other hand, produce events < 10 mm when the observed is < 5 mm. In other words, the extent to which the model over predicts is not as extreme. Also notable for WSM3-Tiedtke-cudt0 is that the false alarms totals are around 5 mm, while the other scenarios have much higher rainfall totals from false alarms.

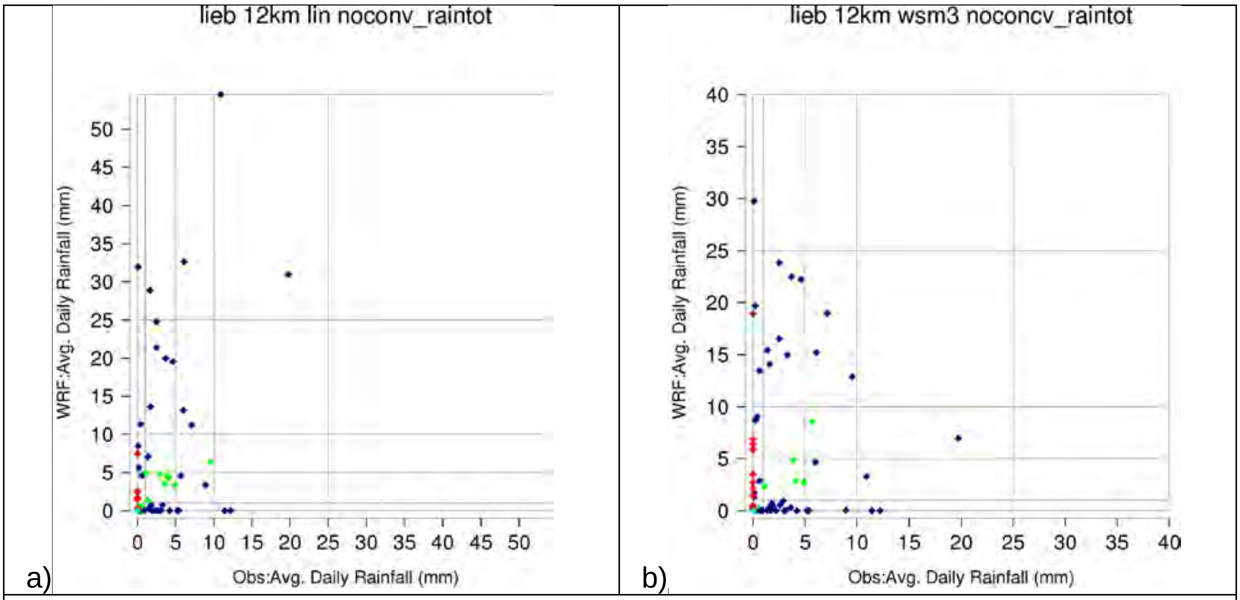

Figure 8-15: Scatter plots of 24hour rainfall for a) Lin noconv and; b) WSM noconv. Green=hit inside category, Blue=hit outside category, Red=False Alarm, Cyan=Correct negative

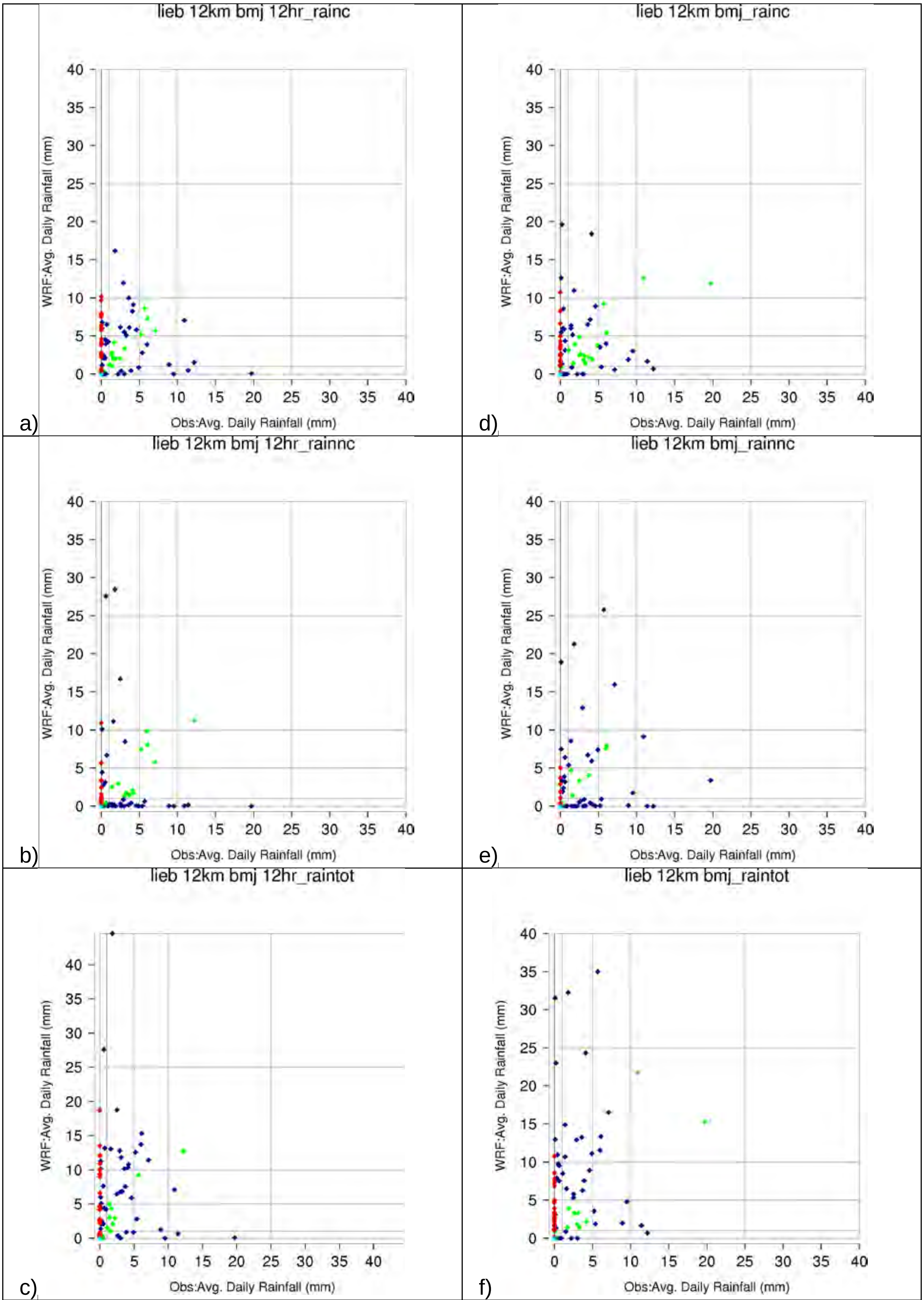

Figure 8-16: Scatter plots of 24hour rainfall for rainc rainnc and rain total
a)wsm3-bmj 12hr rainc; b)rainnc ; c)rain total ; d)wsm3-bmj rainc ; e)rainnc; f)rain total.
Green=hit inside category, Blue=hit outside category, Red=False Alarm, Cyan=Correct negative

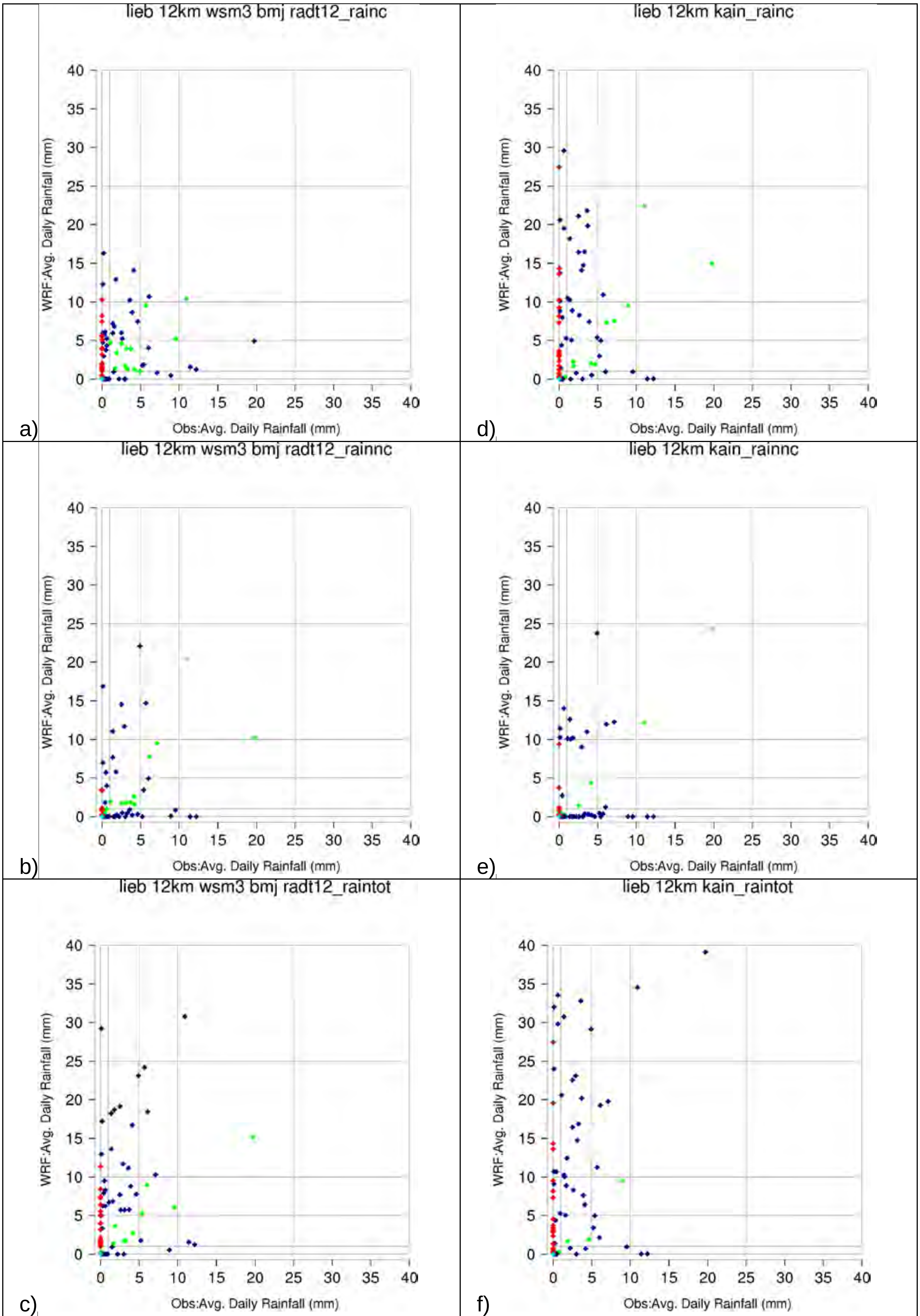

Figure 8-17: Scatter plots of 24hour rainfall for rainc rainnc and rain total a)wsm3-bmj-radt12 rainc; b)rainnc ; c)rain total ; d)wsm3-kain rainc ; e)rainnc; f)rain total.

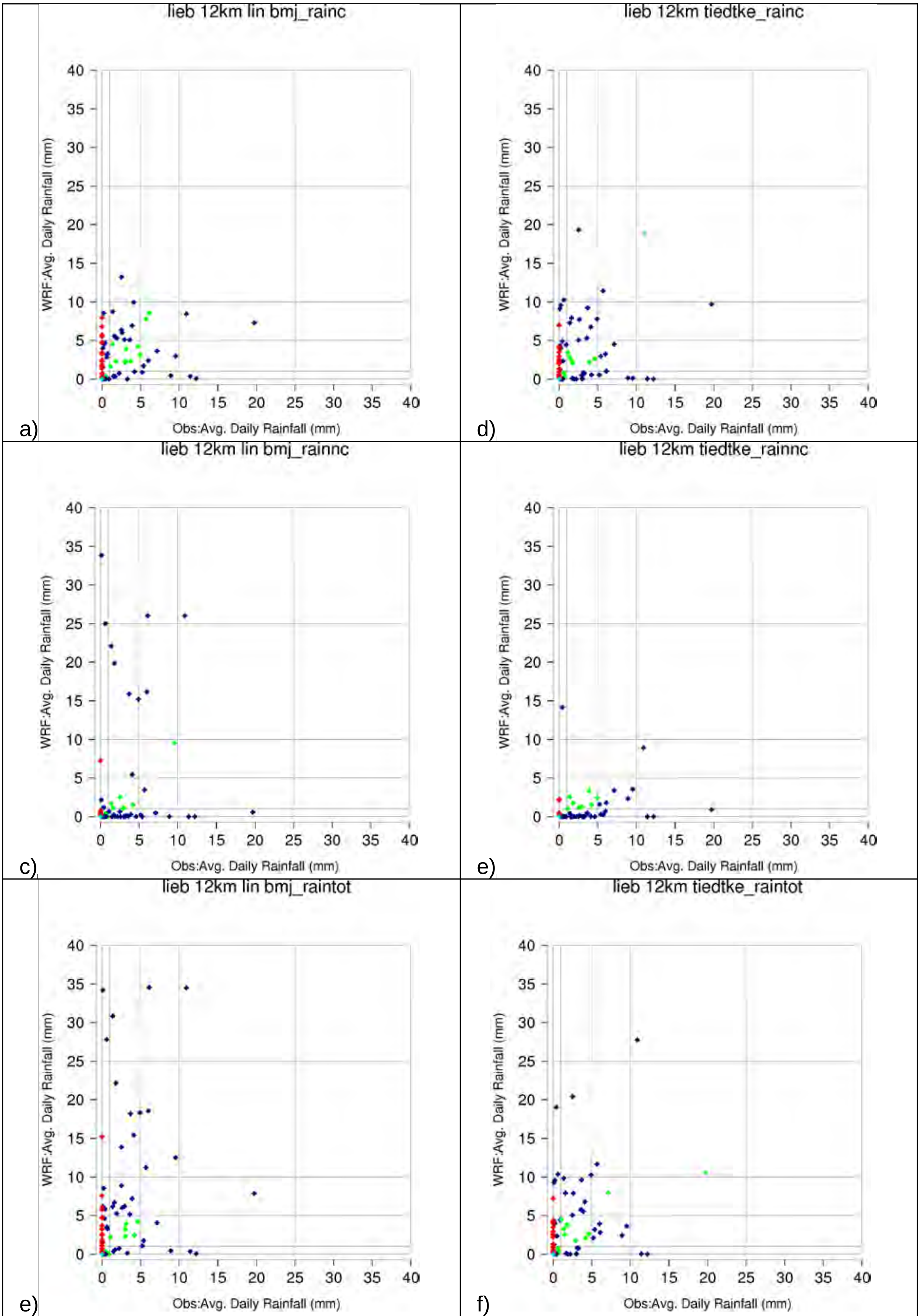

Figure 8-18: Scatter plots of 24hour rainfall for rainc rainnc and rain total
a)Lin-bmj 12hr rainc; b)rainnc ; c)rain total ; d)wsm3-tiedtke rainc ; e)rainnc; f)rain total.

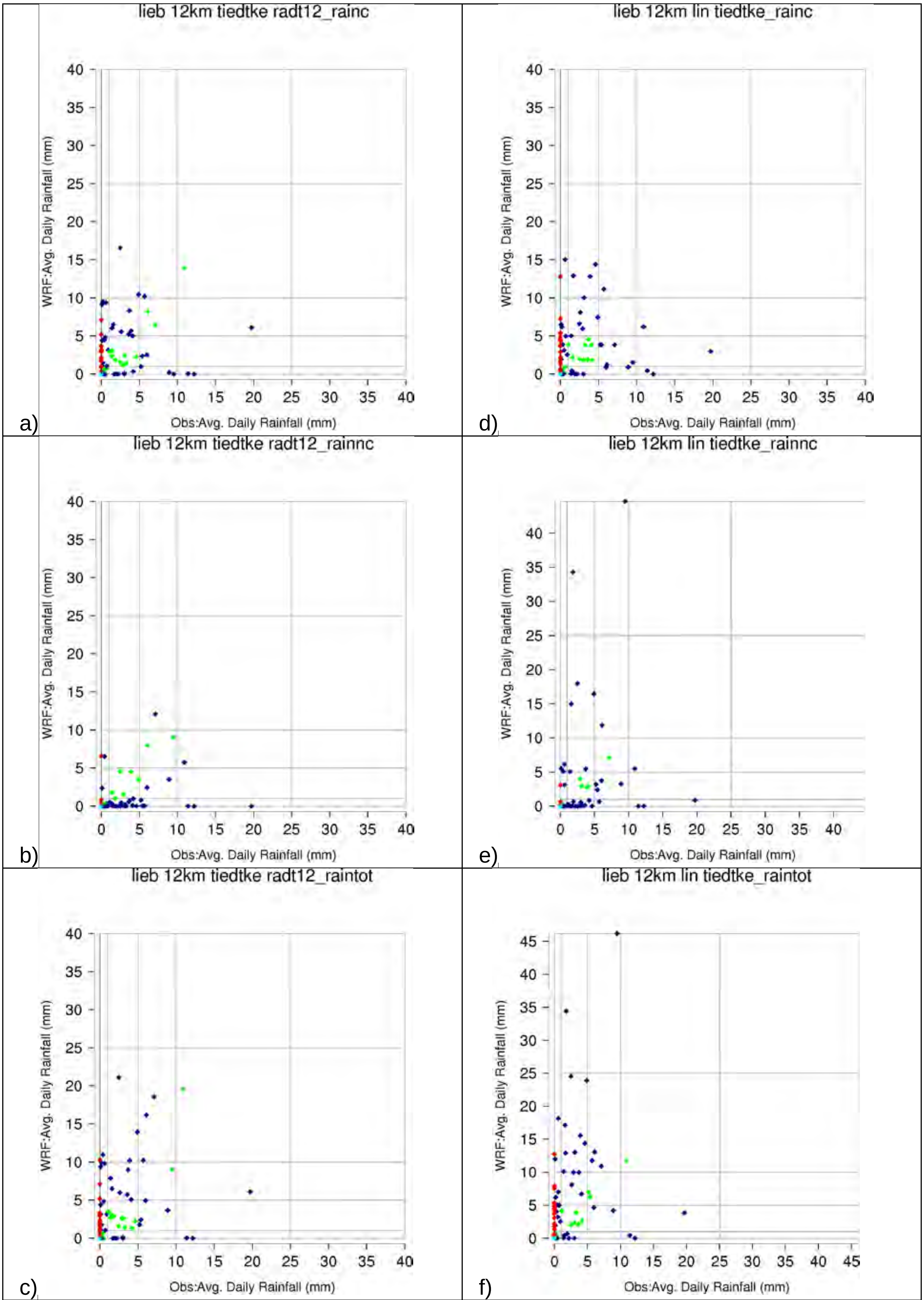

Figure 8-19: Scatter plots of 24hour rainfall for rainc rainnc and rain total
a)wsm3-tiedtke-radt12 12hr rainc; b)rainnc ; c)rain total ; d)Lin-tiedtke rainc ; e)rainnc; f)rain total

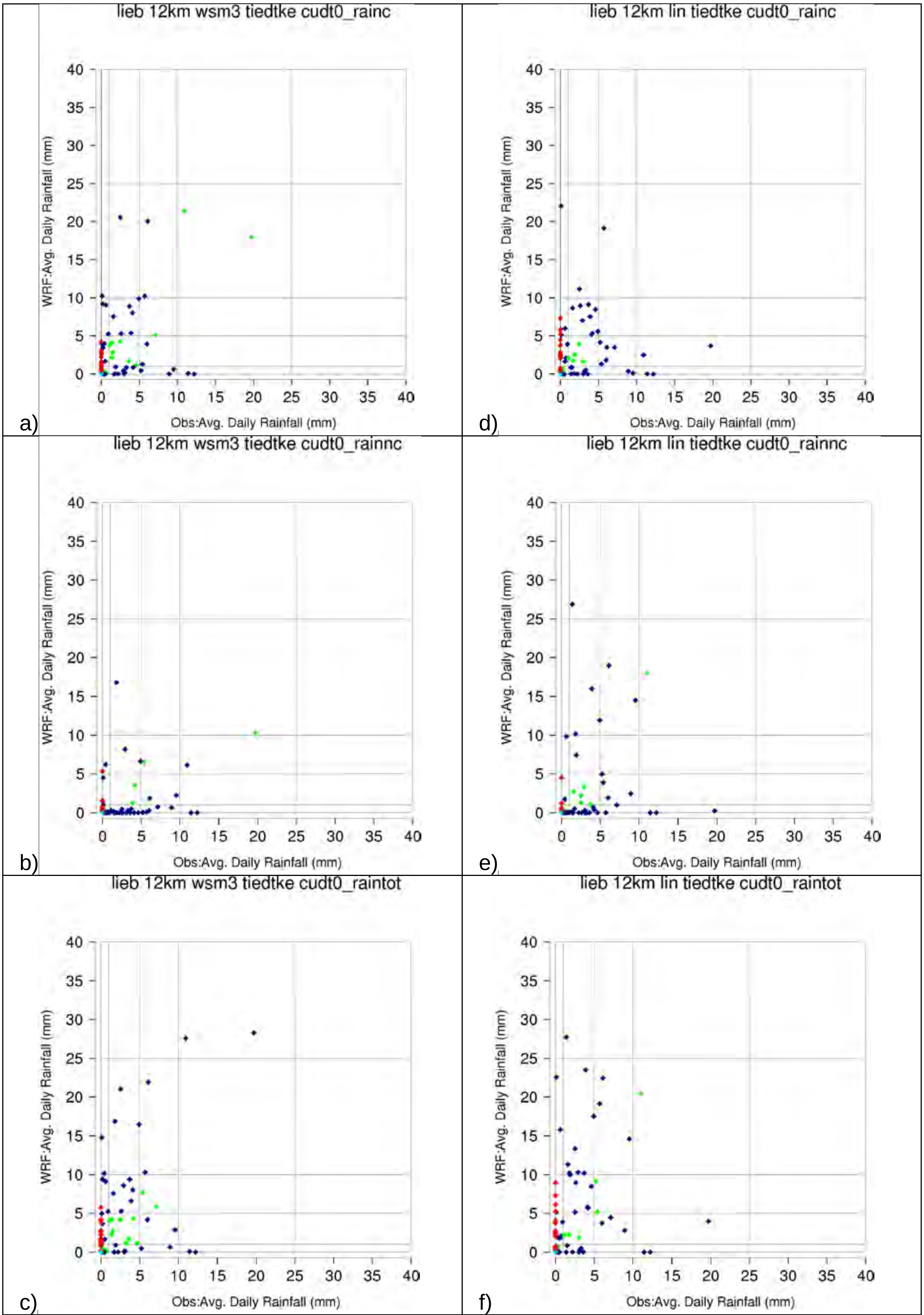

Figure 8-20: Scatter plots of 24hour rainfall for rainc rainnc and rain total
a)wsm3-tiedtke-cudt0 12hr rainc; b)rainnc ; c)rain total ; d)Lin-tiedtke-cudt0 rainc ; e)rainnc; f)rain total

8.6 Berg River Rain Days and Bias: WRF 12 km

Overall, the Berg scenarios performed much better than Liebenbergsvlei as the rainfall systems are synoptic scale non-convective rainfall which is treated well by the microphysics schemes in the model. All bias results for a 24 hour period were less than 2 mm for all parameterisation schemes (Figure 8-21). The Berg River experienced 28 rain days out of the possible maximum of 92, of which only the Kain and Tiedtke schemes produced excess rain days. Both schemes produced a greater number of false alarms than the BMJ scenarios (Figure 8-22), which produced daily bias results of less than 1 mm.

The probability of detection (POD) is approaching the ideal value of 1 for all scenarios (Figure 8-23), which is similar to the Liebenbergsvlei results presented in (Figure 8-3). However, unlike the Liebenbergsvlei results, which achieved high POD due to high false alarm counts, the Berg results have a low false alarm ratio (Figure 8-23). Thus we can conclude that the WRF model simulates rainfall formation more adequately over the Berg catchment, and that convective rainfall over the Liebenbergsvlei remains challenging

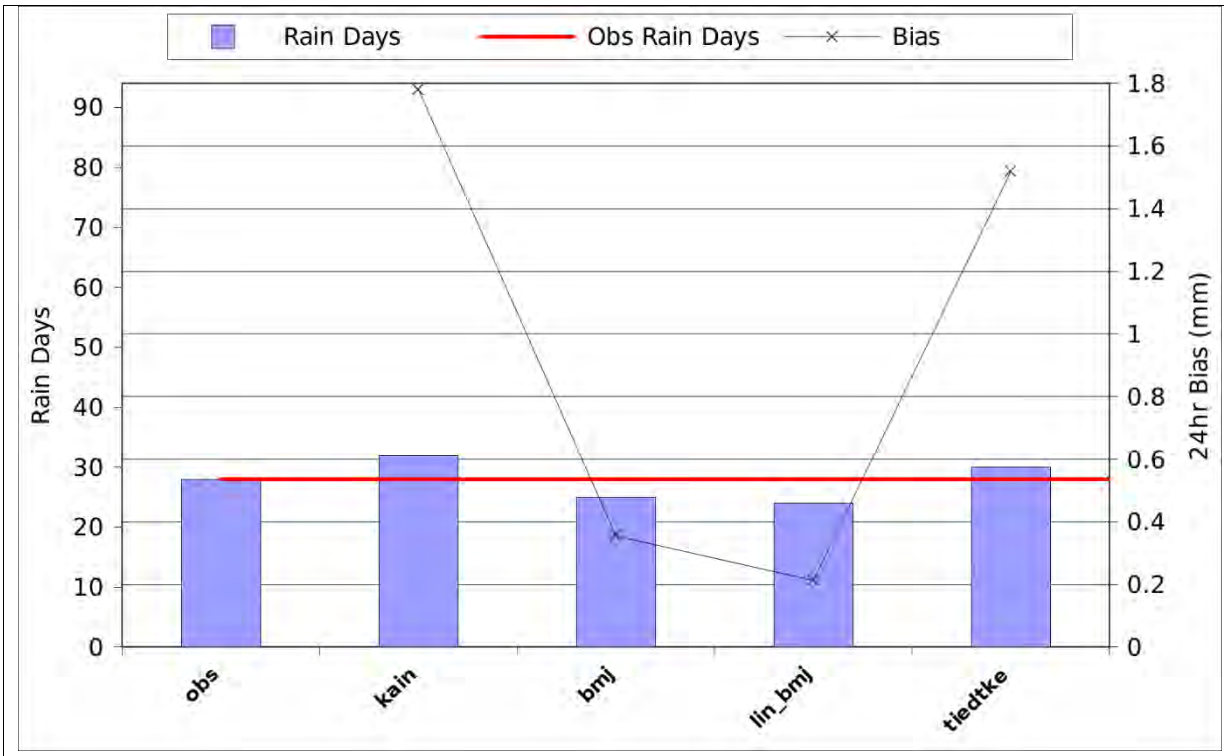

Figure 8-21: Rain days (>1 mm/d threshold) and 24hr bias for Berg River Catchment 12 km WRF domain.

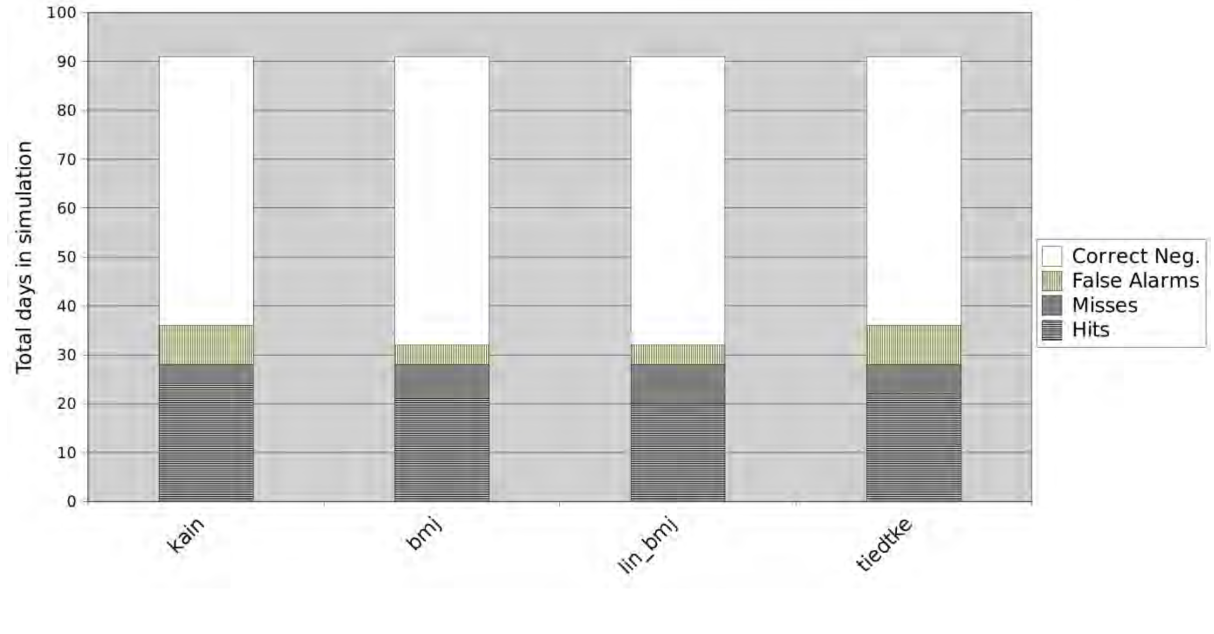

Figure 8-22: Contingency tables counts of hits, misses, false alarms and correct negative (no rainfall) for daily threshold of >1 mm/d for Berg River catchment 12 km WRF domain.

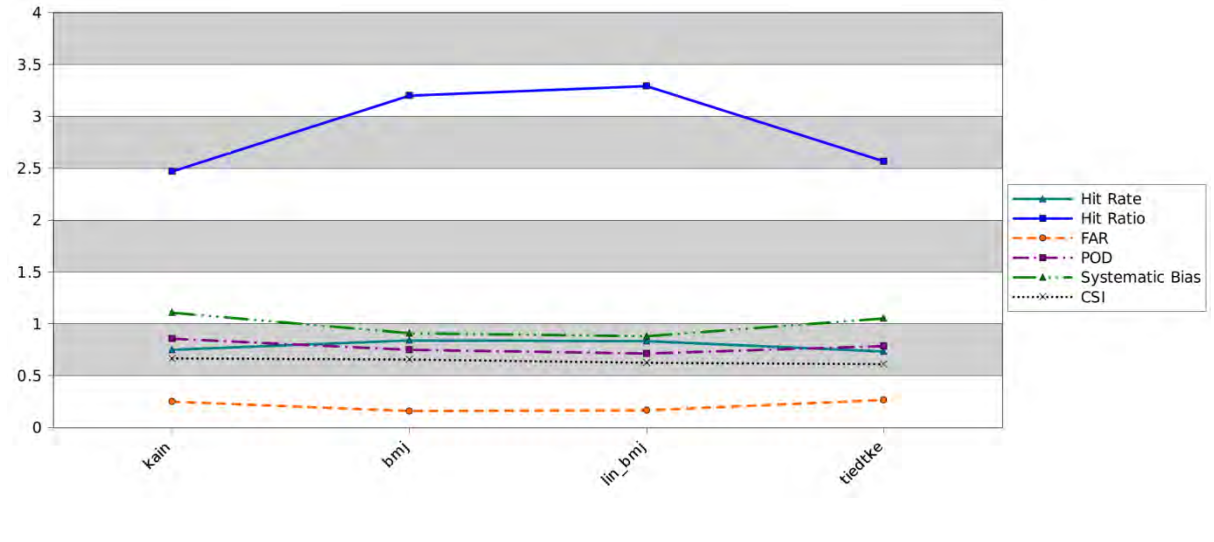

Figure 8-23: Scores derived from contingency table counts (>1 mm/d threshold) for Berg River 12 km WRF domain. Optimum score is 1 for Hit Rate, POD (probability of detection) and CSI (critical success index). Ideal score for FAR (false alarm ratio) is 0.

8.7 Berg River Rainfall Maps

Firstly, the Berg River receives winter rainfall and annual totals are higher than for Liebenbergsvlei. There is a rainfall gradient, as the catchment is in a complex area with respect to rainfall (Figure 8-5), from South East to the drier North West. Observed rainfall totals from May to July 2000 range from 183 to 477 mm (Figure 8-24).

Modelled totals for the same period range from 200 to 400 mm for four modelled scenarios (Figure 8-25). The 24 hour bias is less than 2 mm for all scenarios; 0.355 for WSM3-BMJ, 1.780 for WSM3-Kain, 0.214 for Lin-BMJ and 1.520 for WSM3-Tiedtke.

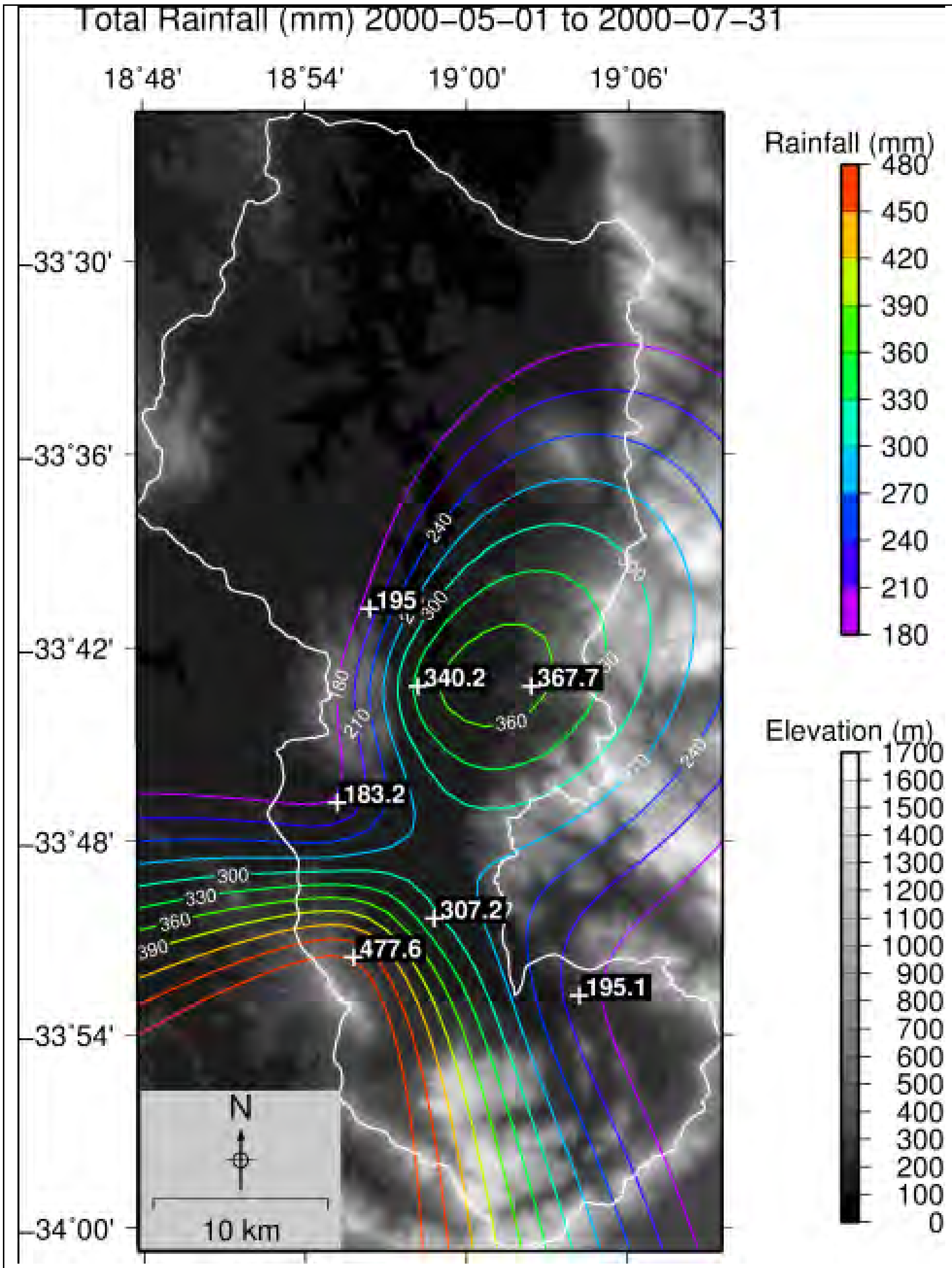

Figure 8-24: Observed rainfall over the Berg River from 2000-05-01 to 2000-07-31. Contours created using simple tracing of each contour through a grid.

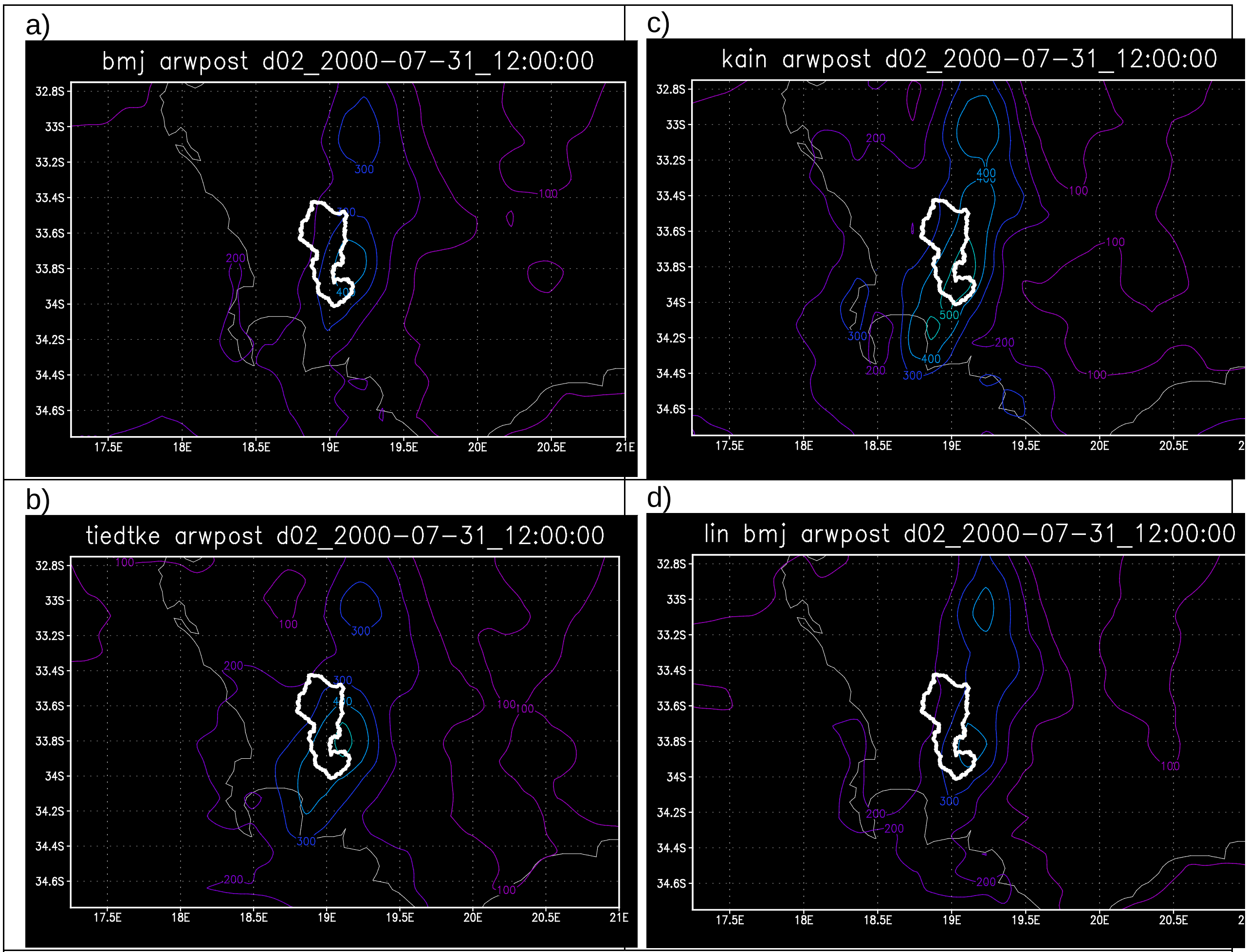

Figure 8-25: Berg River WRF results for a)WSM3-BMJ ; b)WSM3-Tiedtke ; c) WSM3-Kain; d) .Lin-BMJ

8.8 Berg River Diurnal Cycle

There is no obvious diurnal cycle in observed rainfall as was seen for Liebenbergsvlei (Figure 8-26). Furthermore, convective rainfall is not triggered as easily in the model and most rainfall is produced by non-convective physics.

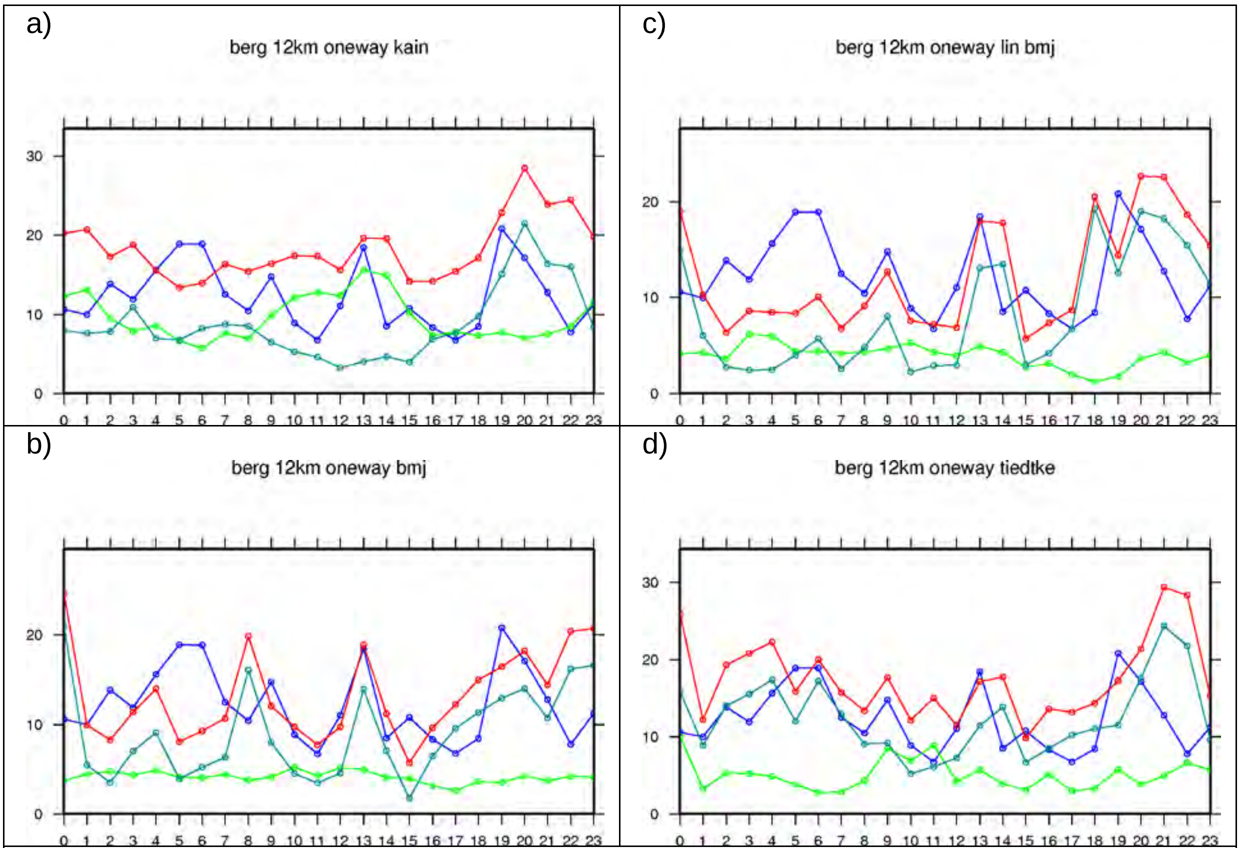

Figure 8-26: Diurnal cycle of average rainfall over the catchment. Blue=Observed, Red=WRF total, Green=WRF Convective, Cyan= WRF Non-convective.
a)wsm3-kain ; b) wsm3-bmj; c) lin-bmj; d) wsm3-tiedtke

8.9 Berg River Catchment Scatter Plots

The Kain and Tiedtke schemes both produce over predictions for daily rainfall between 20 and 25 mm, which are not observed in the BMJ scenarios (Figure 8-27). Rainfall totals are divided using thresholds of 1, 5, 10, 25 and >25 mm. Totals represent an average 24 hour total for the catchment. Furthermore, two days occurred where observed rainfall exceeded 25 mm. For one of these events, Kain and Tiedtke produced totals in excess by 15 to 25 mm. These single overestimations could be responsible for daily bias results exceeding 1 mm. Nevertheless, the BMJ scenarios performed much better for events between 10 and 25 mm and >25 mm, as indicated by the green dots in Figure 8-27b and d.

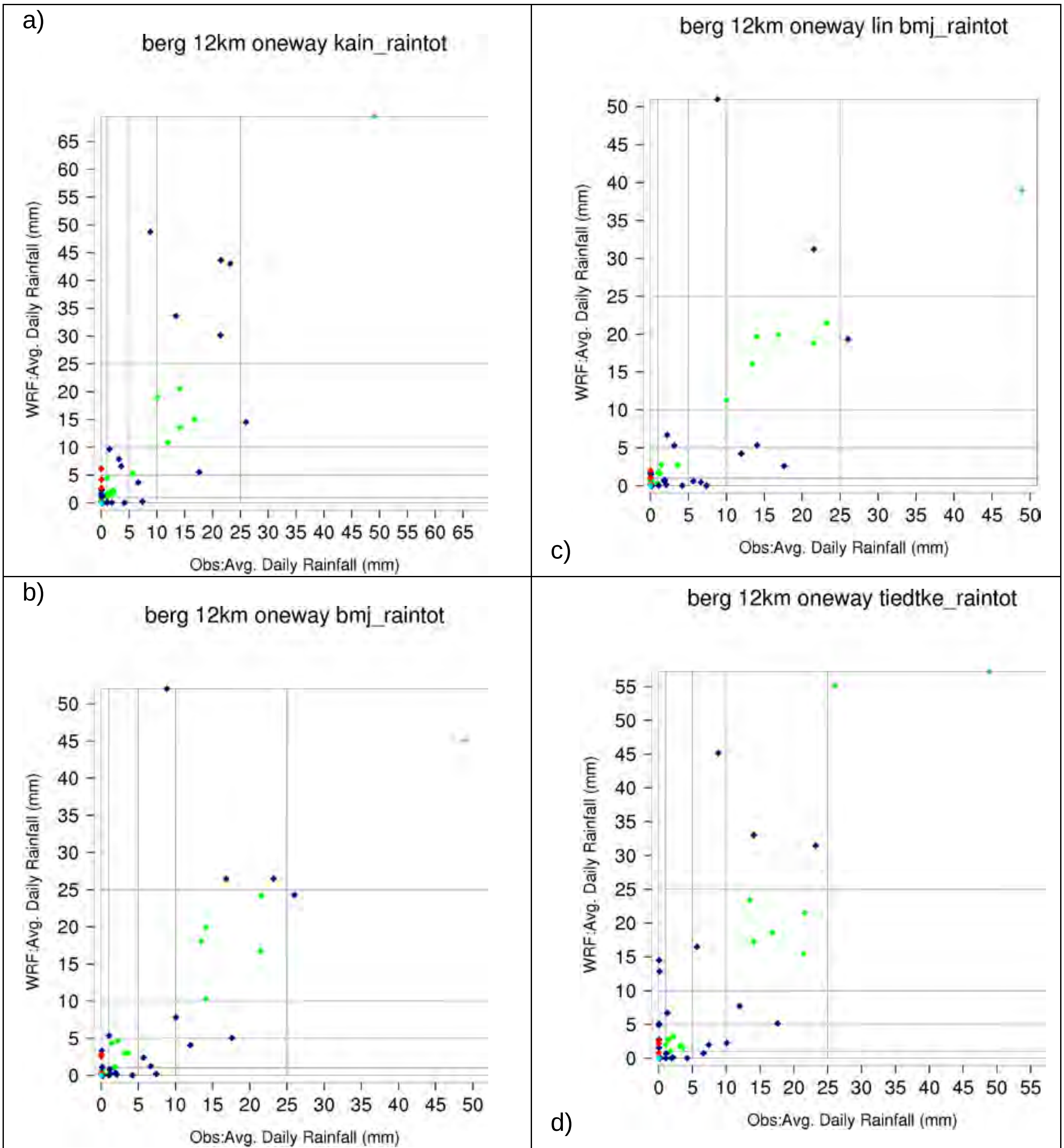

Figure 8-27: Scatter plots of 24hour rainfall for rain total a)wsm3-kain; b)WSM3-BMJ ; c)Lin-BMJ ; d)WSM3-Tiedtke. Green=hit inside category, Blue=hit outside category, Red=False Alarm, Cyan=Correct negative

8.10 Liebenbergsvlei Rain days and Bias: WRF 4 KM

Four scenarios were simulated for Liebenbergsvlei at 4 km resolution, three of which made use of microphysics alone. These were the Thompson. WSM3 and WSM6 scenarios. One run made use of the grell-3D cumulus scheme which is designed for sub 10 km grid resolution. The WSM3-Grell3D scenario produced too many rain days and achieved a daily bias of 1.8 mm (Figure 8-28). However, the microphysics scenarios produced lower daily bias results due to a good resemblance of simulated rain days observed. However, an improvement in bias was not really evident in comparison to 12 km results, where WSM3-tiedtke-cudt0 and Lin-tiedtke-cudt0 produces bias between 1 and 2 mm. Here, the more sophisticated microphysics schemes, Thompson and WSM6, produced results in the same range. Only the 3-class microphysics scheme, WSM3 produced a bias of less than 1 mm.

Although the modelled rain day totals are similar to the observed, they may not occur on the same day, which is evident in the number of misses and false alarms presented in (Figure 8-29). As such, the model performance may not be an improvement on the 12 km results as is discussed below.

Upon further inspection of the probability of detection (POD) and false alarm ratio (FAR), the 12 km results compared more favourably, achieving higher POD while maintaining a FAR of less than 0.5. For the 4 km results, only WSM3-Grell3D achieves a comparable POD, but achieves a FAR greater than 0.5 (Figure 8-30), which means the model is wrong more often than it is right. The microphysics schemes do achieve FAR lower than 0.5, which is desirable, but score less strongly than the 12 km results in terms of probability of detection.

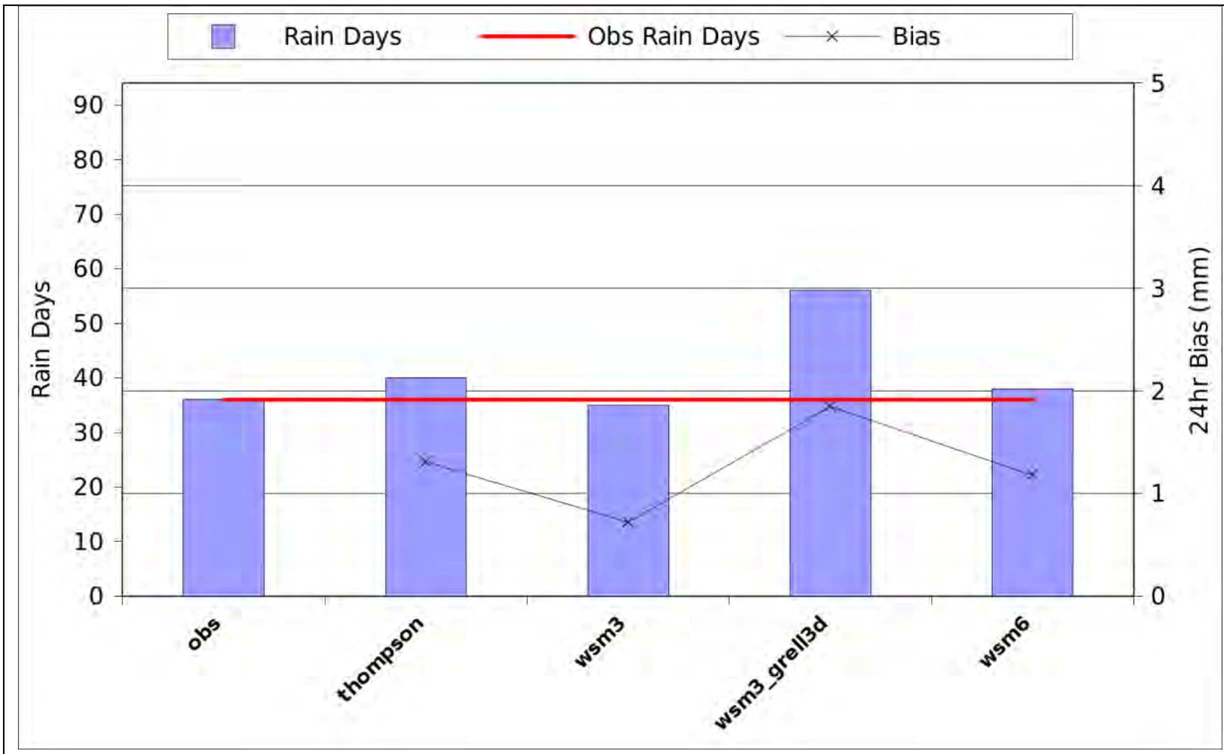

Figure 8-28: Rain days (>1 mm/d threshold) and 24hr bias for Liebenbergsvlei 4 km WRF domain.

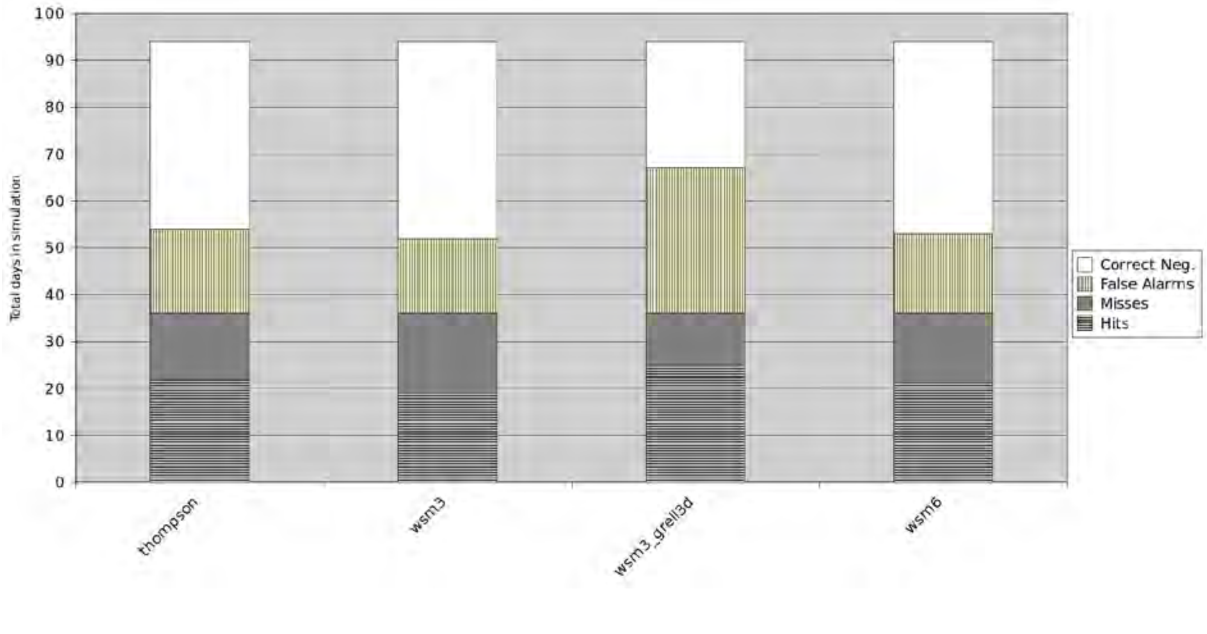

Figure 8-29: Contingency tables counts of hits, misses, false alarms and correct negative (no rainfall) for daily threshold of >1 mm/d for Liebenbergsvlei 4 km WRF domain.

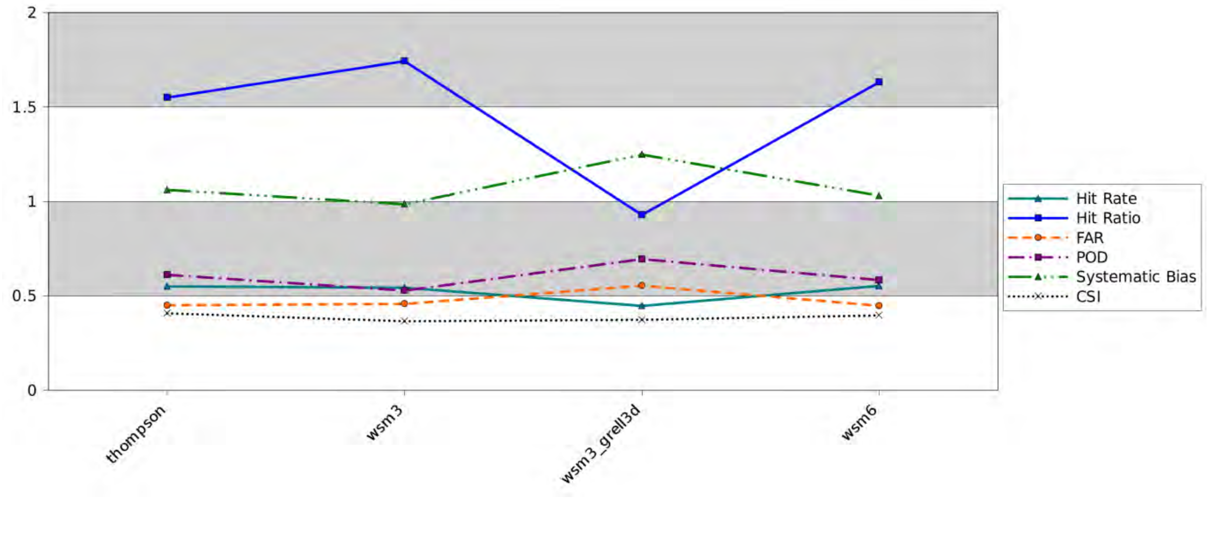

Figure 8-30: Scores derived from contingency table counts (>1 mm/d threshold) for Liebenbergsvlei 4 km WRF domain. Optimum score is 1 for Hit Rate, POD (probability of detection) and CSI (critical success index). Ideal score for FAR (false alarm ratio) is 0.

8.11 Liebenbergsvlei River Rainfall Maps

Total Rainfall

Where the 4 km results are an improvement on the 12 km results is in rainfall totals. Rainfall totals in the catchment range from 300-400 mm, compared to 300-700 mm from the 12 km results. The WSM3 produced the lowest totals over the catchment (Figure 8-31c) while Grell3D produced the highest, as well as high values over the remainder of the domain

(Figure 8-31b). Outside of the domain, the Thompson microphysics scheme produces lower rainfall totals over the escarpment WSM3 or WSM6. However, WSM3 produced more realistic results over the low lying areas of KwaZulu-Natal. Thus, overall, when considering the metrics in Section 8.10 and the totals here, the WSM3 4 km results perform most favourably.

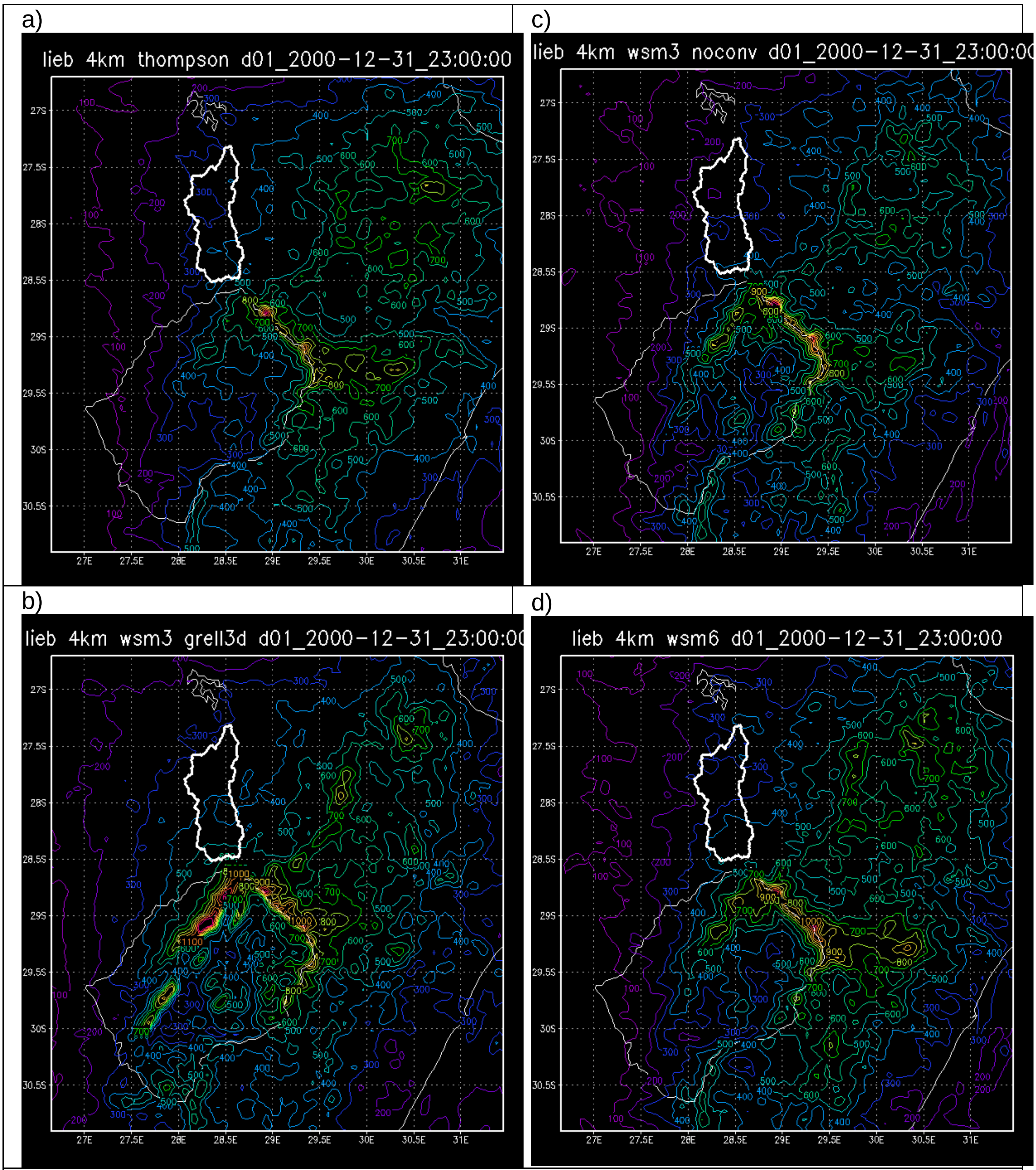

Figure 8-31: Total rainfall maps from WRF for 2000-09-28 00:00:00 to 2000-12-31 23:00:00.a) Thompson; b) WSM3-Grell; c) WSM3 no conv; d) WSM6

8.12 Liebenbergsvlei River Catchment Diurnal Cycle

The WSM3-Grell3D scheme still triggers convection too early, as was seen in the 12 km results. However, this serves to highlight the allocation of moisture between the microphysics and cumulus schemes, as the microphysics does not become overactive in this scenario (Figure 8-32b). When cumulus parameterisation is not present, the microphysics has to deal with all the moisture and so produces excess rainfall when it is triggered. The model diurnal cycle does follow the observed for the microphysics scenarios, and the peak rainfall does coincide, indicating that the timing is good (Figure 8-32 a, c and d). This suggests that there is either too much moisture in the model, which condenses and rains, or that the temperature profile is not correct causing too much cooling, or it is a combination of both.

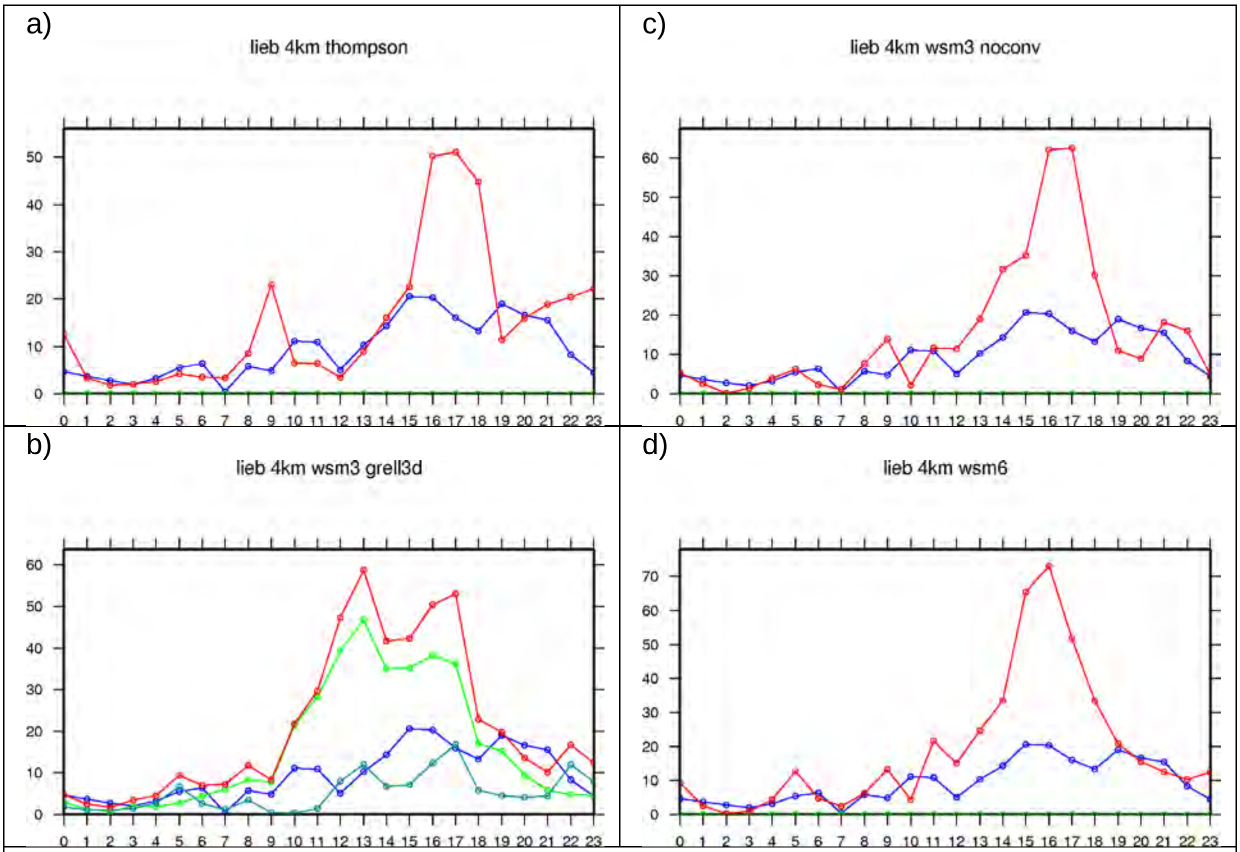

Figure 8-32: Diurnal cycle of average rainfall over the catchment. Blue=Observed, Red=WRF total, Green=WRF Convective, Cyan= WRF Non-convective.
a)wsm3-kain ; b) wsm3-bmj; c) lin-bmj; d) wsm3-tiedtke

8.13 Liebenbergsvlei River Catchment Scatter Plots

Results from the 4 km domain show similar scatter plots to the 12 km results. False alarms cause single rainfall events in excess of 15 mm, while observed totals between 1 and 5 mm are often overestimated. Furthermore, WSM3 and WSM6 produced single rain days in excess of 60 mm. These are outlier events that may be caused by a single cell. While no data pruning was conducted, these events may have a significant effect on the statistics and total rainfall presented earlier in this chapter.

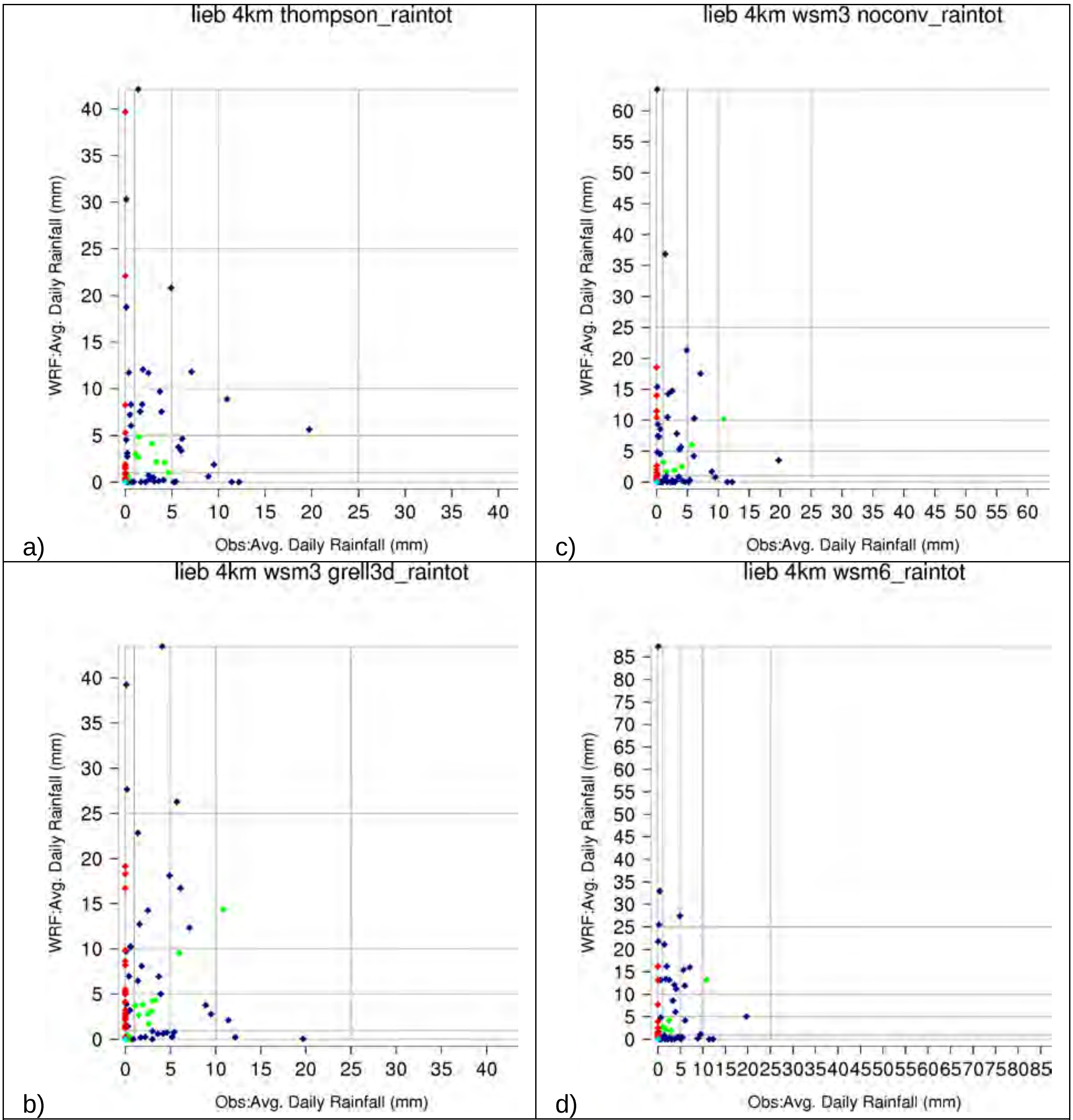

Figure 8-33: Scatter plots of 24hour rainfall for rain total
a)Thompson ; b)WSM3-Grell; c) WSM3; d)WSM6 .
Green=hit inside category, Blue=hit outside category, Red=False Alarm, Cyan=Correct negative

8.14 Berg River Rain days and Bias: WRF 4 KM

Three scenarios were modelled making use of microphysics schemes only. These were the Lin, WSM3 and WSM6 schemes respectively. A total of 28 rain days were observed during the modelled period from May-July 2000. All three scenarios produced daily bias of less than

2 mm (Figure 8-34), but none less than 1 mm. This is in contrast to the 12 km domain simulations, where daily bias results of less than 1 mm were achieved when convection schemes were active (WSM3-BMJ and Lin-BMJ. Figure 8-21).

The Lin scheme produced the lowest bias but this was due to a high number of missed rainfall events (Figure 8-35). WSM3 produced the most hits, but also produced a higher false alarm count than WSM6. All schemes performed well when considering the Hit rate, scoring 0.72, which is in the preferred range between 0.5 and 1 as discussed in section 8.2. WSM3 and WSM6 performed almost identically, but it can be said that WSM6 slightly out performed WSM3, but only slightly. This is due to the hit ratio being higher for WSM6. Both schemes produce almost identical hit rates, but the hit ratio is the ratio between total correctly modelled rain/non-rain days (hits + correct neg.) to total modelled rain days, including false alarms (Hits + false alarms). Ideally, false alarms would be zero and the ratio would be high, e.g. 4:1. However, if the false alarm count is too high, the ratio evens out, e.g. 2:1. Thus, a higher hit ratio is preferred, which WSM6 produces while maintaining a hit rate similar to WSM3, suggesting that WSM6 is more adequate than WSM3 when considering all metrics presented in Figure 8-36.

Arguably, the 4 km domain results did not outperform the 12 km results presented in section 8.6, as the hit rates, hit ratios and daily bias results were less favourable compared to the WSM3-BMJ and Lin-BMJ scenarios.

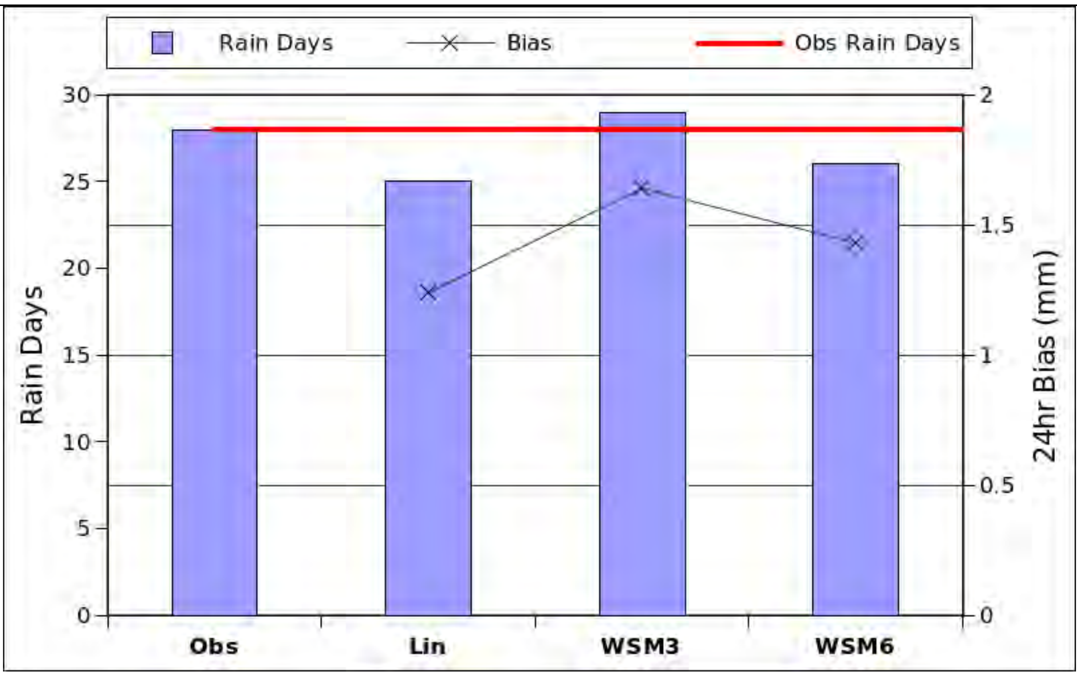

Figure 8-34: Rain days (>1 mm/d threshold) and 24hr bias for Berg River 4 km WRF domain.

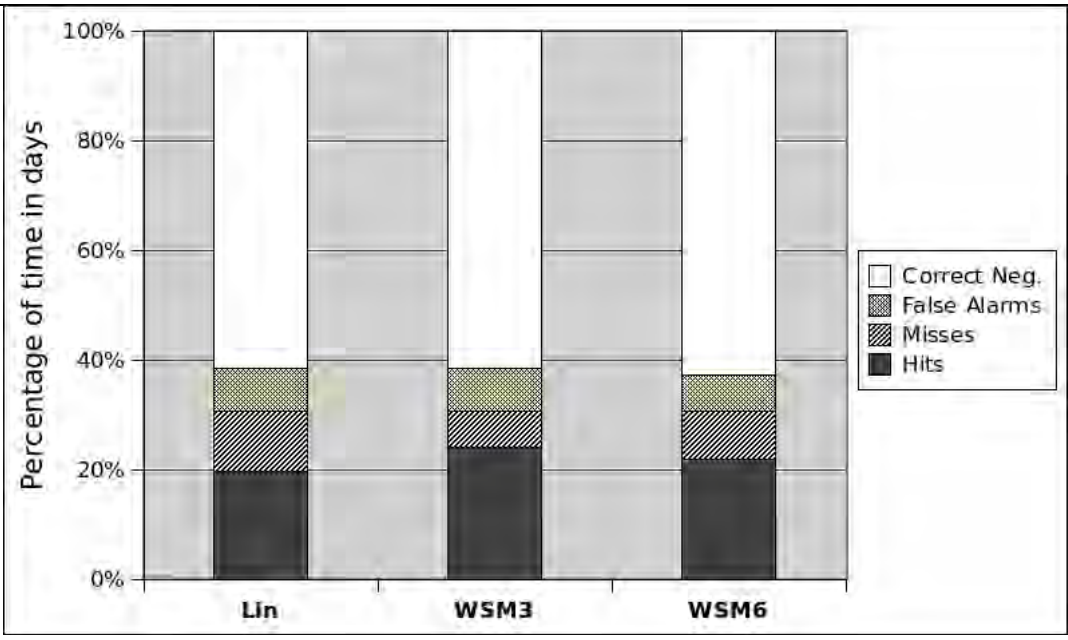

Figure 8-35: Contingency tables counts of hits, misses, false alarms and correct negative (no rainfall) for daily threshold of >1 mm/d for Berg River 4 km WRF domain.

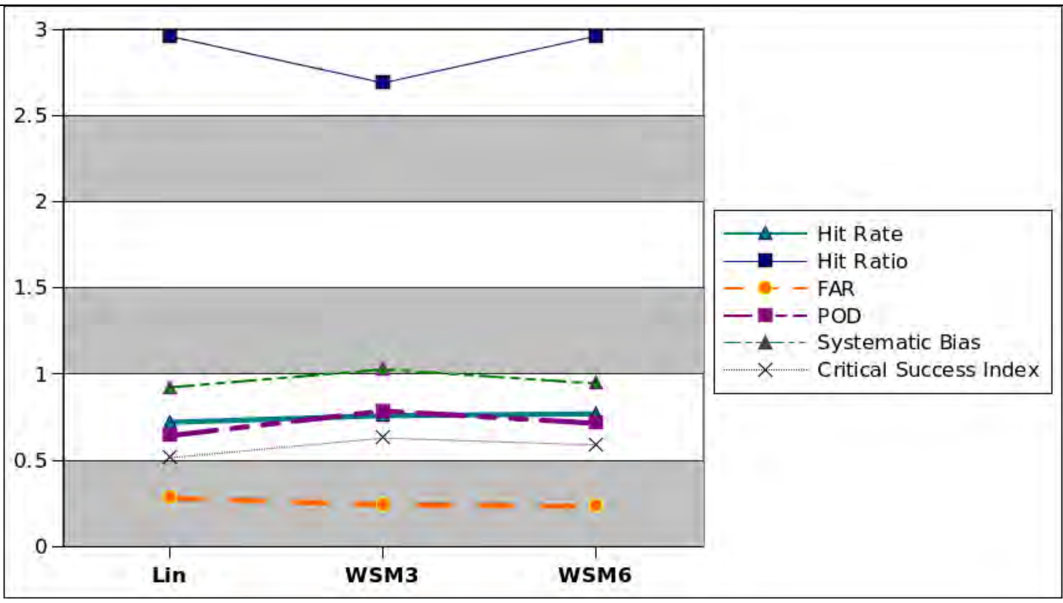

Figure 8-36: Scores derived from contingency table counts (>1 mm/d threshold) for Berg River4 km WRF domain. Optimum score is 1 for Hit Rate, POD (probability of detection) and CSI (critical success index). Ideal score for FAR (false alarm ratio) is 0.

8.15 Berg River Rainfall Maps

The higher resolution domain has highlighted the individual mountains around the catchment and subsequently has produced high rainfall totals possibly due to orographic uplift (Figure 8-37). Thus, the major difference between the 12 km domain scenarios and these is that high rainfall totals are observed on the escarpment and over the elevation features to the south of the catchment. Inside the catchment rainfall totals are from 300-400 mm, but totals over the escarpment now rain too much, producing rainfall totals of 1000 mm, which is equivalent to annual rainfall totals. Nevertheless, these totals may be more realistic that the 12 km escarpment totals presented in section 8.7, although cannot be confirmed in this study.

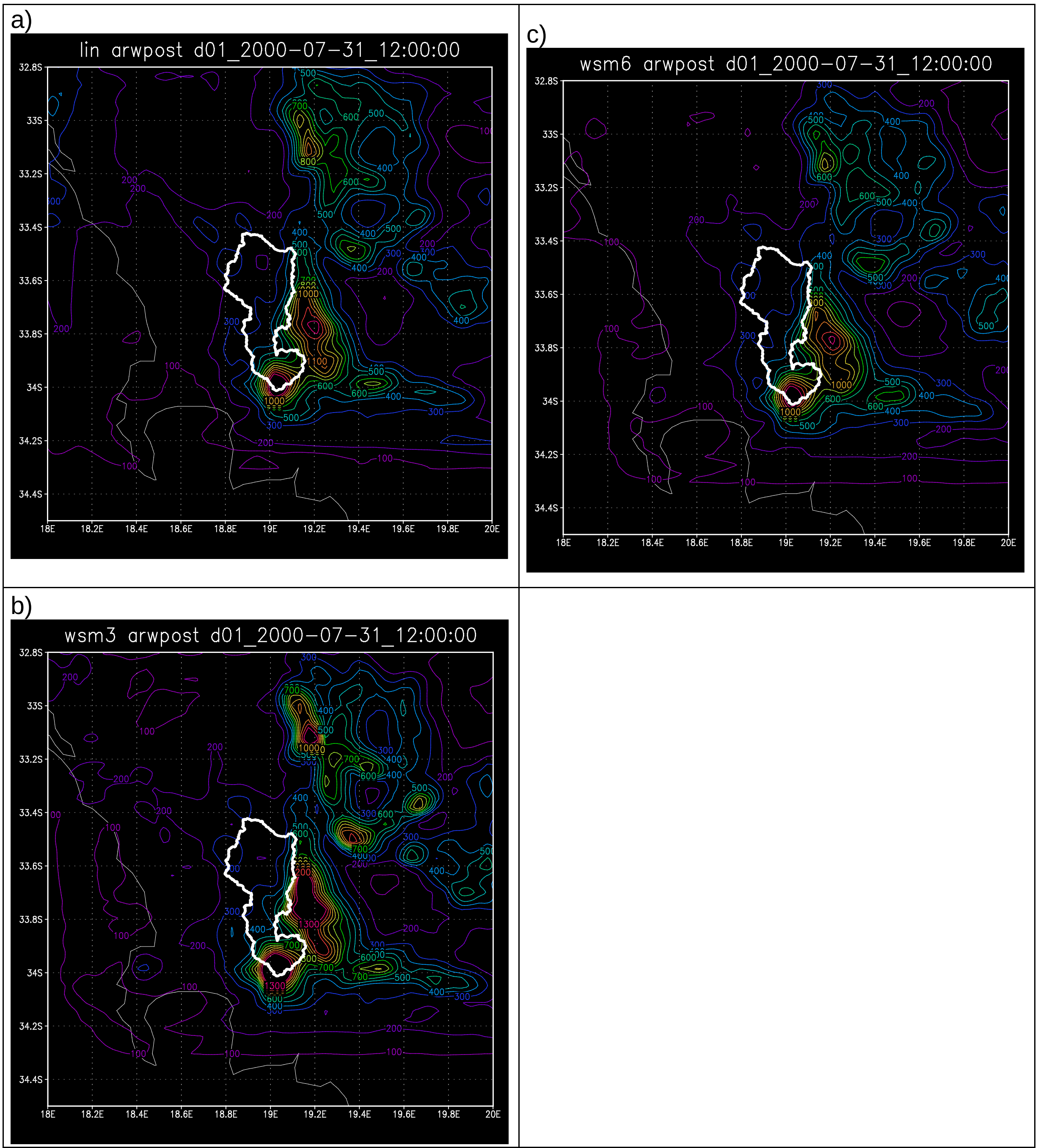

Figure 8-37: Berg 4 km total rainfall maps from WRF for 2000-04-28 00:00:00 to 2000-07-31 12:00:00. a) Lin; b) WSM3 c) WSM6.

8.16 Berg River Catchment Diurnal Cycle

The model and observed data follow a similar diurnal pattern in rainfall when averaged over the catchment (Figure 8-38). However, the 4 km domain produces excess rainfall between 5h00-10h00 and 14h00-17h00 which was not observed in the model results from the 12 km domain. This increase is possibly due to the improved terrain in the higher resolution domain which produced high rainfall totals presented in the previous section.

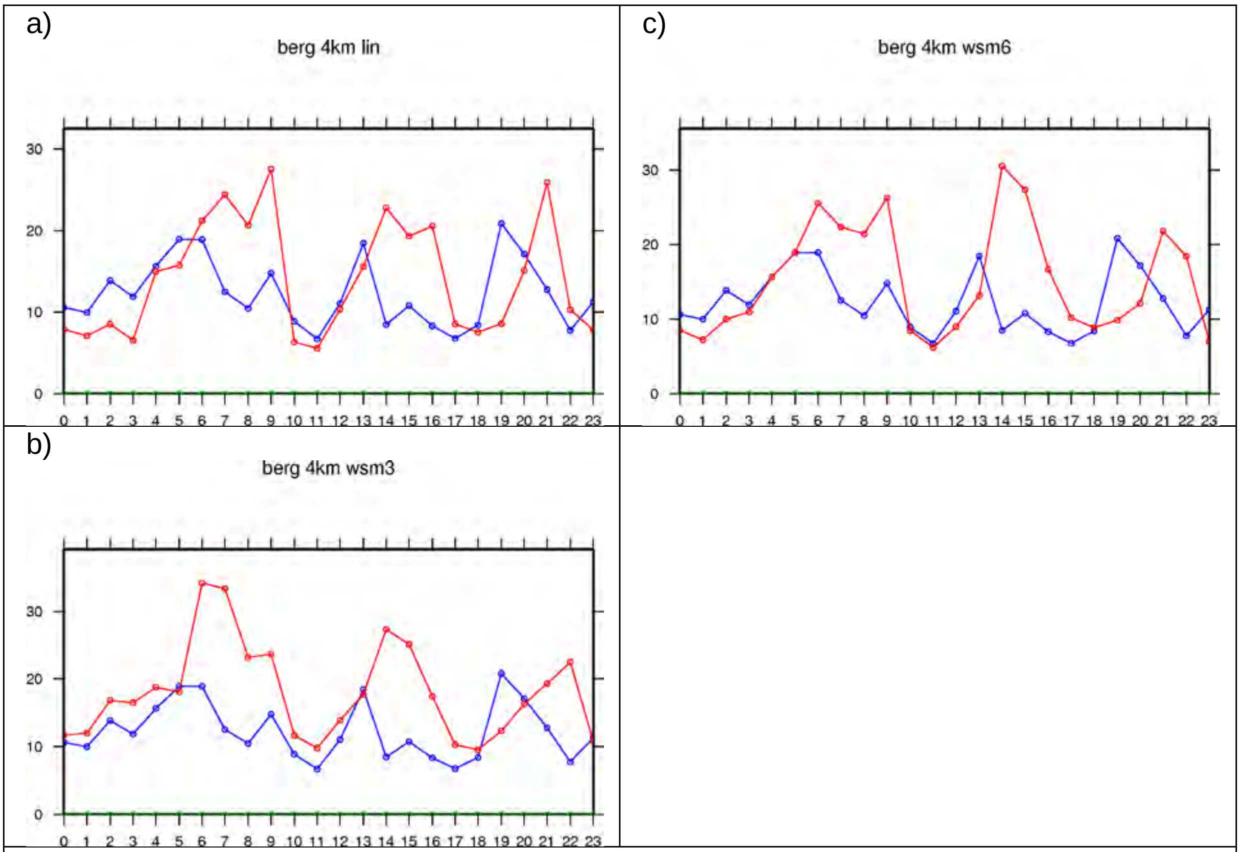

Figure 8-38: Diurnal cycle of average rainfall over the catchment. Blue=Observed, Red=WRF total, Green=WRF Convective, Cyan= WRF Non-convective.
a)Lin ; b) WSM3; c) WSM6

8.17 Berg River Catchment Scatter Plots

All three schemes show good correlation between observed and modelled events, indicated by the green dots in the scatter plots below. Unlike the 12 km results, where many over predictions were made for rain days of 10 to 25 mm, there are not as many over predictions in the 4 km domain results. Two outliers are identifiable for all three schemes, the first being a modelled event of over 50 mm when there was no observed rainfall. The second being a modelled event of >70 mm when the observed was only 50 mm over 24 hours. These modelled events cold drastically skew the daily bias results and highlight the need for the scores like hit rate and hit ratio.

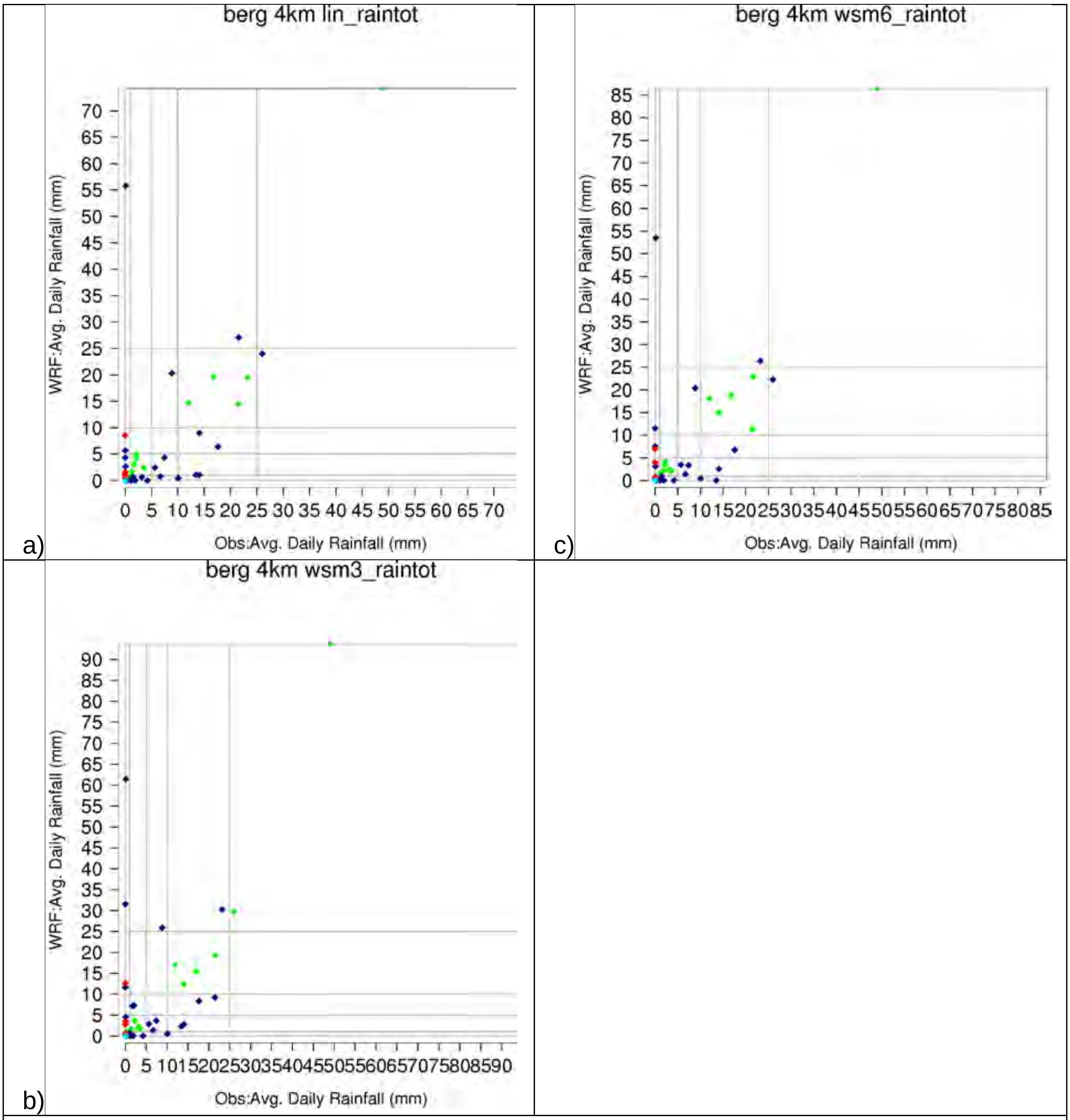

Figure 8-39: Scatter plots of 24hour rainfall for rain total
a)Lin ; b) WSM3; c)WSM6 .
Green=hit inside category, Blue=hit outside category, Red=False Alarm, Cyan=Correct negative

9 PYTOPKAPI RESULTS AND DISCUSSION

Having set up the TOPKAPI model for both the Berg and the Liebenbergsvlei Catchments, the models were run at a time step of 6 hours each. The Berg River simulation was run for 2 years from 2000-2001. The Liebenbergsvlei simulation was run for 3 months from 1 Oct 2000 - 1 May 2001. The results obtained from the simulations are presented in Figure 9-1 and Figure 9-3.

A visual inspection of the plots comparing the observed flows to the simulated flows suggests satisfactory model performance particularly with respect to the Berg River Catchment in Figure 9-1. For this catchment, a Nash-Sutcliffe Efficiency (NSE) of 0.48 is achieved and the only discrepancy appearing to be the model's failure to reproduce the flood peaks particularly towards the end of the simulation period (Figure 9-1) where this failure is significant. Simulations with WRF rainfall data performed well, achieving a Nash-Sutcliffe Efficiency (NSE) of 0.479 (Figure 9-2).

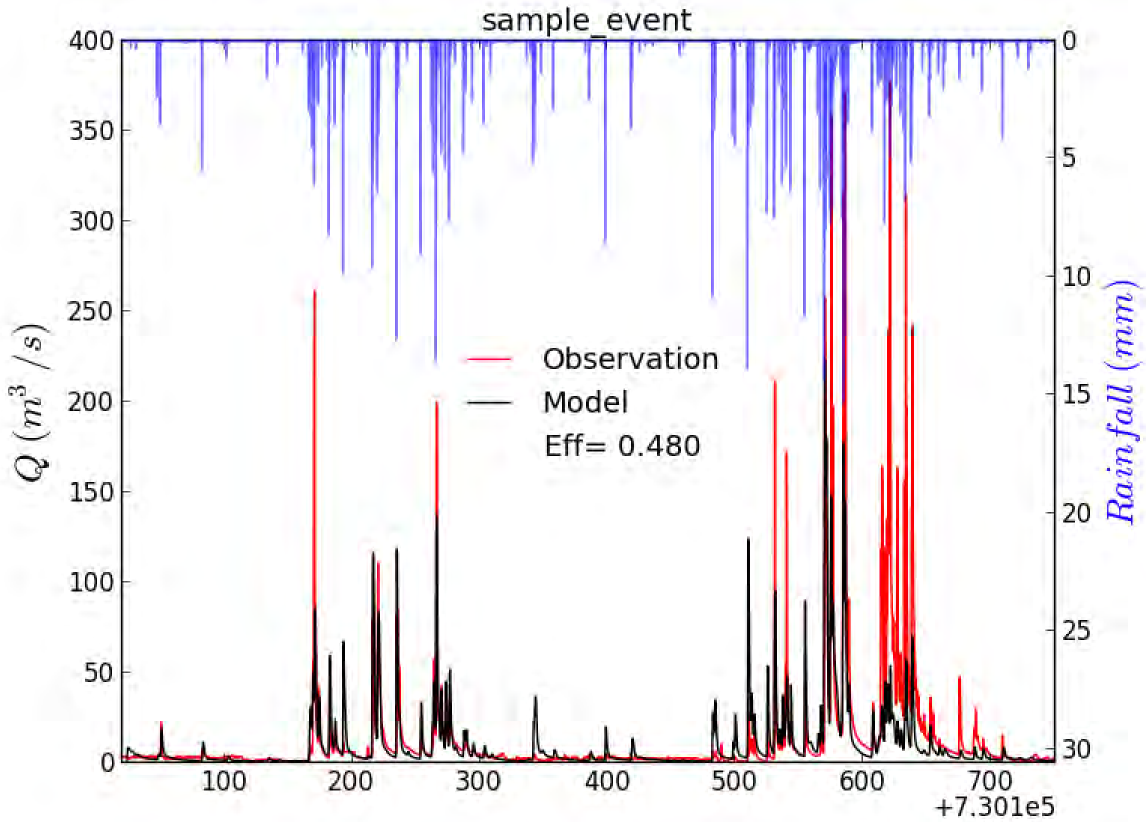

Figure 9-1: Berg River – Simulated and observed stream flow.

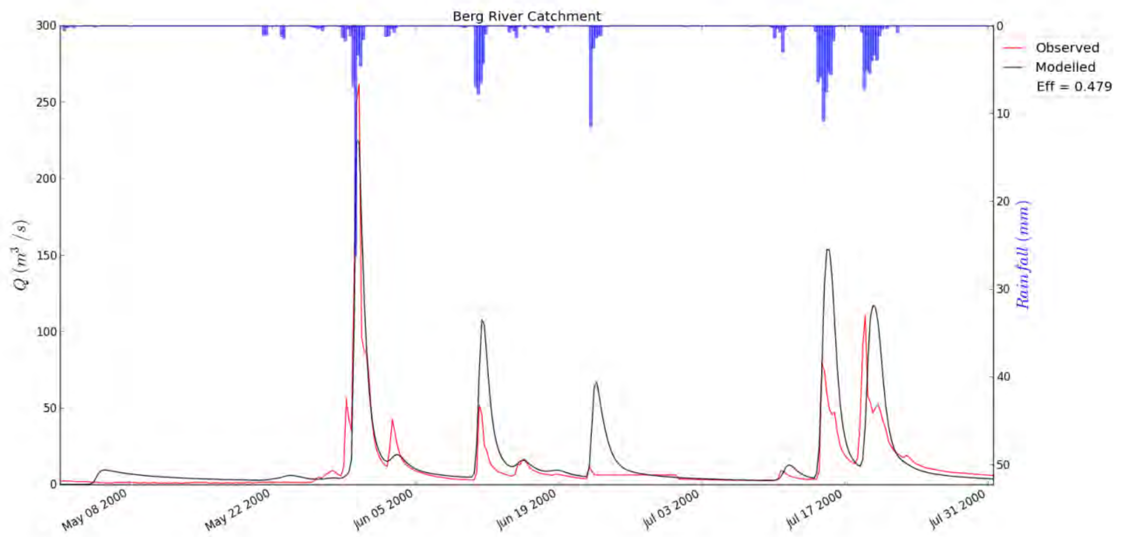

Figure 9-2: Berg River – WRF (scenario Lin/BMJ 12 km) vs. calibrated stream flow from May-Jul 2000.

Initially, the model setup on the Liebenbergsvlei catchment was markedly less successful (Figure 9-3). This was due to using gauge C8H020 which had missing data that was patched using a well-known methodology. However, the patching method created erroneous peak flows which were not observed in adjacent gauges in the same stream. At this point gauge C8H037 was used for verification instead.

Using gauge C8H037, we ran the model with zero rainfall and external flow only with a Manning channel roughness factor of 1. This showed good timing of external flow in the downstream gauges, but showed an initial peak in the simulation that was not in the observed data set (Figure 9-4). Rainfall was then introduced to simulate the rainfall peaks in stream flow. This was successful, but the simulated peak discharge from rainfall was too high (Figure 9-5). To adjust the peaks, the flow from soil water was decreased by decreasing the soil depth. This effectively decreases the volume of flux of water transported through the soil. The result was that the initial peak in the model no longer occurred and the peak discharge from rainfall events decreased to observed levels (Figure 9-6). Finally, Manning overland and channel roughness factors were adjusted with rainfall present in the simulation. Suitable values were reached where peak flows from rainfall events were simulated well both in start time, duration and intensity and a Nash-Sutcliffe Efficiency (NSE) of 0.744 was achieved (Figure 9-7 and Figure 9-8).

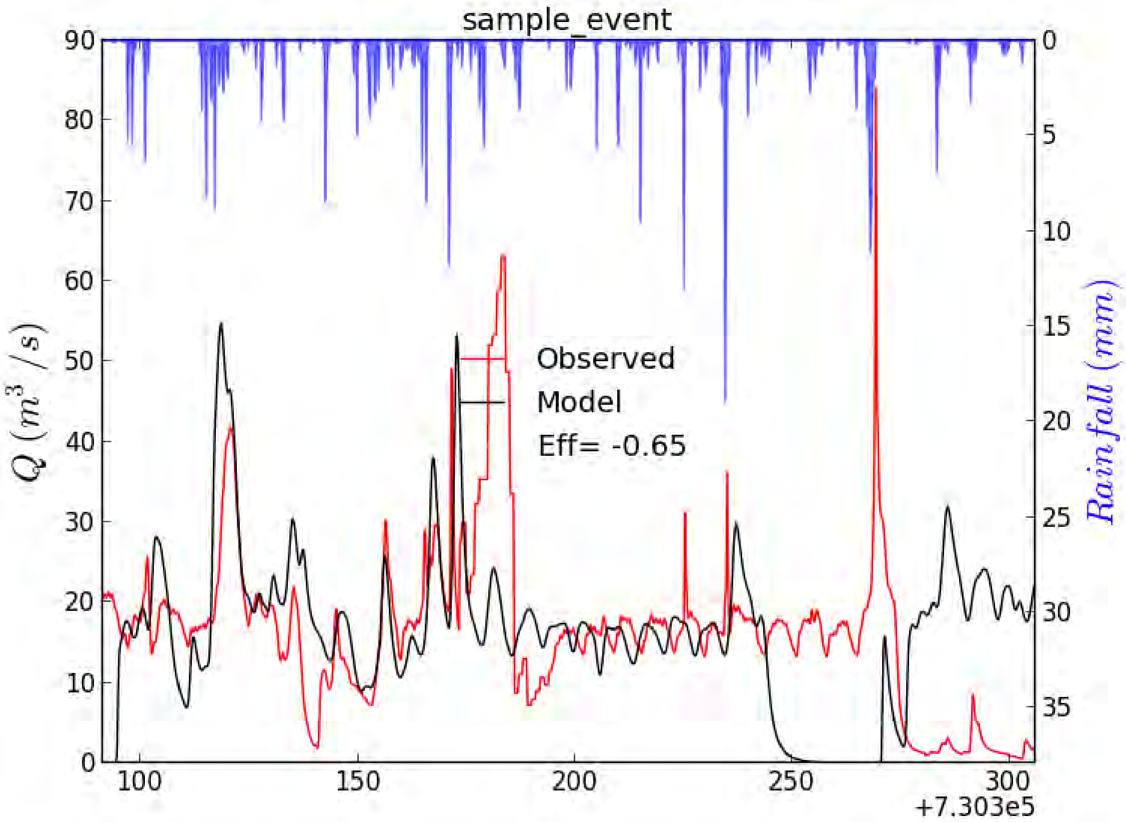

Figure 9-3: Liebenbergsvlei – Simulated and observed stream flow.

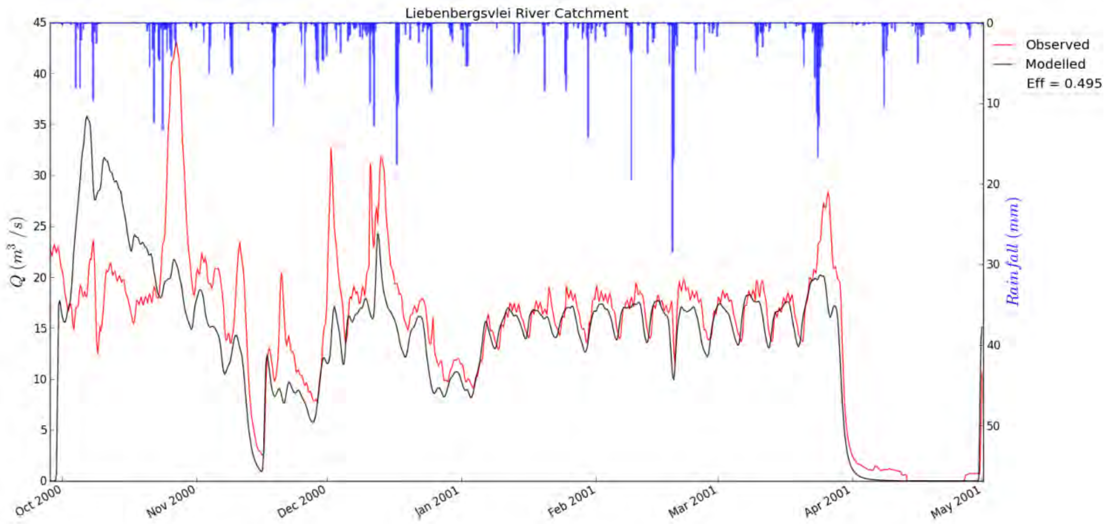

Figure 9-4: Liebenbergsvlei. No rainfall; External Flow only.

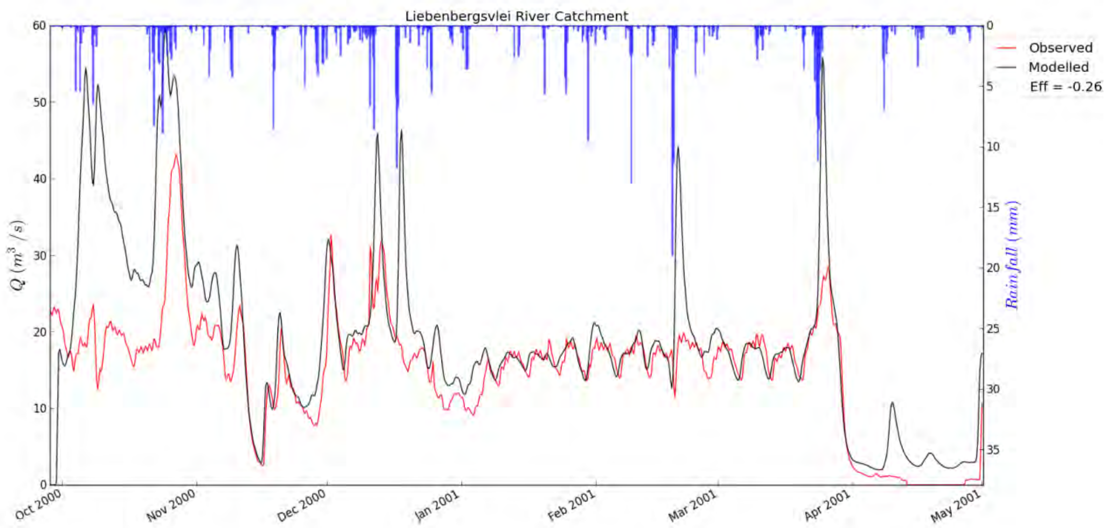

Figure 9-5: Liebenbergsvlei. Rainfall and initial parameters (fac_L=1, fac_Ks=1.2, fac_n_o=1, fac_n_c=1)
Timing was great. Peaks too high. Initial peak too high.

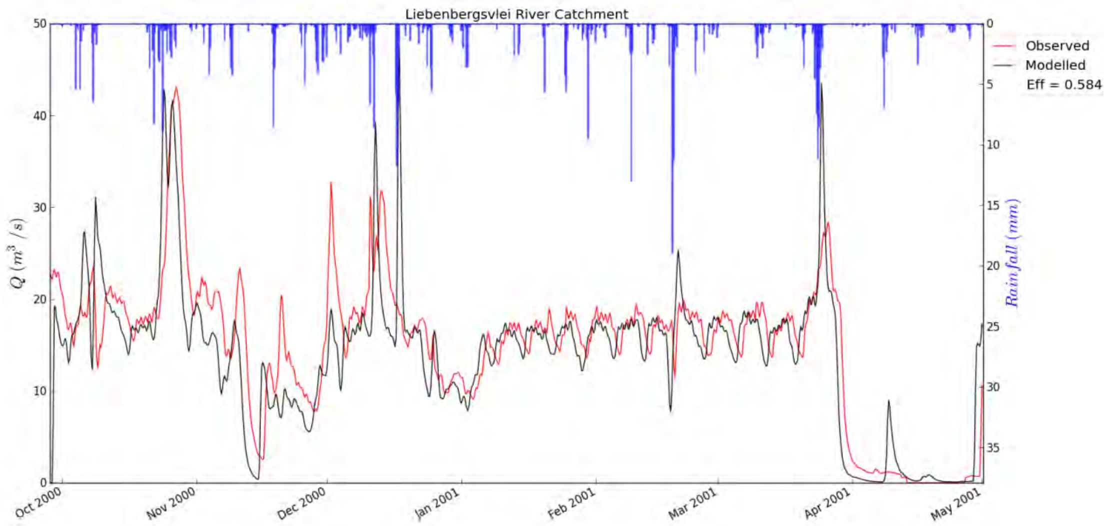

Figure 9-6: Liebenbergsvlei. (fac_ L=0.5, fac_Ks=1.2, fac_n_c=0.6, fac_n_o=0.6. Removed initial peak. Rainfall peaks decreased. Timing was too early.

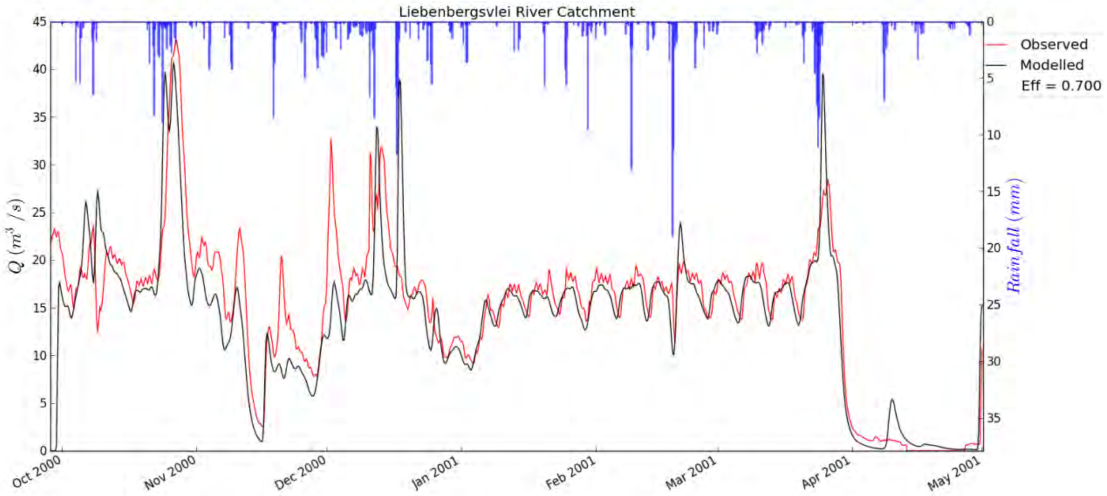

Figure 9-7: Liebenbergsvlei. (fac_L=0.5, fac_Ks=1.2, fac_n_c=1, fac_n_o=0.6) Peaks too high. Improved timing.

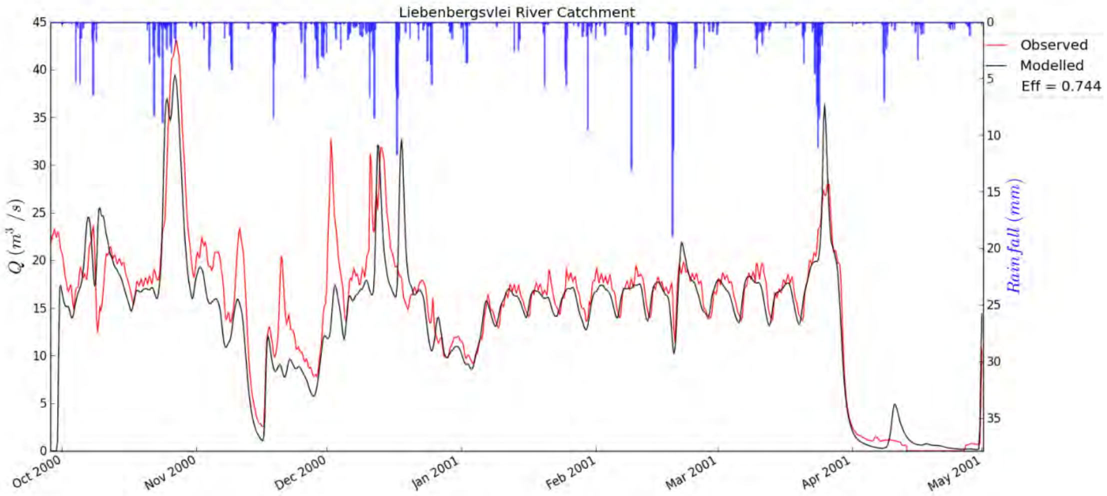

Figure 9-8: Liebenbergsvlei. (fac_n_c=1.2, fac_ n_o=0.6) Start and end of rain peaks match observations and peaks decrease. Timing was good.

An initial run of PyTopkapi with WRF rainfall results from the Tiedtke convective scheme (best performing scheme for rainfall totals) is presented in Figure 9-9. While WRF is known to be overactive, as demonstrated by the large discharge peaks produced by rainfall, we can say that PyTopkapi has been suitably calibrated, as the base flow is not adversely affected.

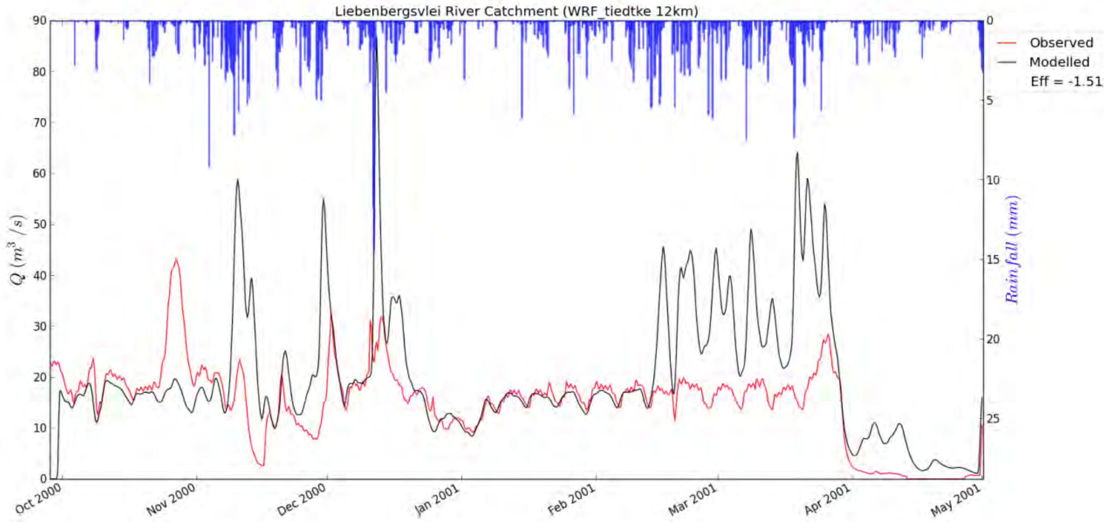

Figure 9-9: Simulation using WRF total rainfall from Tiedtke 12 km.

10 WRFCHEM RESULTS AND DISCUSSION

WRFChem results are presented here for 1-5 Oct 2000 using a 36 km domain over Africa South of the Equator. Global emissions inventories for anthropogenic and biomass SO_2 and $PM_{2.5}$ from the RETRO emissions inventory was used (Figure 7-4 and Figure 7-5). Rainfall totals are presented for the Highveld area using the Lin-BMJ microphysics and cumulus physics respectively. Three scenarios were run, one with chemistry from the global emissions inventory (Chem), one with chemistry from a South African emissions Inventory (Chem Ind.) and one without chemistry (NoChem), but all had identical physics schemes implemented.

The introduction of aerosols and sulphates in the form of SO_2 conversation was expected to increase rainfall by providing more cloud condensation nuclei. However, a uniform increase in rainfall is not observed over the region. Instead, rainfall increased in places and decreased in others, evident by the peak rainfall over Gauteng (NoChem, high rainfall) the 30 mm contour over the Kwazulu-Natal and Mpumalanga boundary (Chem, High rainfall) (Figure 10-1 and Figure 10-2). The global emissions inventory produced identical results to the South African emissions inventory.

The Chem run produced 200 mm more total rainfall over the region presented in Figure 10-1, totalling 3945 mm over the entire area, compared to 3781 mm for the NoChem scenario. A time series of total rainfall for the area shows that most rainfall is produced by cumulus physics in the model, however, the chemistry affects non-convective rainfall. Total convective rainfall is 3328 mm and 3361 mm for Chem and NoChem respectively, but non-convective rainfall is 616 mm and 419 mm, accounting for the increase of 200 mm.

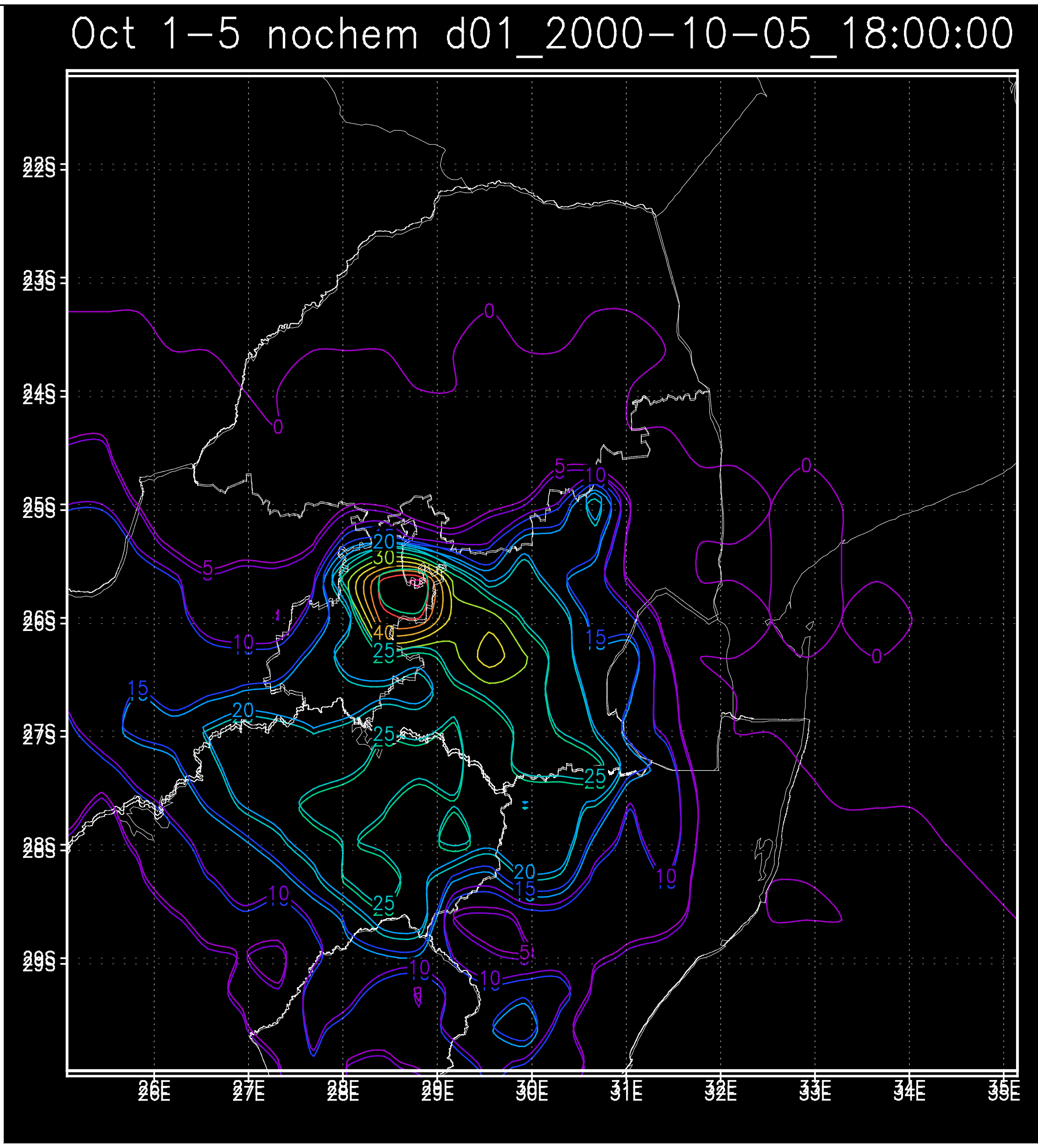

Figure 10-1: No Chemistry: Total rainfall from 1-5 October 2000, over the Highveld of South Africa using the WRF 36 km domain

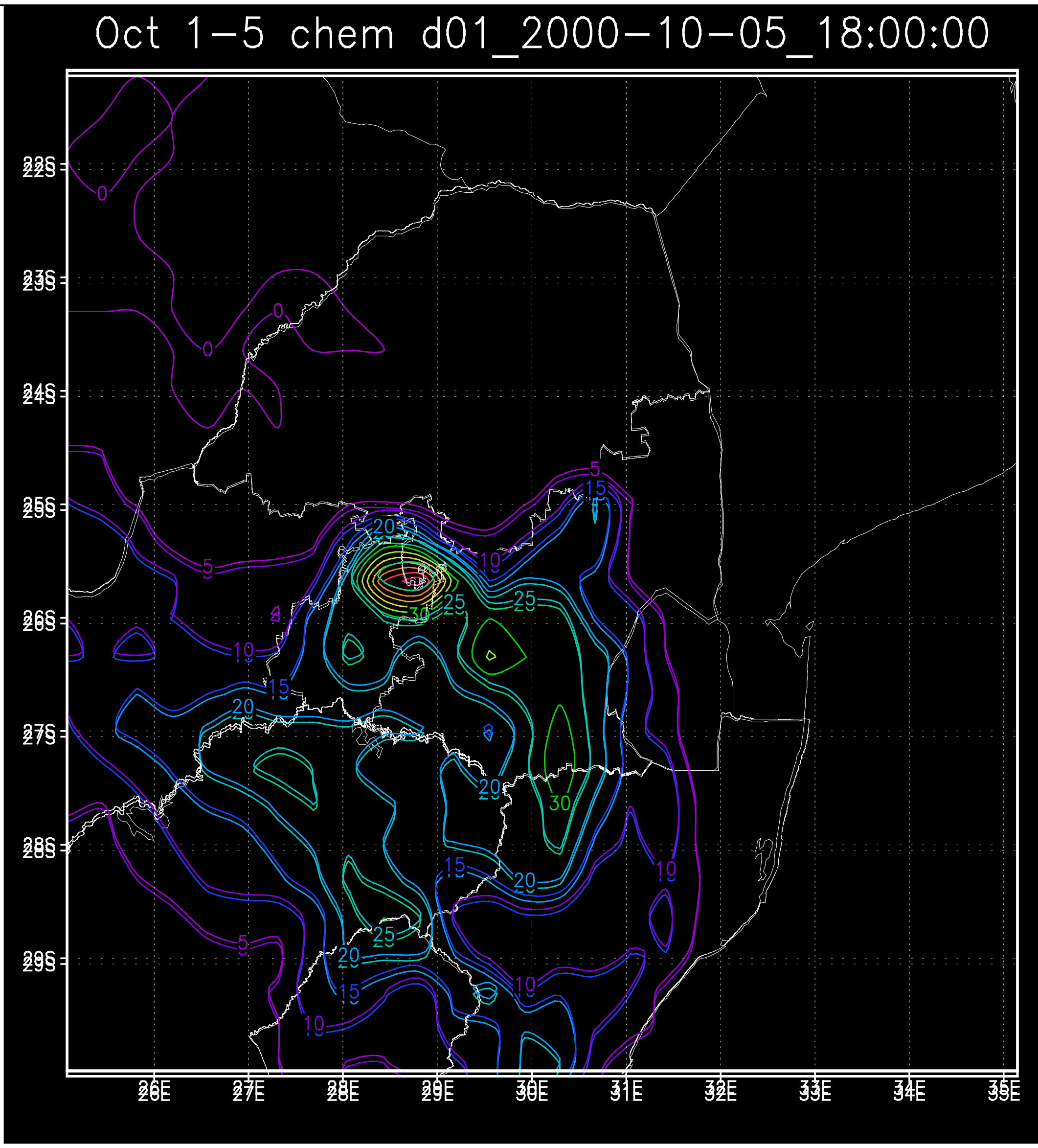

Figure 10-2: Chemistry On: Total rainfall from 1-5 October 2000, over the Highveld of South Africa using the WRF 36 km domain.

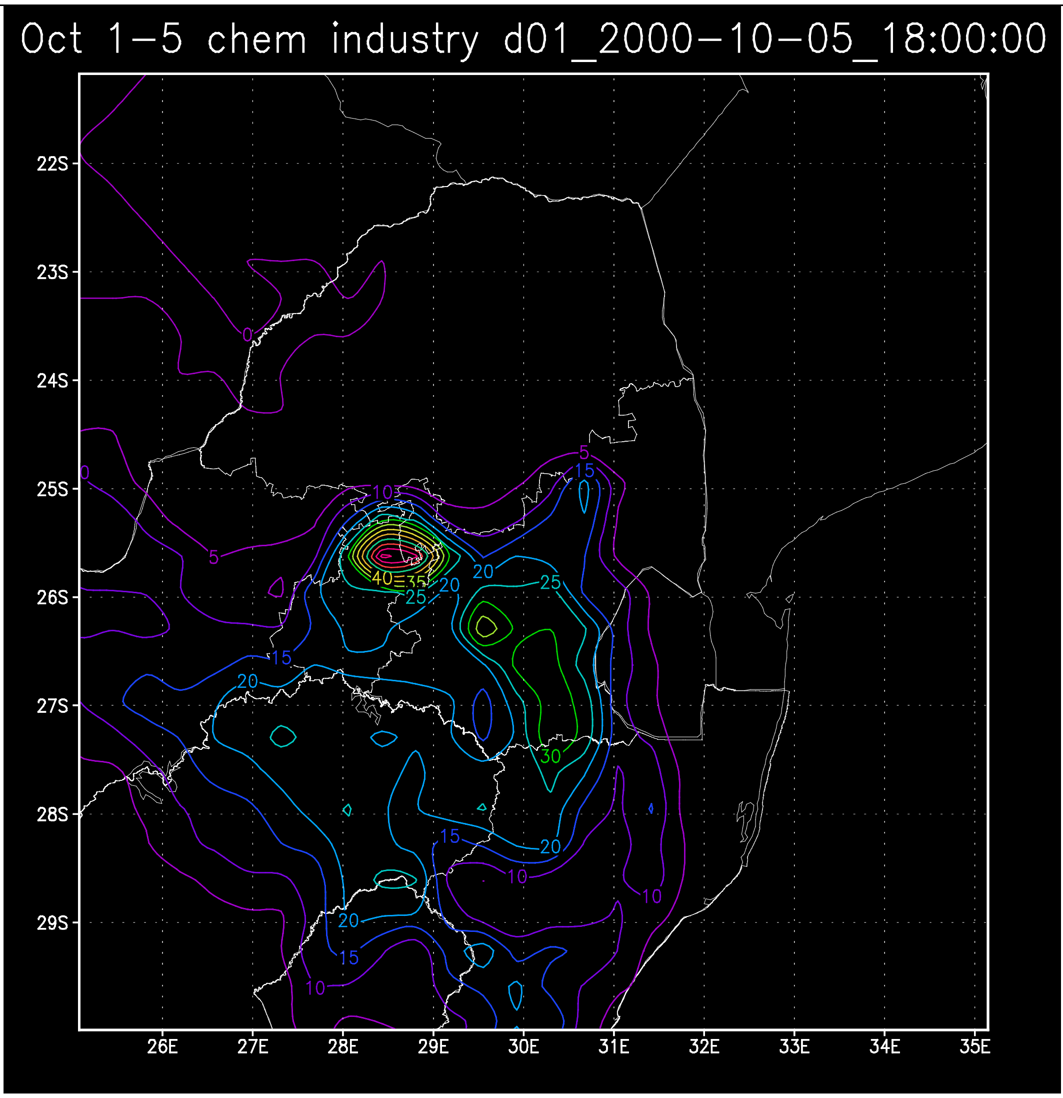

Figure 10-3: Local Industrial Chemistry On: Total rainfall from 1-5 October 2000, over the Highveld of South Africa using the WRF 36 km domain.

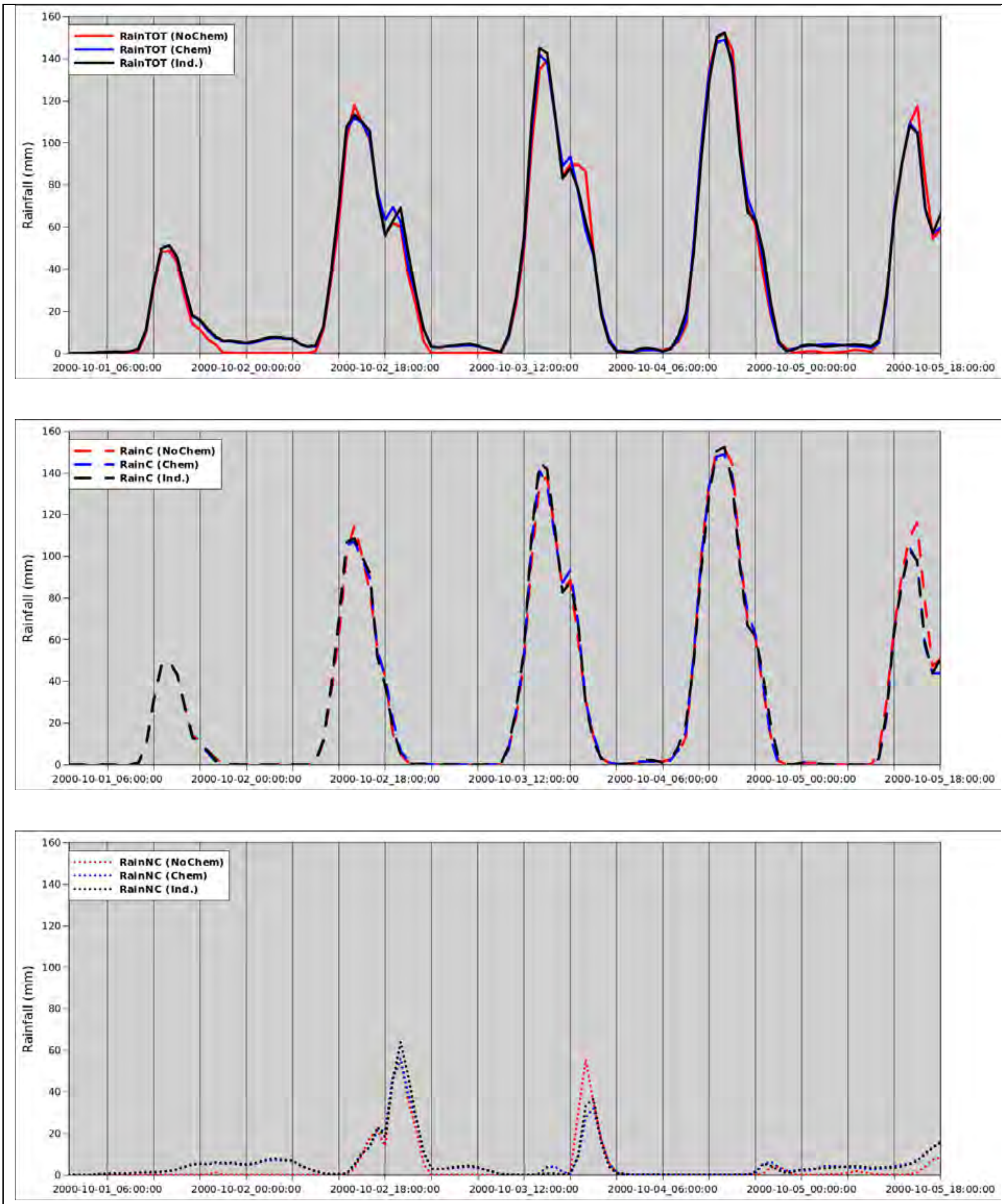

Figure 10-4: Time series of area total rainfall of Figure 10-1, Figure 10-2 and Figure 10-3.

The increase in non-convective rainfall in the chemistry simulations is due to rainfall over KwaZulu-Natal and not over the Highveld (Figure 10-5). This suggests that emissions from the Highveld are transported down the escarpment to effect rainfall patterns. Although this simulation only represents a few days in October when a specific synoptic condition is present, it indicates that other transport routes out of the Highveld, e.g. east over Mpumalanga, will experience altered rainfall patterns when emissions are activated in WRF.

a.) b.) c.)

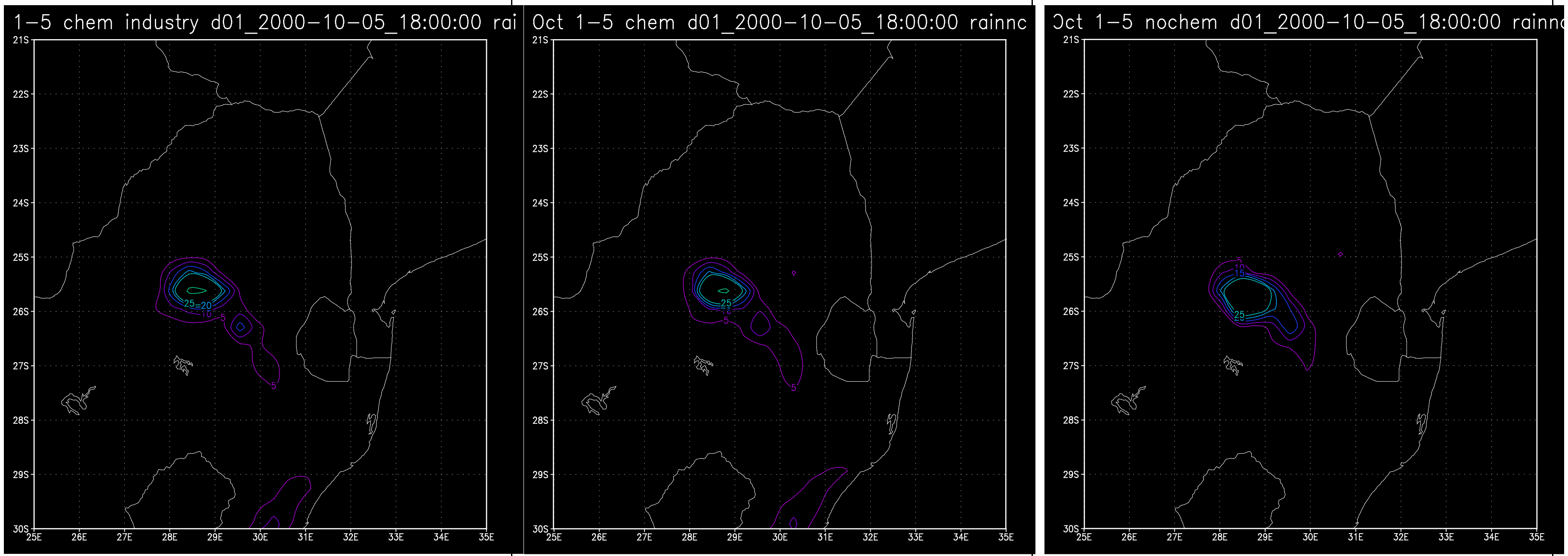

Figure 10-5: Non-convective rainfall: Total rainfall from 1-5 October 2000, over the Highveld of South Africa using the WRF 36 km domain. a.) Chem Ind. b.) Chem and c.) No Chem.

11 CONCLUSIONS

11.1 WRF

Each catchment required different schemes to suitably model daily rainfall when running 12 km model domains. The best performing schemes for modelling rainfall over Liebenbergsvlei were the WSM3-Tiedtke-cudt0 and Lin-Tiedtke-cudt0. These schemes were implemented at a 12 km resolution, but both schemes trigger too early in the day and cause excessive rain days. Subsequently WRF is currently over active at modelling convective rainfall over the Eastern Part of South Africa at this resolution and improvements to the model are required when modelling at this resolution.

The Liebenbergsvlei 4 km results did not show a significant improvement, but may indicate why the model is over predicting rainfall. These results suggests that there is either too much moisture in the model, which condenses and rains, or that the temperature profile is not correct causing too much cooling, or it is a combination of both.

The Betts-Miller-Janjic convective scheme, with either the WSM3 or Lin microphysics was suitable for the Berg River 12 km domain. However, these schemes did not perform well for Liebenbergsvlei.

Arguably, the 4 km domain results did not outperform the 12 km results presented in section 8.6, as the hit rates, hit ratios and daily bias results were less favourable compared to the WSM3-BMJ and Lin-BMJ scenarios.

11.2 PyTopkapi

PyTopkapi was adequately calibrated for each catchment and proved to simulate observed flow well when using observed rain gauge data as input. However, the coupling of WRF to PyTopkapi did not produce suitable results, and further improvement in the WRF forecast is needed before linking to PyTopkapi.

11.3 WRFChem

Much progress was made in introducing emissions and dynamic chemistry into WRF. Results indicated that over a period of five days, emissions effectively altered rainfall patterns and totals, affecting rainfall in KwaZulu-Natal. This has implications for Mpumalanga and Lowveld rainfall when transport patterns out from the Highveld shift slightly with synoptic conditions. These results are promising and open the door for future research into this field.

12 RECOMMENDATIONS

12.1 WRF Rainfall

Future research could include the following. Firstly, a larger sample size for comparing the model to observed data could be used. This would require modelling six months, instead of three, over five seasons, instead of one season. This may be long enough to negate any bias in choosing a single observed rainfall season, where individual rainfall events hold higher waiting in effecting diurnal cycles of observed rainfall and geographic distribution. Secondly, the model code could be investigated to determine why rainfall is triggered early. If identified, this can then be adjusted so that the early trigger is delayed or modified. This requires much testing of trigger variables to first identify why the model triggers early. Lastly, this research did not include any spatial bias, or account for correctly modelled events that occurred in the wrong area. This proved to be difficult with the rain gauge data which is not arranged on a regular grid. Thus, the possibility exists to run this research over a larger area than the catchments, and verify the model against gridded observed data such as radar or satellite.

Two recommendations are made. The first is to model at 4 km resolution whenever possible using the WSM3 for convective areas. However, this is not always feasible in which case the following suggestion is made for modelling rainfall at 12 km resolution. Choose the correct schemes for your area of interest (e.g. Tiedtke performed well for convective rainfall in the Eastern escarpment). If your domain contains both areas, e.g. Western Cape and Eastern Escarpment, and you are running a forecast, run two instances of the model, one with each set up.

13 LIST OF REFERENCES

Bartholomes J and Todini E (2005) Coupling meteorological and hydrological model for flood forecasting. Hydrol. Earth Syst. Sci. 9 (4) 333-346.

Beven, K.J. and Kirkby, M.J., 1979. A physically based, variable contributing area model of basin hydrology. Hydrol. Sci. Bull., 24, 1-3.

Beven, K.J., Kirkby, M.J., Schofield, N. and Tagg, A.F., 1984. Testing a physically-based flood forecasting model (TOPMODEL) for three U.K. catchments. J. Hydrol., 69, 119-143.

Borge, R. et al., 2008. A comprehensive sensitivity analysis of the WRF model for air quality applications over the Iberian Peninsula. Atmospheric Environment, Volume 42, pp. 8560-8574.

Brooks R.H. and Corey A.T., Hydraulic properties of porous media, Hydrology papers, No. 3, Colorado State University, Colorado, 1964.

Bruen and Parmentier, 2005, Deliverable 9.4 – Fitting the spatially-distributed catchment model TOPKAPI to the Dargle catchment, comparison of modelled and measured flows and investigation of its parameter sensitivity, CARPE DIEM – EVG1-CT-2001-00045

Bugan, R. D. H., 2008. Hydrosalinity Fluxes in a Small Scale Catchment of the Berg River (Western Cape). Unpublished Master's Thesis. University of Western Cape.

Cheng, W. Y. Y. & Steenburgh, W. J., 2005. Evaluation of Surface Sensible Weather Forecasts by the WRF and the Eta Models. American Meteorological Society, 18 May, Volume 20, pp. 812-821.

DLSI (1996) A Digital Elevation Model for South Africa. Directorate of Land Surveys and Information, South Africa.

Doorembos, J., Pruitt, W.O., Aboukhaled, A., Damagnez, J., Dastane, N.G., van den Berg, C., Rijtema, P.E., Ashford, O.M. and Frere, M., 1984. Guidelines for predicting crop water requirements. FAO Irrig. Drainage Pap., 24.

Dunne, T (1978) Field studies of hillslope flow process. In: MJ Kirkby (ed.) Hillslope Hydrology. Wiley, New York. 227-293.

Efstathiou, G., Melas, D., Zoumakis, N. & Kassomenos, P. A., 2013. Evaluation of WRF-ARW Model in Reproducing a Heavy Rainfall Event Over Chalkidiki, Greece: The Effect of Land-Surface Features on Rainfall. s.l.:Springer Berlin Heidelberg.

Franchini, M., Wendling, J., Obled, C. and Todini, E., 1996. Physical interpretation and sensitivity analysis of the TOPMODEL. J. Hydrol., 175, 293-338.

Gallus, W. A. & Bresch, J. F., 2006. Comparison of Impacts of WRF Dynamic Core, Physics Package, and Initial Conditions on Warm Season Rainfall Forecasts. American Meteorological Society, Volume 134, pp. 2632-2641.

Gallus, W. A. & Pfeifer, M., 2008. Intercomparison of simulations using 5 WRF microphysical schemes with dual-Polarization data for a German squall line. Advances in Geosciences, Volume 16, pp. 109-116.

GAW, 2008, Schlunzen, k.h. and Sokhi, R.S. (eds). Overview of Tools and Methods used for Meteorological and Air Pollution Mesoscale Model Evaluation and User Training. Joint Report of COST action 728 (Enhancing Mesoscale Meteorological Modelling Capabilities for Air Pollution and Dispersion Applications) and GURME (GAW Urban Research Meteorology and Environment Project). WMO/TD-No. 1457

GLCC (1997) Global Land Cover Characteristics. United States Geo-logical Survey (USGS) http://edcdaac.usgs.gov/glcc

Grell, G. A., S. E. Peckham, R. Schmitz, S. A. McKeen, G. Frost, W. C. Skamarock and B. Eder, 2005: Fully coupled online chemistry within the WRF model, Atmos. Environ., 39, 6957-6975.

Grell, G., 2012. Parameterizing Convection on “Almost” Cloud-Resolving Scales (“Gray Scales”). s.l., s.n.

Hong, 2010. Progresses in PBL parameterization in atmospheric models. Jeju, Korea, s.n.

Hong, S. & Dudhia, J., 2012. Next-generation numerical weather prediction. American Meteorological Society, pp. 6-9.

Hong, S., Noh, Y. & Dudhia, J., 2006. A New Vertical Diffusion Package with an Explicit Treatment of Entrainment Processes. Monthly Weather Review, Volume 134, pp. 2314-2341.

Janko, I. et al., 2010. An Evaluation of Five ARW-WRF Microphysics Schemes Using Synthetic GOES Imagery for an Atmospheric River Event Affecting the California Coast. Journal of Hydrometeorology, Volume 12, pp. 618-633.

Jimenez, P. A. & Dudhia, J., 2011. Improving the representation of resolved and unresolved topographic effects on surface wind in the WRF model. s.l., s.n.

Kwun, J. H., Kim, Y. K., Seo, J. W. & You, S. H., 2009. Sensitivity of MM5 and WRF meso-scale model predictions of surface winds in a typhoon to planetary boundary layer parameterizations. Natural Hazards, 51(1), pp. 63-77.

Landman, S., Engelbrecht, F, A., Engelbrecht, C., Dyson L, L., and Landman, W, A., 2012, A short-range weather prediction system for South Africa based on multi-model approach. Water SA, 38.

Liu Z. and Todini E., 2002. Towards a comprehensive physically-based rainfall-runoff model, Hydrol. Earth Syst. Sci., 6(5), 859-881.

Mark DM (1988) Modelling geomorphological systems (Chapter 4). In: MG Anderson (ed.) Network Models in Geomorphology. John Wiley & Sons Ltd.

Marshall, J. S. & Palmer, W. M., 1948. The distribution of raindrops with size. Journal of Meteorology, Volume 5, pp. 165-166.

Martina M.L.V., Todini E and Libralon A (2006) A Bayesian decision approach to rainfall thresholds based flood warning. Hydrol. Earth Syst. Sci. 10 413-426.

Mass, C., 2012. , Improved subgrid drag or hyper PBL/Vertical Resolution? Dealing with the stable PBL problems in WRF. Boulder, s.n.

Midgley DC, Pitman WV and Middleton BJ (1994) Surface Water Resources of South Africa 1990. WRC Report No. 298/2.2/94. Water Research Commission, Pretoria, South Africa

Mohan, M. & Bhati, S., 2011. Analysis of WRF Model Performance over Subtropical Region of Delhi, India. Advances in Meteorology.

Molthan, A. L., 2011. Evaluating the Performance of Single and Double Moment Microphysics Schemes During a Synoptic-Scale Snowfall Event. Seattle, s.n.

Mooney, P. A., Mulligan, F. J. & Fealy, R., 2012. Evaluation of the sensitivity of the Weather Research and Forecasting model to parameterization schemes for regional climates of Europe over the period 1990-1995. Journal of Climate.

Moriasi, D.N., Arnold, J.G., Van Liew, M.W., Bingner, R.L., Harmel, R.D., Veith, T.L.,2007. Model evaluation guidelines for systematic quantification of accuracy in watershed simulations. Transactions of the ASABE 50 (3), 885-900.

Morrison, H. & Thompson, G., 2009. Impact of Cloud Microphysics on the Development of Trailing Stratiform Precipitation in a Simulated Squall Line: Comparison of One- and Two-Moment Schemes. American Meteorological Society, Volume 137, pp. 991-1007.

Pegram G.G.S., Nxumalo N. and Sinclair S., 2006. Soil Moisture Mapping from Satellites. Report K8/598 on a consultancy to the Water Research Commission, Pretoria.

Pegram G.G.S., Sinclair S., Parak M. and Nxumalo N., 2007. National Flood Nowcasting System: Towards an Integrated Mitigation Strategy. Report 1429/1/06. Water Research Commission, Pretoria

Pytharoulis, I. et al., 2010. Sensitivity of WRF precipitation on microphysical and boundary layer parameterizations during extreme events in Eastern Mediterranean. Plinius Conference Abstracts, Volume 12, pp. 12-76.

Rajeevan, M. et al., 2010. Sensitivity of WRF cloud microphysics to simulations of a severe thunderstorm event over Southeast India. Annales Geophysicae, Volume 28, pp. 603-619.

Ratna, S, B., Ratnam, J, V., Behera, S., Takahashi, K., and Yamagat, T., 2011, Simulation of 2010.2011 Summer Season Heavy Rainfall Events Over Southern Africa Using WRF Model. South African Society of Atmospheric Scientists (SASAS)27th Annual Conference, Hartbeespoort, North-West Province, South Africa

Rogers, E. et al., 2001. Changes to the NCEP Meso Eta Analysis and Forecast System : Assimilation of observed precipitation, upgrades to land-surface physics, modified 3DVAR analysis. [Online] Available at: http://www.emc.ncep.noaa.gov/mmb/mmbpll/spring2001/tpb/ [Accessed 10 02 2013].

Romine, G. S. et al., 2012. Model bias in a continuously cycled assimilation system and its influence on convection-permitting forecasts. Monthly Weather Review.

Ross, K. E., S. J. Piketh, R. T. Bruintjes, R. P. Burger, R. J. Swap, and H. J. Annegarn, 2003 Spatial and seasonal variations in CCN distribution and the aerosol-CCN relationship over southern Africa, J. Geophys. Res., 108(D13), 8481.

Shin, H. H. & Hong, S., 2011. Intercomparison of Planetary Boundary-Layer Parametrizations in the WRF Model for a Single Day from CASES-99. Springer Science, 139(2011), pp. 261-281.

SIRI (1987) Land Type Series. Department of Agriculture and Water Supply, Soil and Irrigation Research Institute. Memoirs on the Agri- cultural Natural Resources of South Africa. Pretoria, South Africa.

Skamarock, W. C. et al., 2008. A Description of the Advanced Research WRF Version 3. Boulder, Colorado.

Steeneveld, G. J., van de Wiel, B. J. H. & Holtslag, A. A. M., 2005. Modeling the Evolution of the Atmospheric boundary layer coupled to the land surface for three contrasting nights in cases-99. Journal of the Atmospheric Sciences, pp. 1-57.

Stensrud, D. J., 2007. Parameterization Schemes: Keys to Understanding Numerical Weather Prediction Models. Norman(Oklahoma): Cambridge University Press.

Stull, R. B., 2000. Meteorology for Scientists and Engineers. 2nd ed. s.l.:Brooks/Cole Thomson Learning .

Thompson, G., Rasmussen, R. M. & Manning, K., 2004. Explicit Forecasts of Winter Precipitation Using an Improved Bulk Microphysics Scheme. Part I: Description and Sensitivity Analysis. American Meteorological Society, Volume 132, pp. 519-542.

Todini E (1996) The ARNO rainfall-runoff model. J. Hydrol. 175 339-382.

UCAR, 2006 www.meted.ucar.edu/nwp/afwa_wrf/print.htm

Vischel T., Pegram G. G. S., Sinclair S., Parak M, 2008. Implementation of the TOPKAPI model in South Africa. Initial results from the Liebenbergsvlei catchment. Water SA Vol. 34 No.

Vischel T, Pegram GGS, Sinclair S, Wagner W and Bartsch A (2007) Comparison of soil moisture fields estimated by catchment modelling and remote sensing: a case study in South Africa. Hydrol. Earth Syst. Sci. Discuss. 4 2273-2306.

Weisman, M. L., Davis, C. A. & Manning, K., 2008. Experiences with 0-36h explicit convective forecasts with the WRF-ARW model. Weather and Forecasting, Volume 23, pp. 407-437.

Zhang, C, Wang, Y and Hamilton, K., 2011, Improved Representation of Boundary Layer Clouds over the Southeast Pacific in ARW-WRF Using a Modified Tiedtke Cumulus Parameterization Scheme, Monthly Weather Review, Vol. 139, pp 3489-3513.